Abstract

Ayres, Jennifer. Characterization of Titanium Alkoxide-Based Sol-Gel Systems and their Behavior in Icephobic Coatings.
(Under the direction of Dr. C.M. Balik)

New coatings have been developed that display resistance to the nucleation and adhesion of ice and are therefore termed 'icephobic'. These coatings are comprised of sub-micron sized phase domains of a hydrophobic matrix and a multi-component melt-point depressant. The melt-point depresssant complex consists of a titanium alkoxide-based sol-gel system designed to facilitate the slow-release of tripropylene glycol (TPG) and glycerol to the coating surface. The presence of these compounds is necessary for effective prevention of the nucleation and adhesion of ice; however, their concentrations are depleted with time and exposure to water. Thus, the rate at which TPG and glycerol are released to the surface is critical to both the coating's performance and its lifetime.

The morphology of the coating was verified using SEM, EDS and AFM techniques. Mass loss kinetics were studied over the temperature range 30 to 90°C ,for two coating formulations and indicated that the rate at which

TPG and glycerol are released to the surface is limited by diffusion through the coating matrix. Additives can also be used to control the mass loss behavior in these coatings. Similar studies performed on the isolated melt-point depressant complex combined with chemical analyses from FT-IR, NMR and TGA techniques indicate mass loss in the melt-point depressant is controlled by diffusion of TPG through the sol-gel network. TPG is the only species released through sol-gel reactions; glycerol remains bound to the network. The chemistry of the sol-gel network was altered by changing the reaction conditions. This had only minimal effects on the mass loss kinetics, which were affected primarily by changes in the diffusion environment rather than by reaction kinetics.

The original design of this coating was based on the assumption that the kinetics of the sol-gel reaction would control the rate at which TPG was released to the coating surface. This study found that the release of TPG is controlled by diffusion rather than by chemical reaction kinetics. Nevertheless, this coating was still found to be effective for preventing the nucleation and adhesion of ice.

CHARACTERIZATION OF TITANIUM ALKOXIDE-BASED SOL-GEL SYSTEMS AND THEIR BEHAVIOR IN ICEPHOBIC COATINGS

by
JENNIFER AYRES

A thesis submitted to the Graduate Faculty of North Carolina State University in partial fulfillment of the requirements for the Degree of Master of Science

MATERIALS SCIENCE AND ENGINEERING

Raleigh
2004

APPROVED BY:

_____

_____ Co-chair of Advisory Committee

_____ Co-chair of Advisory Committee

This work is dedicated to my family and friends without whom this would not be possible.

Biography

Jennifer Ayres grew up in Chapel Hill, N.C. and got a B.S. in Applied Science from UNC-Chapel Hill with a concentration in polymeric materials. She spent two years working in product development for fiber optic assemblies before returning to school as a graduate student at North Carolina State University. After completing her M.S. in Materials Science and Engineering, Jennifer plans to pursue a PhD in chemistry.

Acknowledgments

The following people are acknowledged for their contribution to this work:

Dr. C.M. Balik, advisor

Dr. Michael Rigsbee, co-chair of advisory committee

Dr. Richard Spontak, advisory committee

Dr. William Simendinger and Shawn Miller of Microphase Coatings, Inc.,

Rich Fiore, AFM technical assistance

Birgit Andersen, FT-IR assistance

Dr. Hanna Gracz, NMR assistance

Drs. Cristian and Marianna Rusa, TGA assistance

Marcus A. Hunt and Brad Busche

Microphase Coatings, Inc. is also acknowledged for funding this project

Table of Contents

List of Tables vii

List of Figures viii

1. Introduction 1
    - 1.1 Problem of Ice Adhesion 1
    - 1.2 Proposed Solution 5
    - 1.3 Sol-Gel Chemistry 7
    - 1.4 Applications of Sol-gel Chemistry 17
    - 1.5 Sol-Gel Chemistry Applied to Prevent the Nucleation and Adhesion of Ice 23
    - 1.6 Objectives 25

2. Experimental 27

3. Coating Morphology, Performance and Practice 31
    - 3.1 Contact Angle 31
    - 3.2 Coating Morphology 33
    - 3.3 Release of Tripropylene Glycol and Glycerol 36
    - 3.4 Coating Morphology after Water Immersion 41
    - 3.5 Coating Performance 43
    - 3.6 Summary and Conclusions 46

4. Mass Loss Depressant in the Coating and the Melt-Point Depressant Complex 47
    - 4.1 Mass Loss in Coating 48
    - 4.2 Mass Loss in the Melt-Point Depressant 56
    - 4.3 Mass Loss Kinetics for the Melt-Point Depressant 66
    - 4.4 Coating Formulations Compared to the Melt-Point Depressant 72
    - 4.5 Summary and Conclusions 74

5. Chemistry of the Melt-Point Depressant 76
5.1 Fourier Transform-Infrared Spectroscopy 78
5.2 Predictive Model for the Sol-Gel Reaction 88
5.3 Extension of Predictive Model 106
5.4 Verification of Model 113
5.5 Mass Loss Kinetics 133
5.6 Summary and Conclusions 148

6.0 Summary and Conclusions 152

7.0 Future Work 155

References 156

Appendices 159
Appendix 1: Possible Reaction Paths for Sol-Gel System Synthesized Under Ambient Conditions 160
Appendix 2: Possible Reaction Paths for Sol-Gel System Synthesized Under Ambient Conditions; Glycerol Added Last 168
Appendix 3: Possible Reaction Paths for Sol-Gel System Synthesized Under Nitrogen 173
Appendix 4: Possible Reaction Paths for Sol-Gel System Synthesized Under Nitrogen; Glycerol Added Last 177

List of Tables

3-1 Contact Angle Measurements for Polymeric Coating Matrix 33

4-1 Additives in Two Coating Formulations 49
4-2 Diffusion Coefficients for Coating Formulations A and B 54
4-3 Diffusion Coefficients for IPA out of the Melt-Point Depressant 67
4-4 Diffusion Coefficients for TPG and Glycerol out of the Melt-Point Depressant 71

5-1 Reported Vibrational Frequencies for Silica Gels 82
5-2 Partial Charge Calculations for TIP Reacted with Acetic Acid 93
5-3 Reaction of TIP with Acetic Acid 96
5-4 Partial Charge Calculations for Reactants Involved in Sol-Gel Reaction 98
5-5 Charge Distributions for All Possible Reaction Intermediates of Sol-Gel System Synthesized in Ambient Conditions 99
5-6 Predicted Reaction Products for Melt-Point Depressant Synthesized in Ambient Conditions 101
5-7 Predicted Reaction Products for Melt-Point Depressant Synthesized in Ambient Conditions, Continued 102
5-8 Ionic Components of Bond Energy Approximated Using Pauling's Bond Energy Equation 103
5-9 Charge Distribution of $Ti(C_3H_70)_3(C_3H_7O_3)$ 106
5-10 Summary of Reaction Paths for Sol-Gel System Synthesized in Ambient Conditions, Glycerol Added Last 109
5-11 Summary of Reaction Paths for Sol-Gel System Synthesized Under Nitrogen 111
5-12 Summary of Reaction Paths for Sol-Gel System Synthesized Under Nitrogen with Glycerol Added Last 112
5-13 Summary of Predicted Reactions 113
5-14 Signals Expected in Various Systems Analyzed with ^1H NMR 130
5-15 Diffusion Coefficients for IPA in Sol-Gel System at 70°C 138
5-16 Diffusion Coefficients for Final Region of Mass Loss in Sol-Gel System at 70°C 140
5-17 Calculated Mass Percentages for Sol-Gel System 145
5-18 Mass Percentages Loss for Sol-Gel System 146

List of Figures

1-1 Schematic of coating design 5
1-2 Hydrolysis of tetraethoxysilane 7
1-3 Alcoxolation of hydrolyzed TEOS 8
1-4 Oxolation of hydrolyzed TEOS 8
1-5 Shrinkage of gel with condensation 9
1-6 TEOS precursor substitution and the resulting reaction rates 12
1-7 Acid catalyzed hydrolysis of TEOS 15
1-8 Base catalyzed hydrolysis of TEOS 15
1-9 Gel structures for acid and base catalyzed reactions 16
1-10 Entrapment of guest molecules in a sol-gel network 18
1-11 Possible structures for organic-inorganic hybrids 19
1-12 Property regimes for organically modified sol-gel 21
1-13 Reaction of TIP with TPG and glycerol 24
1-14 Condensation reaction resulting in slow release of TPG and glycerol to coating surface 25

3-1 Schematic of contact angle for hydrophobic and hydrophilic surfaces 32
3-2 Scanning electron microscopy and EDS images of coating 34
3-3 Topographical and Phase AFM Images of Coating, 5μm^2 35
3-4 Topographical and Phase AFM Images of Coating, 1 μm^2 35
3-5 Mass loss measurements made during water immersion at 30°C 37
3-6 FT-IR spectrum of leachant obtained during water immersion 38
3-7 Optical images of coating taken at room temperature 39
3-8 Mass loss measurements made in an oven at 50°C 40
3-9 SEM images before and after water immersion 42
3-10 AFM images before and after water immersion 42
3-11 Vortex generator after being in the icing wind tunnel for approximately 20 minutes at -2°C 44
3-12 Vortex generator after being in the icing wind tunnel for only a few minutes at -9°C 44
3-13 Airfoil after being in the icing wind tunnel for approximately 12 minutes at -15°C 45

List of Figures (continued)

4-1 Mass loss behavior in coating formulation A 50
4-2 Mass loss behavior in coating formulation B 52
4-3 Diffusion model curve fit for mass loss data collected for formulation A at 90°C 53
4-4 Arrhenius plots for coating formulations A and B 55
4-5 Mass loss behavior for the melt-point depressant 57
4-6 Three regions of mass loss in a sol-gel 58
4-7 Three regions of mass loss observed for the melt-point depressant at 70°C 60
4-8 Physical changes in the melt-point depressant during mass loss at 70°C 62
4-9 Three regions of mass loss observed for the melt-point depressant at 22°C 63
4-10 Physical changes observed for the melt-point depressant at 22°C 64
4-11 TGA scan for the melt-point depressant from 25 to 400°C 66
4-12 Curve fit for diffusion of IPA out of the melt-point depressant at 70°C 67
4-13 Arrhenius plot for diffusion of IPA out of the melt-point depressant at 70°C 68
4-14 Curve fit for diffusion of TPG and glycerol out of melt-point depressant at 70°C 70
4-15 Arrhenius plot for diffusion of TPG and glycerol out of the melt-point depressant 72
4-16 Arrhenius plots for coating formulations compared to the isolated melt-point depressant 73

5-1 Reaction of titanium isopropoxide with tripropylene glycol and glycerol 76
5-2 Sol-gel reaction 77
5-3 FT-IR spectrum of reacted melt-point depressant compared to the sum of the individual reactants 79
5-4 FT-IR spectrum of the reacted melt-point depressant compared to IPA and TIP 80
5-5 FT-IR spectra of dried melt-point depressant and hydrolyzed TIP 83
5-6 FT-IR spectrum of the liquid released from the melt-point depressant 86

List of Figures (continued)

5-7 Chemistry resulting in Ti-O-R-O-Ti infrared band 87
5-8 Reaction of TIP with acetic acid 92
5-9 Flowchart showing reaction of TIP with acetic acid 96
5-10 FT-IR spectra of sol-gel system reacted under different conditions 114
5-11 FT-IR spectra of dried sol-gel systems reacted under different conditions 115
5-12 FT-IR spectra of dried MPD reacted under nitrogen for different time periods 118
5-13 Protons affecting 'H NMR chemical shifts 121
5-14 'H NMR of melt-point depressant 122
5-15 Magnified view of ^{1}H NMR of melt-point depressant 123
5-16 Chemical shift changes expected for 'H NMR of sol-gel 125
5-17 ^{1}H NMR spectra for melt-point depressant synthesized under different conditions 129
5-18 Chemical shift changes expected for ^{13}C NMR of sol-gel 132
5-19 Mass loss kinetics at 70°C for melt-point depressant synthesized under different conditions 134
5-20 Physical changes in melt point depressant 136
5-21 Thermogravimetric analysis of melt-point depressant synthesized under different conditions 144
5-22 Thermogravimetric analysis of melt-point depressant synthesized under different conditions 148

A1-1 Possible reaction paths for TIP after initial reaction with glycerol; ambient conditions 160
A1-2 Possible reaction paths for TIP after initial reaction with water; ambient conditions 161
A1-3 Possible reaction paths for TIP after initial reaction with water and TPG; ambient conditions 162
A1-4 Possible reaction paths for TIP after initial reaction with water and two TPG groups; ambient conditions 163
A1-5 Possible reaction paths for TIP After initial reaction with TPG and glycerol; ambient conditions 164

List of Figures (continued)

A1-6 Possible reaction paths for TIP after initial reaction with TPG and water; ambient conditions 165

A1-7 Possible reaction paths for sol-gel system TIP after initial reaction with TPG, water and then a second TPG group; ambient conditions 166

A1-8 Possible reaction paths for TIP after initial reaction with three TPG groups; ambient conditions 167

A2-1 Possible reaction paths for TIP after initial reaction with water; ambient conditions, glycerol not yet added 168

A2-2 Possible reaction paths for TIP after initial reaction with water; ambient conditions, glycerol added to system 169

A2-3 Possible reaction paths for TIP after initial reaction with TPG; ambient conditions, glycerol not yet added to the system 170

A2-4 Possible reaction paths for $Ti(C_3H_70)(C_9H_{19}O_4)_3$ upon addition of glycerol; ambient conditions 171

A2-5 Possible reaction paths for $Ti(C_9H_{19}O_4)_3OH$ upon addition of glycerol; ambient conditions 172

A3-1 Possible reaction paths for TIP under nitrogen 173

A3-2 Possible reaction paths for $Ti(C_9H_{19}O_4)_3(C_3H_7O_3)$ and $Ti(C_3H_7O)_2(C_9H_{19}O_4)(C_3H_7O_3)$ upon exposure to atmosphere 174

A3-3 Possible reaction paths for $Ti(C_3H_7O)(C_9H_{19}O_4)_2(C_3H_7O_3)$ and $Ti(C_3H_7O)(C_9H_{19}O_4)_3$ upon exposure to atmosphere 175

A4-1 Possible reaction paths for TIP under nitrogen, glycerol added last 176

A4-2 Possible reaction paths for system reacted under nitrogen; glycerol added last, exposed to atmosphere 177

1. Introduction

1.1 Problem of Ice Adhesion

Since the dawn of aviation, ice, frost and snow have posed obstacles to flight. Ice build-up on the exterior of an aircraft affects the aerodynamics and consequently the lift capabilities of a plane in addition to causing the malfunction of individual components. Various techniques have been explored to rectify this problem; mechanical, electrical and chemical methods have been employed both to remove ice and limit its adhesion.[1, 2]

Ice is commonly removed by mechanical cutting and scraping. These methods are only effective for removing ice while the aircraft is grounded and do not prevent ice from reforming. In addition to ice build-up that occurs on the ground, in flight icing poses a significant threat, especially to small planes which fly at or below cloud level. Supercooled water droplets freeze upon contact with an aircraft in flight. To counter this problem, rubber tubes are placed along the front of many airplane wings.[1, 2] These tubes can be periodically inflated to break ice on the surface. However, this approach is much less effective than ice removal performed on the ground.

Electrical methods have also been applied to remove ice from aircraft in flight. Ice has been melted using heaters and redirecting heat generated by the engine. Currently, small engines do not generate sufficient heat for effective ice removal; the development of engines with increased energy efficiency further limits the use of this technique.

Electrodes have also been used to facilitate ice removal. A power supply generates DC current between multiple closely-spaced electrodes on the surface of the aircraft and generates an electric field at the ice-surface interface.[3] The electric field initiates electrolysis reactions, which create bubbles of hydrogen and oxygen gas at the interface. These bubbles reduce the surface area of ice in direct contact with the aircraft, creating cracks and reducing the force required for ice removal to that created by normal aerodynamic forces while in the air.[1, 3] Electric current is also used to facilitate the mechanical removal of ice. Short bursts of current are applied in opposite directions through two parallel wires. The resulting electromagnetic field creates a force, which pushes the wires apart and cracks the ice.[1]

Of all the techniques explored, chemical methods show the greatest potential for solving the problem of ice build-up on aircraft. Not only can chemicals be used to remove ice from surfaces, but they can prevent further ice adhesion.

Two different chemical approaches have been studied: hydrophobic coatings have been developed to limit the contact area between the ice and the surface of the aircraft, and freezing point (melt-point) depressants have been used to melt ice already the surface.

One of the most commonly used hydrophobic coatings is polytetrafluoroethylene (PTFE, Teflon®). Recently, comparable hydrophobic properties have been found in polysiloxanes[1], and one company found increased hydrophobicity in a copolymer containing both fluoralkyl and silicon-containing monomer units.[4] This composition also included silica particles with an average particle size less than 5 μm, which increased the smoothness of the surface and improved its hydrophobic capabilities.[2, 4]

The other chemical approach to removing ice from surfaces involves the use of melt-point depressants, which create a liquid layer on the surface and consequently limit ice adhesion. The most commonly used melt-point depressants are mixtures of water and either ethylene glycol or propylene glycol. These solutions are applied to the aircraft while on the ground. Because the adhesive forces between ice and a metal surface are significant[5, 6], large amounts of these solutions are required for ice removal; this is not only expensive and time consuming, but poses a significant threat to the

environment. In addition, these low-viscosity fluids quickly run off the surface and do not provide any protection against further ice formation. Many attempts have been made to thicken solutions of melt-point depressant to increase their viscosity so that they remain on the surface of the aircraft. Both pure polyacrylic acid[7] and a hydrophobically modified acrylic acid copolymer[8] have been crosslinked and added to these solutions as thickening agents. These solutions provide protection against further ice adhesion while the aircraft is grounded; however, the solutions must be removed before flight. Liquids on the exterior of an aircraft can result in appreciable lift loss[6], and therefore must be removed prior to take-off or by shearing action during take off.[6-8] Thickened melt-point depressants pose additional challenges in that they must wet the surface to be effective, they must be stable enough that they do not gel or separate during storage[6] and they must be thinned with another substance, generally an alkanol, so that they can be sprayed.[6, 7] Compounds that exhibit all of these properties still only provide protection for a limited amount of time, on the order of hours, while the plane is grounded. Attempts have been reported to mix ethylene glycol with a gelatin that can be painted on a metal surface and subsequently hardened to form a fixed coating.[2] However, no success in this area has been documented.

1.2 Proposed Solution

This study investigates a long-term solution to the aircraft icing problem which incorporates both a hydrophobic surface and melt-point depressants. This coating, designed to prevent the nucleation and adhesion of ice, consists of heterogeneous, sub-micron sized phase domains of a multi-component melt-point depressant dispersed in a hydrophobic polymer matrix as shown in figure 1-1. The size and distribution of the phase regions ensures that each droplet that comes in contact with the surface will be exposed to both the hydrophobic matrix, which limits the contact area of the droplet, and the melt-point depressant, which forms a thin layer on the surface and prevents ice formation.

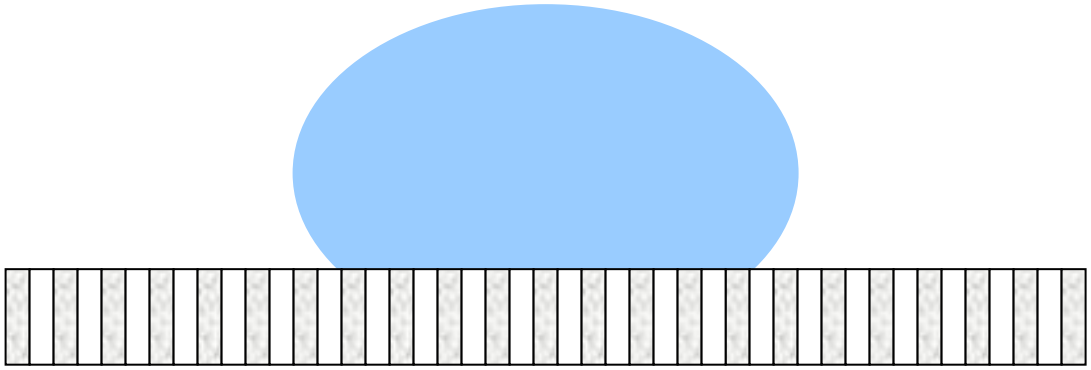

Figure 1-1: Schematic of coating design

The hydrophobicity of the matrix was achieved through the addition of poly(diethoxysiloxane) (PDES), which has documented hydrophobic properties.

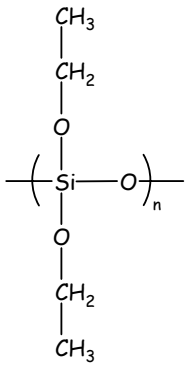

Poly(diethoxysiloxane)

The melt-point depressants used in this system are tripropylene glycol (TPG) and glycerol. Like the melt-point depressants described above, these compounds offer only short term protection. Because of their low viscosity and water-solubility, surface concentrations of these molecules are depleted with both time and exposure to water. This coating is therefore designed to slowly release TPG and glycerol to the surface offering long term protection both on the ground and in flight.

The slow release of TPG and glycerol is achieved by incorporating a sol-gel system into the coating. The exact nature of the gel used in this system is described after the brief discussion of sol-gels below.

1.3 Sol-Gel Chemistry

The term, 'sol,' describes a colloidal suspension in a fluid matrix, and a gel is defined as a two-phase system including a molecular backbone and an interstitial liquid. 'Sol-gel' refers to the process of forming metal oxides from metal alkoxide precursors; both a 'sol' and a 'gel' are formed in the intermediate stages of this process.

Sol-gel reactions were used to synthesize glasses and ceramics long before the chemistry was understood. The most common sol-gel reaction involves the hydrolysis and condensation of tetraethoxysilane (TEOS) to form silica. The sol consists of TEOS molecules suspended in solution. Upon exposure to water, the TEOS molecules undergo hydrolysis as shown in figure 1-2.

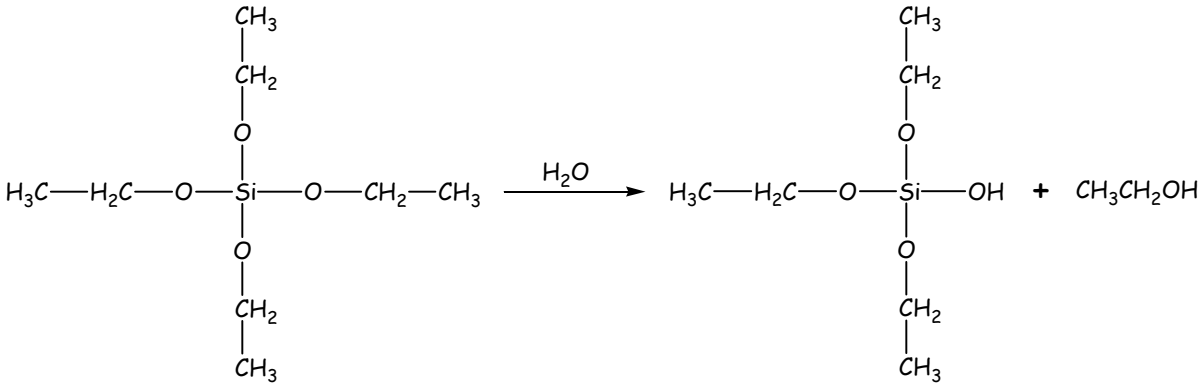

Figure 1-2: Hydrolysis of tetraethoxysilane

After hydrolysis, TEOS undergoes one of two possible condensation reactions. The most common process is alcoxolation in which the hydroxide group reacts

with an adjacent ethoxy group to produce ethanol and a siloxane oligomer as shown in figure 1-3.

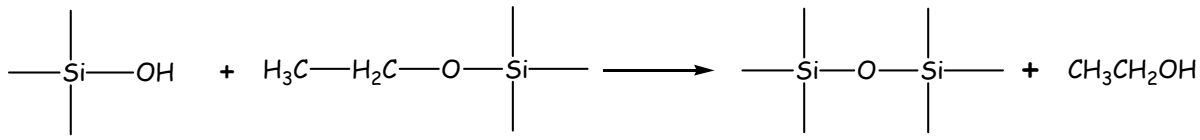

Figure 1-3: Alcoxolation of hydrolyzed TEOS

The hydroxide group can also react with another hydroxide group in the process of oxolation as shown in figure 1-4. This reaction produces water in addition to the siloxane oligomer.

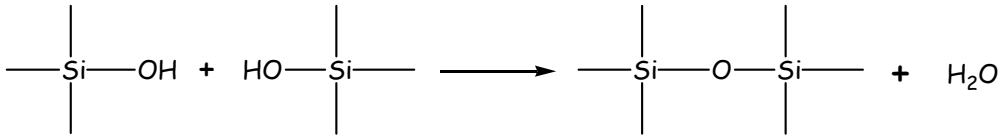

Figure 1-4: Oxolation of hydrolyzed TEOS

Alcoxolation occurs much more often than oxolation, because the ethoxy group is less electronegative and consequently makes a much better leaving group. In addition, there is a larger concentration of ethoxy groups in the early stages of the reaction. Condensation reactions proceed through several additional stages until a pure SiO_2 network is formed.

The first stage associated with the sol-gel process is, of course, the formation of gel, which consists of growing metal-oxide chains surrounding solvent molecules. This stage is accompanied by a sharp increase in viscosity. Gelation is succeeded by the formation of additional metal-oxide crosslinks, which pull chains together and result in shrinkage of the gel as shown in figure 1-5. This contraction brings additional –OH groups together, resulting in further condensation.

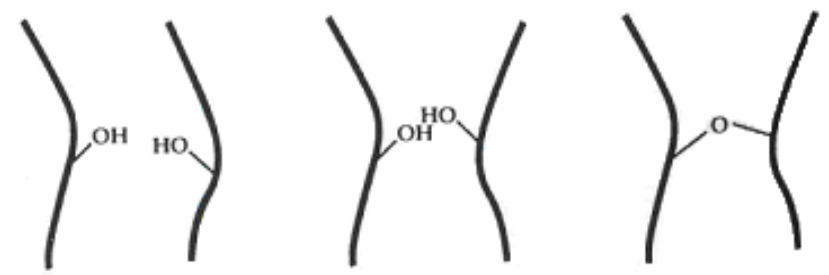

Figure 1-5: Shrinkage of gel with condensation
Image was taken from Brickner and Scherer's book, *Sol Gel Science: The Physics and Chemistry of Sol-Gel Processing* (reference 10).

Ostwald ripening also occurs during this stage[11, 13]; small oligomeric metal-oxide structures migrate towards each other to form larger polymeric structures. The result is phase separation of the solid network from the solvent, and precipitation of solid crystals is often observed. This process is thermodynamically driven to reduce energy associated with the solid-liquid interface. However since this process is not kinetically favored, Ostwald ripening is limited in systems with high reaction rates. Condensation occurs

with minimal migration, yielding a final product with significant cracking and a high concentration of oligomers.

The next stage of the sol-gel process is aging, which involves the loss of water, solvent and any alcohols produced during hydrolysis and condensation.[10, 11]. These liquids are first removed through syneresis; a consequence of the gel shrinkage shown in figure 1-5 which expels liquids from the pores. Liquid on the surface of the gel evaporates, creating a concentration gradient that leads to diffusion. Liquid evaporation can also cause pressure gradients and capillary stresses within the network, which are relieved by cracking and the release of additional liquid.[10]

Once aging is complete, the resulting network can be subjected to thermal treatment; above approximately 1000°C, densification occurs.[10] This process involves additional condensation reactions and structural relaxation which cause shrinkage and produce a dense ceramic.[10, 11]

This procedure for producing glasses and ceramics has the advantage that the chemical reactions occur at much lower temperatures than other methods

yielding the same products.[11-12] Sol-gel processes also yield extremely pure materials. This is due to both the purity of the starting materials, which can be easily distilled, and the fact that lower processing temperatures reduce the risk of contamination and thermal degradation.[11-12] However, sol-gel techniques have not replaced other more traditional methods for preparing glasses and ceramics for several reasons. No glasses have been prepared using sol-gel methods that have not been prepared by other means and metal alkoxide precursors are expensive and moisture-sensitive, which limits large-scale production. Sol-gel reactions are also complicated, time consuming and difficult to control.

All stages of the sol-gel process require strict kinetic control in order to create a solid network with limited cracking. Many different factors affect the kinetics of sol-gel reactions including the rates of hydrolysis and condensation.

The hydrolysis rate is dependent the concentration of water in the system and the nature of the alkoxy substituents. The rate of hydrolysis is limited by steric effects, and therefore decreases with the length of the alkyl

substituent on the alkoxide precursor. Because slow kinetics yield larger networks with limited cracking, alcohol exchange, also known as precursor substitution, reactions are often utilized to increase the length of the alkoxy substituents on the precursor molecules and limit the hydrolysis rate. Figure 1-6 shows two alcohol exchange reactions involving TEOS and indicates their effects on hydrolysis rates. Nucleophilic substitution of butanol decreases the hydrolysis rate by a factor of approximately 2.7 while substitution of 2, 6 dimethyl-heptanol decreases the hydrolysis rate by a factor of 17.[10]

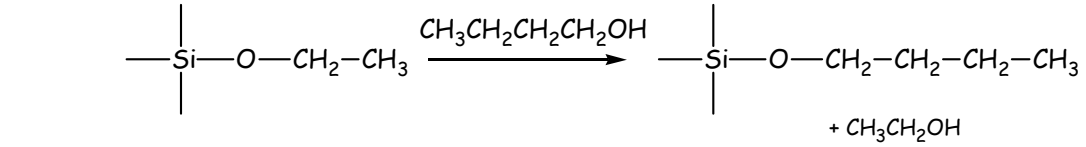

k_h = 0.051/(mol*s*[H^+]) k_h = 0.019/(mol*s*[H^+])

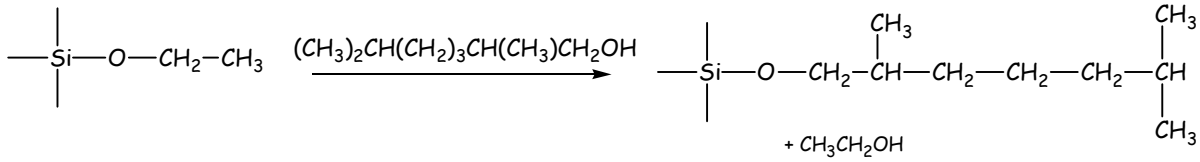

k_h = 0.051/(mol*s*[H^+]) k_h = 0.003/(mol*s*[H^+])

Figure 1-6: TEOS precursor substitution reactions and the resulting hydrolysis rates

Data was taken from Brickner and Scherer's book, *Sol Gel Science: The Physics and Chemistry of Sol-Gel Processing* (reference 10).

Precursor substitution reactions are especially important for controlling the hydrolysis rate of transition metal alkoxides. Titanium metal alkoxides exhibit greater hydrolysis rates than siloxanes, because transition metals are more electrophilic (less electronegative) than silicon and consequently more susceptible to nucleophilic attack.

The length of the alkoxy chain affects the rate of condensation as well as hydrolysis reactions. Steric hindrance limits condensation reactions; consequently, precursor substitution yields smaller oligomers.

Another factor that affects both the rate and extent of condensation reactions is the flexibility of the inorganic chains. The condensation reaction shown in figure 1-5 assumes some flexibility in the backbone chains. This reaction would not occur in an extremely rigid system. Chain flexibility decreases with the extent of condensation in any given gel. Likewise, the viscosity of the pore liquid affects condensation as its movement through the network is required for condensation and concurrent shrinkage. Increasing the temperature of reaction often increases the reaction rates; however, the proportional increases in the liquid viscosity and chain flexibility are not

observed. When liquid is not expelled at a rate comparable to the rate of condensation, pressure builds up in the network and causes additional cracking.[10]

As indicated above, any small change in reaction conditions including precursor chemistry, temperature, pH and solvent can affect not only the rates of hydrolysis and condensation, but also the structure of the final product. A more specific example of how small changes in reaction rates affect structures is shown in the following example involving the addition of acids and bases to the sol-gel solution. An acid added to a sol-gel system protonates hydroxo ligands and facilitates the departure of water or alcohol in both hydrolysis and condensation reactions. Figure 1-7 shows this for the hydrolysis of TEOS. Protonation increases the rate of hydrolysis by stabilizing the transition state and facilitating the removal of ethanol. The added proton creates a positive charge, which is stabilized by the electron-donating substituents on the alkoxide. Consequently, the transition state is less stable with each successive reaction and the reaction rates decrease accordingly. Decreasing rates of hydrolysis and condensation result in significant Ostwald ripening and a highly crosslinked network as shown in figure 1-9.[10, 11]

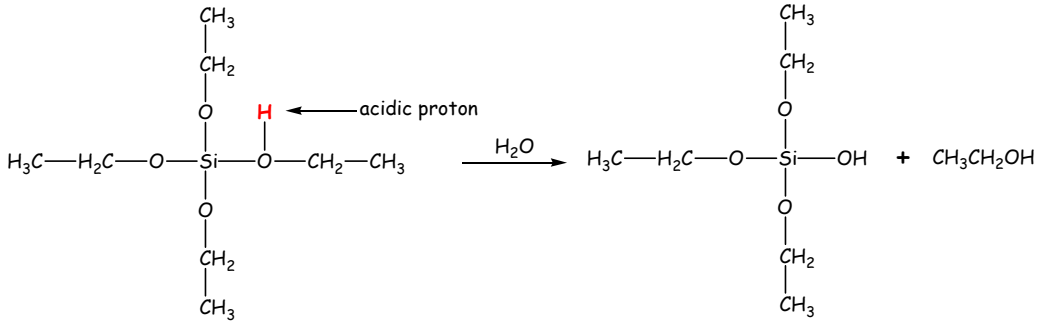

Figure 1-7: Acid catalyzed hydrolysis of TEOS

In contrast, a base added to a sol-gel solution deprotonates hydroxyl ligands and creates stronger nucleophiles. The base-catalyzed hydrolysis of TEOS is shown in figure 1-8. In this case, the transition state is negatively charged and becomes increasingly stable as electron-donating groups are removed through successive hydrolysis and condensation. The slow kinetics in the early stage of the condensation process result in highly crosslinked particles. However, as reaction rates increase there is not sufficient time for Ostwald ripening and the resulting structure is extremely porous as shown in figure 1-9.

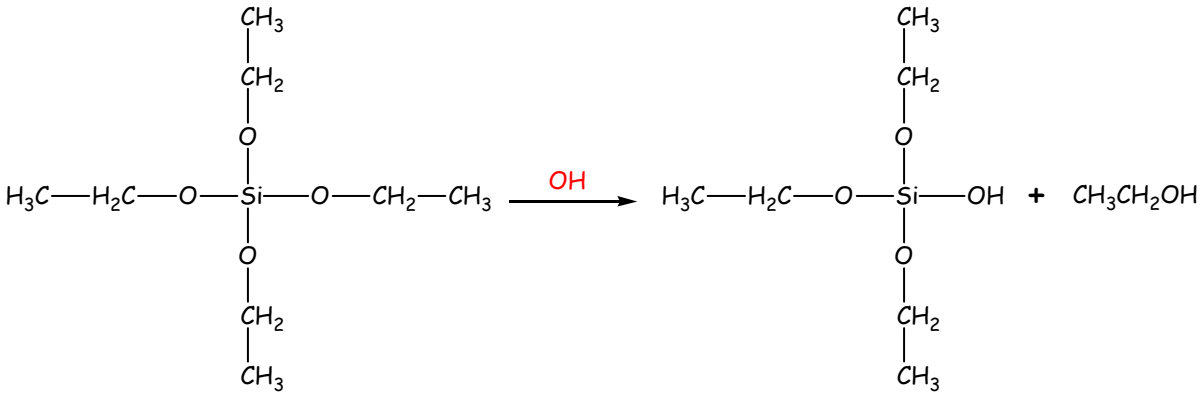

Figure 1-8: Base catalyzed hydrolysis of TEOS

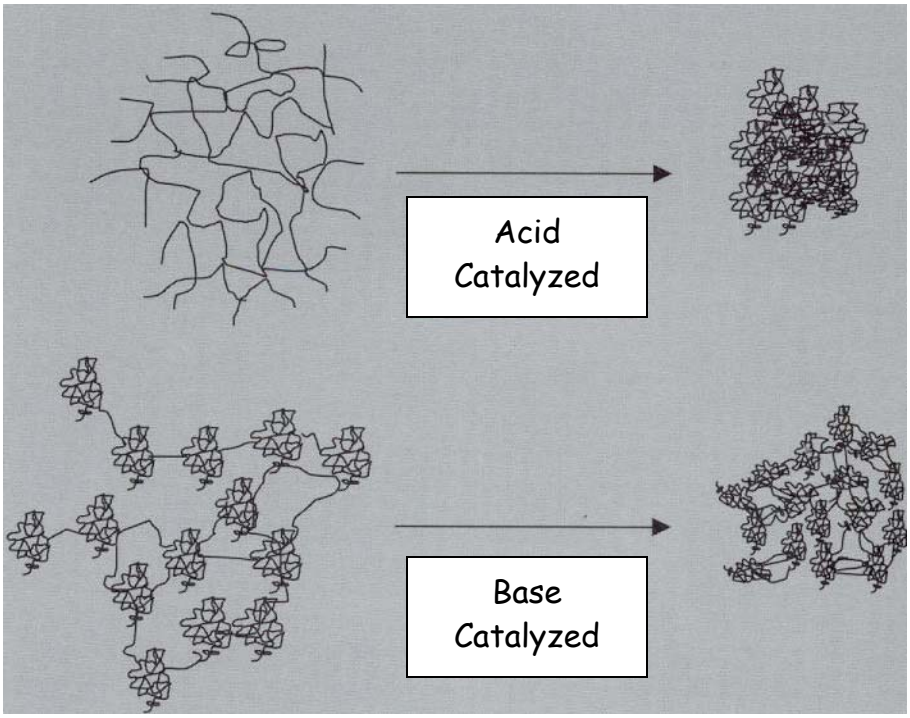

Figure 1-9: Gel structures for acid and base catalyzed reactions
Figure was taken from Wright, Nico and Sommerdijk's book, *Sol Gel Materials: Chemistry and Applications* (reference 11).

The significant structural differences observed for products of acidic and basic sol-gel solutions are yet another indication that strict control of reaction conditions is required to achieve a desired product. While this is a significant disadvantage in the production of ceramics and glasses, the complexity of the sol-gel process allows for the synthesis of a wide range of new materials not achievable through other methods. The study of sol-gel science is no longer focused on the production of ceramics, but has expanded to a much broader range of applications.

1.4 Applications of Sol-Gel Chemistry

The complexity of sol-gel systems allows for synthesis of many different structures and paves the way for the development of a variety of materials for many applications.

While sol-gel techniques are not currently used for bulk glasses, their ability to form extremely pure metal oxides has led to their use for the production of optical components including lenses and optical fibers.[12, 13] In addition, the liquid nature of precursor solutions creates the ability to mold ceramics to unique shapes and, more importantly, thin films. Sol-gel solutions are applied to polymer and glass surfaces using spin or dip coating techniques to create coatings resistant to heat, abrasion and chemicals. There is also interest in using sol-gel materials for electronic applications. They form extremely pure, transparent, conductive films for coating semi-conductor wafers[11] and have been explored as alternatives to sputtering.[13]

Sol-gel systems have also been developed to serve merely as a host matrix for other molecules, creating homogenous mixtures on a molecular scale as shown in figure 1-10. Guest molecules are added to the precursor solution and become

entrapped and eventually immobilized in the sol-gel network as crosslinks form. The low-temperature processing conditions allow for the addition of organic molecules such as dyes. One study reported the successful incorporation of 1-nitro-2-naphthol into silica sol-gels.[13] This molecule detects cobalt ions, and the sol-gel network immobilizes these molecules in an array. Thin films of these materials can then be used as chemical sensors. A carbon monoxide sensor has been developed similarly by incorporating a rhodium (I) complex into titania and zirconia sol-gel films.[13]

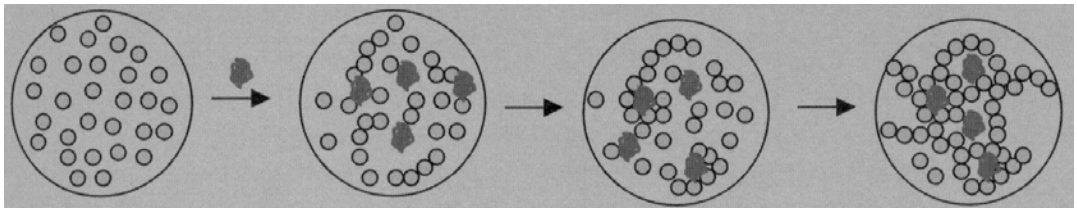

Figure 1-10: Entrapment of guest molecules in a sol-gel network
Figure was taken from Wright, Nico and Sommerdijk's book, *Sol Gel Materials: Chemistry and Applications* (reference 11).

The performance of guest molecules in these systems is limited by their tendency to diffuse out of the gel.[10] Porous networks are therefore less desirable for these applications than high-density gels.

The porous nature of sol-gel networks has made them valuable in separations. They have been used as filters on a sub-micron scale with applications in

wastewater treatment and gas separations.[11, 12] Sol-gel systems inside size-exclusion chromatography columns have yielded extremely efficient separations.

Of all the possible applications for sol-gel materials, the development of organic-inorganic hybrid materials is possibly the most viable. As mentioned above in reference to figure 1-10, the low processing temperatures associated with sol-gel processes allow for the incorporation of organics. Not only can organics be entrapped within the sol-gel network, but they can be covalently bonded to the network.

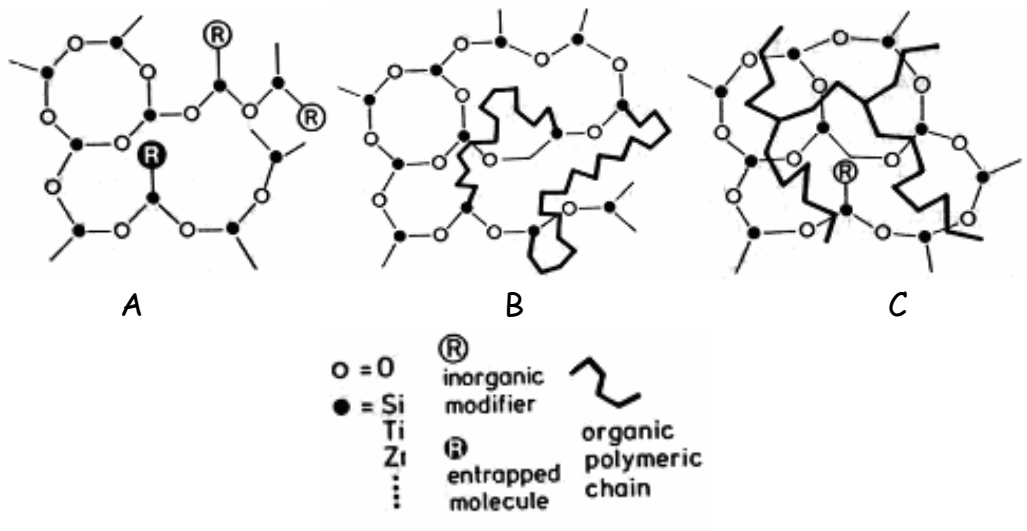

Figure 1-11: Possible structures for organic-inorganic hybrids
(A) sol-gel with organic and inorganic modifiers
(B) polymer chains grafted to sol-gel network
(C) interpenetrating organic and inorganic networks
Figure taken from Helmut Schmidt's article, *"Preparation, Application and Potential of ORMOCERS"* (reference 14)

Figure 1-11 shows several different structures for organic-inorganic hybrid materials. Organic molecules can be added to the inorganic network to alter its structure or add functionality as shown in figure 1-11-A. Figures 1-11-B and C show polymer chains incorporated into sol-gel networks, both covalently grafted to create a single network and polymerized in situ to create interpenetrating organic and inorganic networks.[14]

Because most organic-inorganic hybrids are created from silica sol-gels, they have been given various names such as ORMOSILS (Organically Modified Silicates), ORMOCERS (Organically Modified Ceramics) and CERAMERS (Ceramic Polymers). Organic modifiers are often included in metal oxide coatings for added functionality. For instance, the ORMOCER® line includes coatings for corrosion protection, hydrophobic, anti-static and anti-adhesion applications. The inorganic component in these coatings provides long-term stability with resistance to both heat and abrasion.[15] Organic modifiers for hydrophobic coatings consist of long alkyl chains while polyvalent alcohols, esters and fatty acids provide anti-static properties.[15] The addition of Norbloc 7966 to sol-gel coatings provides UV resistance to transparent, abrasion-resistant coatings for windows in aircraft, public buildings and automobiles.[16]

Not only do hybrid materials add functionality to metal oxides, but they create the ability to develop systems with both the hardness and stability of ceramic materials and the flexibility of organics. The properties vary with the relative concentrations of each component. Figure 1-12 shows property regimes observed in a metal oxide gel and indicates the variation of properties that can be obtained for this single system. MeO_2 indicates the pure metal oxide; the metal is either silicon, titanium or zirconium. SiR_2 and SiR'R'' molecules are added to control the extent of crosslinking in the system; R = C_6H_5, R' = alkyl chain, R'' = vinyl group.

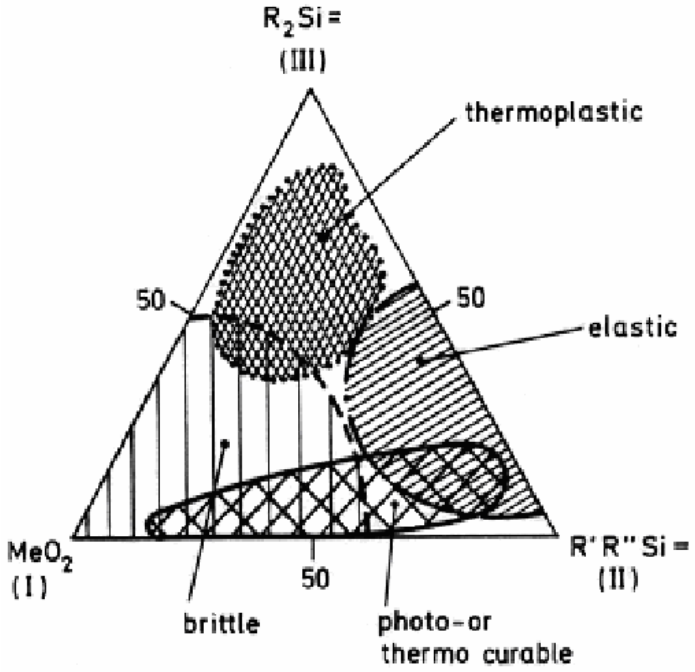

MeO_2 = metal oxide, Me = Si, Ti, Zr
R = C_6H_5, R' = alkyl chain, R'' = vinyl group

Figure 1-12: Property regimes for organically modified sol-gel
Figure taken from Helmut Schmidt's article, *"Preparation, Application and Potential of ORMOCERS"* (reference 14)

The vinyl group can undergo photo or thermal-initiated polymerization reactions with both alkyl and vinyl substituents in the photo-or thermal curable regime.[14] The degree of organic polymerization is another factor that can be optimized to control material properties.

In another example poly(methyl methacrylate) (PMMA) was synthesized in situ with TiO_2 obtained from titanium butoxide. Concentrations of TiO_2 ranging from 6.4 to 53.6 % by weight were included in PMMA and resulted in significantly greater thermal stability than observed for pure PMMA.[17] Another study shows that the ionic and conductive properties of a polyethylene oxide (PEO)-based polymer can be combined with the stability and network-forming capabilities of a titanium sol-gel to create coatings suitable for electrochemical devices.[18]

The examples above describe just a few of the numerous possibilities for sol-gel systems. The next section describes how sol-gel chemistry is applied in this study to prevent the nucleation and adhesion of ice.

1.5 Sol-Gel Chemistry Applied to Prevent the Nucleation and Adhesion of Ice

In all of the examples above, sol-gel chemistry was applied to create an inorganic network. The coating in this work applied sol-gel chemistry to facilitate the slow release of melt-point depressants, specifically tripropylene glycol (TPG) and glycerol to the coating surface. While an inorganic network is formed, it is not the desired product in this application.

Precursor substitution reactions, such as those shown in figure 1-6, are utilized to limit hydrolysis kinetics. For this application, precursor substitution was not performed for the specific purpose of controlling hydrolysis, but to attach the melt-point depressants, TPG and glycerol. The alkoxide precursor used in this reaction is titanium isopropoxide (TIP), which is reacted with a 3:1 stoichiometric ratio of TPG to glycerol. This ratio was chosen by trial and error; product testing indicates this ratio yielded the best performance. Further explanation for this is provided in subsequent chapters.

The reaction of TIP with a 3:1 stoichiometric ratio of TPG to glycerol is shown in figure 1-13. The product of subsequent hydrolysis and condensation

reactions is shown in figure 1-14. In this study the term 'melt-point depressant' is used to describe the entire sol-gel system.

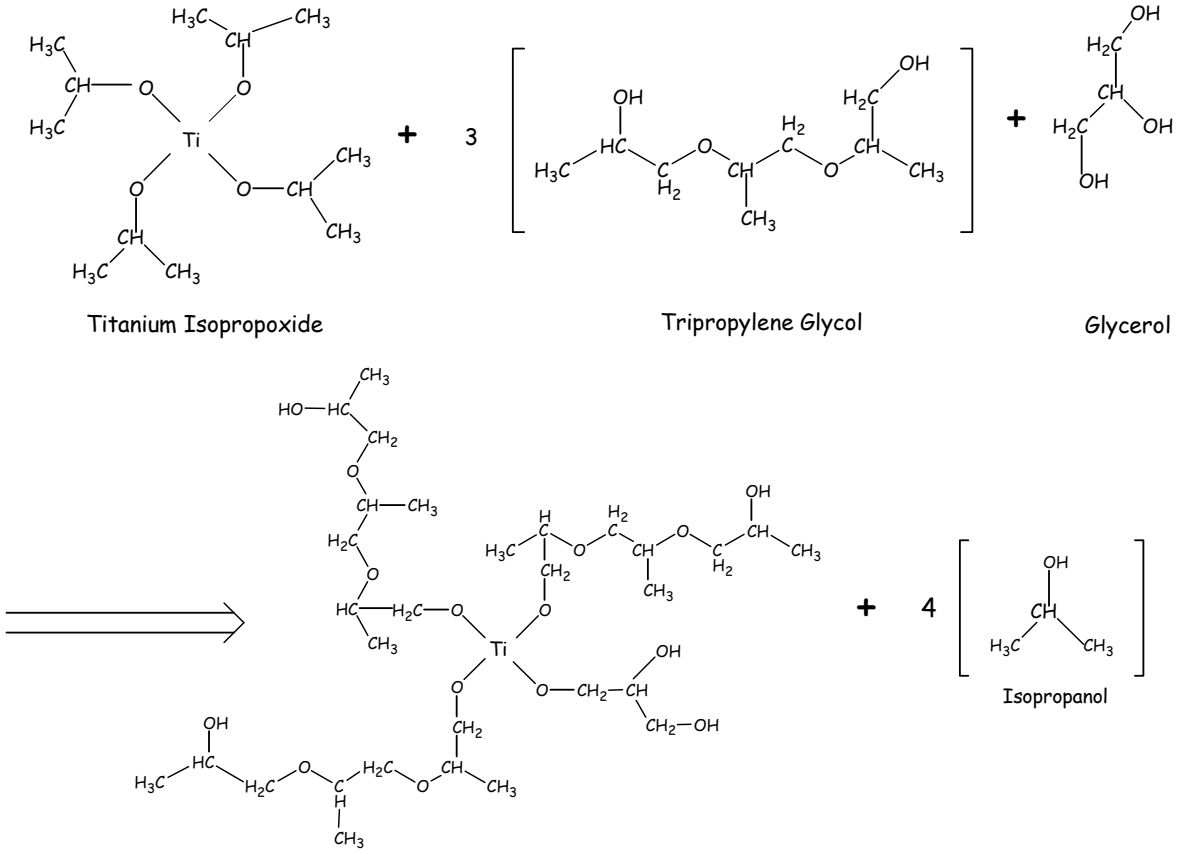

Figure 1-13: Reaction of TIP with TPG and glycerol

Sol-gel condensation reactions were used to facilitate the slow release of TPG and glycerol to the coating surface. This slow-release is crucial to the long term ability of the coating to prevent the adhesion and nucleation of ice. After mixing, the components of the melt-point depressant were added to the coating matrix. The matrix consists of epoxy and PDES crosslinked with silicone. The sol-gel system and coating matrix polymer form an interpenetrating polymer

network.

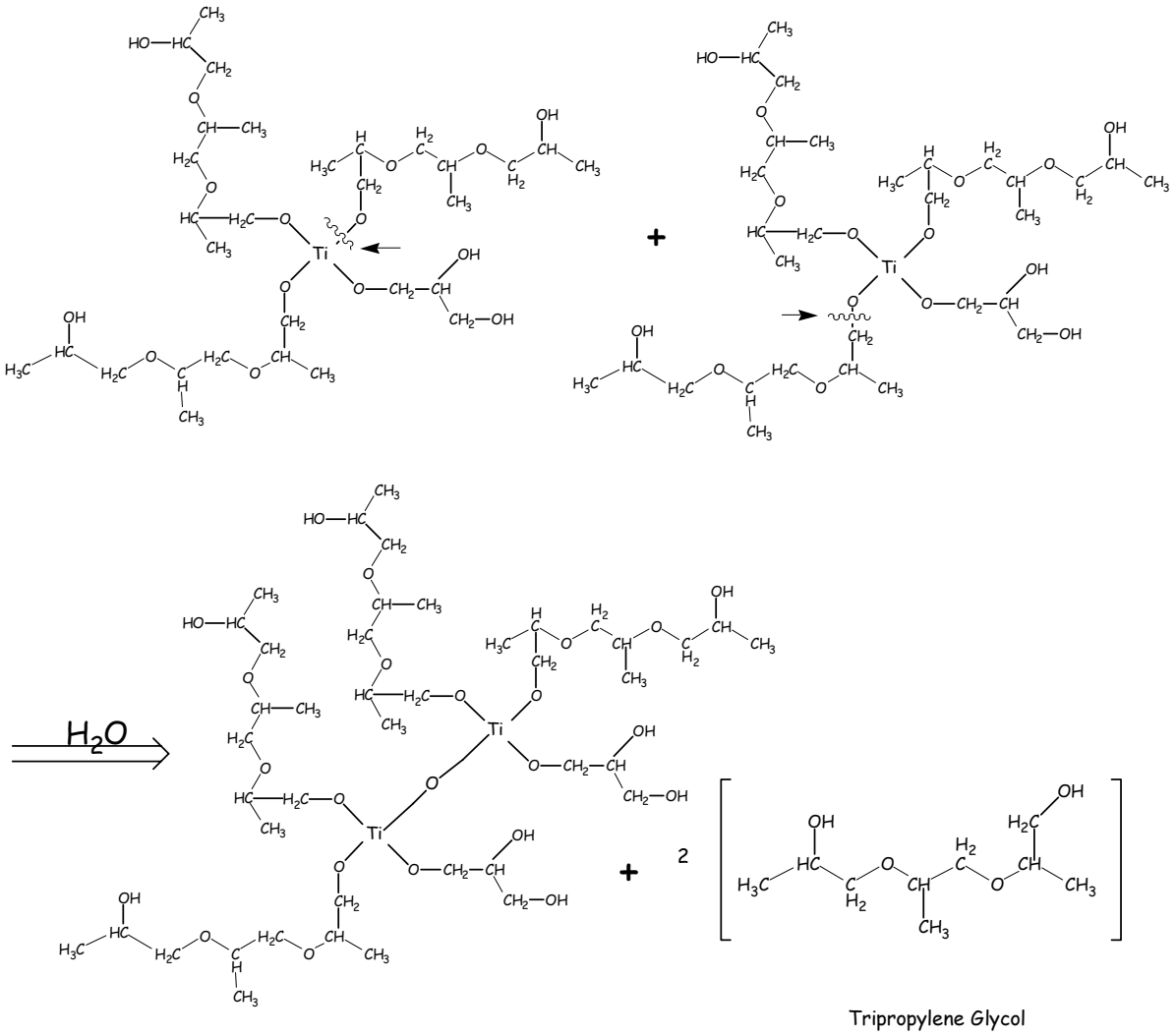

Figure 1-14: Condensation reaction resulting in the slow release of TPG and glycerol to the coating surface

1.6 Objectives

This coating was originally developed by Microphase Coatings, Inc. The objectives of this study included verification of the coating design and the presence of sub-micron sized phase domains of the hydrophobic matrix and

melt-point depressant. Because the slow release of TPG and glycerol is crucial to both the coating's performance and lifetime, the remainder of the study focuses on the kinetics of this process through mass-loss measurements in both the coating and the isolated sol-gel system. The chemistry of the melt-point depressant complex was also studied in order to determine its effect on mass loss kinetics.

2. Experimental

The techniques used in this work are briefly described below.

Contact Angle Goniometry

Contact angle measurements were made using a Rame-Hart Goniometer, Model 100-100. A 6 µL drop of water was brought into contact with a level coating surface, and an image was captured with the attached optical camera. Contact angle was measured on each side of the drop.

Scanning Electron Microscopy (SEM)

SEM imaging was performed using an Hitachi S-3200N Environmental SEM with an secondary electron detector. Measurements were made at 5-10 kV. The low concentration of carbon black in the coating was sufficient to allow imaging without charging.

Energy Dispersive Spectroscopy (EDS)

EDS measurements were made using an x-ray detector attached to the SEM. X-ray maps and secondary electron images were taken simultaneously.

Atomic Force Microscopy (AFM)

AFM images were performed using a Dimension 3000 Scanning Probe Microscope in tapping mode. Both topographical and phase images were collected.

Fourier-Transform Infrared Spectroscopy (FT-IR)

FT-IR measurements were performed using a Nicolet Nexus 470 Fourier Transform Infrared Spectrometer. Liquid samples were placed on AgCl salt plates and analyzed using transmission FT-IR. Solid samples were analyzed with attenuated reflectance spectroscopy (ATR), using the OMNI Sampler^{TM} accessory. Samples were placed on a rounded Ge crystal and analyzed via single bounce attenuated total reflectance.

Nuclear Magnetic Resonance (NMR)

^{1}H and ^{13}C NMR measurements were made using a 500 MHz Bruker Spectrometer. All samples were dissolved in deuterated dimethyl sulfoxide (DMSO) with the exception of titanium isopropoxide, which was dissolved in deuterated toluene.

Thermogravimetric Analysis (TGA)

TGA analysis was performed using a Perkin Elmer Pyris 1

Thermogravimetric Analyzer. Samples were heated from room temperature to 400°C at a constant rate of 20°C/minute.

Mass Loss Measurements

Mass loss measurements were performed by weighing samples maintained at a constant temperature as a function of time. Data was then fit to a diffusion model using the hybrid one-term method[19] in order to determine diffusion coefficients.

Materials

All coating samples were prepared by Microphase Coatings, Inc. Details of coating preparation are included in U.S. Patent # 6,702,953.

The 'melt-point depressant' was synthesized from titanium isopropoxide (TIP), tripropylene glycol (TPG) and glycerol also obtained from Microphase Coatings, Inc. Unless another preparation method is described, synthesis occurred under ambient conditions. 23.32 grams TPG (0.04 mol) and 3.72 grams (0.12 mol) glycerol were mixed using a high speed mixer. 8.0 grams (0.03 mol) TIP was then added dropwise while mixing. The reaction schemes presented all require

a 3:1:1 stoichiometric ratio of TPG:glycerol:TIP. Because the reactions were not performed in solvent, both TPG and glycerol were added in slight excess so that a manageable viscosity was maintained during mixing.

3. Coating Morphology, Performance and Practice

As described in the introduction, this coating was designed to prevent the nucleation and adhesion of ice. The design consisted of heterogeneous, sub-micron sized phase domains incorporating a multi-component melt-point depressant into a hydrophobic polymer matrix as shown in figure 1-1. The hydrophobic matrix limits the contact area between the surface and a water droplet while the slow-release melt-point depressant forms a thin layer on the surface and prevents ice formation.

3.1 Contact Angle

The hydrophobicity of the matrix was achieved through the addition of Poly(diethoxysiloxane), which has documented hydrophobic properties, and was characterized using contact angle goniometry. This technique measures the angle between the surface and the water droplet as shown in figure 3-1.

A contact angle between a surface and a liquid droplet is determined by the thermodynamic balance of three interfacial free energies, γ_{SV}, γ_{LV} and γ_{SL} corresponding to the solid-vapor, liquid-vapor and solid-liquid interfaces. A water droplet on a hydrophobic surface produces a large $\gamma_{SL.}$ Consequently, the

interfacial area is minimized resulting in a large contact angle as shown in figure 3-1-A. Conversely, a water droplet on a hydrophilic surface has a much lower $\gamma_{sL,}$ and wets the surface resulting in a smaller contact angle as shown in figure 3-1-B.

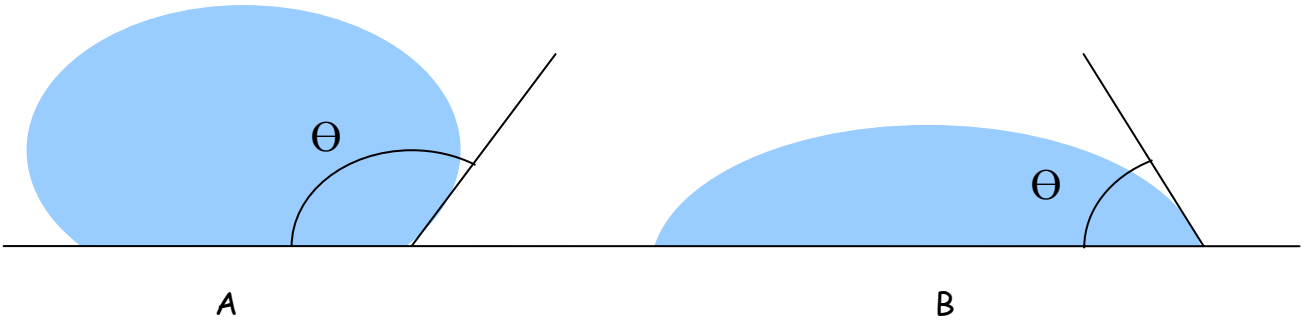

Figure 3-1: Schematic of contact angle for hydrophobic (A) and hydrophilic (B) surfaces

Advancing contact angle measurements were made by bringing a 6 µL drop of water in contact with the surface of the polymer matrix. Measurements were made for five areas on each of three samples which exhibited an average contact angle of 99.9 +/- 6.7 degrees and verified the hydrophobic nature of the coating matrix.

Table 3-1: Contact Angle Measurements for Polymeric Coating Matrix

Sample 1			Sample 2			Sample 3		
Left	**Right**	**Average**	**Left**	**Right**	**Average**	**Left**	**Right**	**Average**
94.1	83.4	88.8	97.2	98.2	97.7	106.8	95.5	101.1
101.5	99.7	97.9	85.8	92.8	89.3	104.6	105.1	104.8
113.1	108.1	110.6	108.4	105.4	106.9	101.7	106.3	104
105.1	102.3	99.5	95.0	91.7	93.3	94.8	102	98.4
108.4	113.4	110.9	98.8	98.7	98.8	97.7	96	96.9
Average		**101.5**	**Average**		**97.2**	**Average**		**101.0**
					Average Over Three Samples	**99.9 +/- 6.7 degrees**		

3.2 Coating Morphology

Scanning Electron Microscopy (SEM), Energy Dispersive Spectroscopy (EDS) and Atomic Force Microscopy (AFM) techniques were used to analyze the coating morphology and verify the presence of sub-micron sized phase domains.

Figure 3-2-A shows a strong silicon K_α peak detected wit EDS. The x-ray map in figure 3-2-B indicates where this signal was detected and corresponds to the SEM image of the coating shown in figure 3-2-C. The coating appears as a relatively flat surface with uniformly distributed pores. These pores are most likely formed as isopropyl alcohol is released during the alcohol exchange reactions involving TPG and glycerol. The x-ray map indicates a uniform distribution of PDES within the coating, even in porous regions.

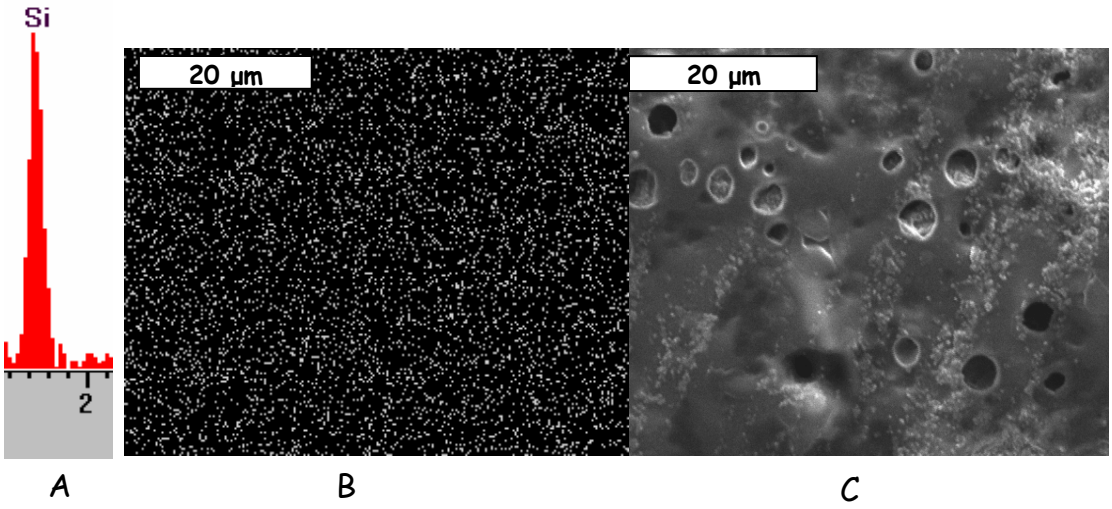

Figure 3-2: (A) Silicon peak in EDS Spectrum (B) x-ray map of silicon corresponding to (C) scanning electron microscopy image of coating

Figures 3-3 and 3-4 show AFM images of much smaller regions of the sample, 5 µm and 1 µm, respectively. In both figures, part (A) is a relatively flat topographical image with root mean squared (rms) roughness values in the nanometer range. Part (B) is a phase image of the area shown in part (A). Phase images reflect differences in mechanical properties across a surface and are constructed by mapping the phase shift in the probe oscillation which occurs after contact with the surface. Softer, more viscoelastic regions of the coating produce a phase lag in the tip oscillation, producing a greater phase shift. The phase images in figures 3-3 and 3-4 show significant compositional differences within relatively flat areas, supporting the belief that the melt-point depressant and the polymer matrix form sub-micron sized phase domains.

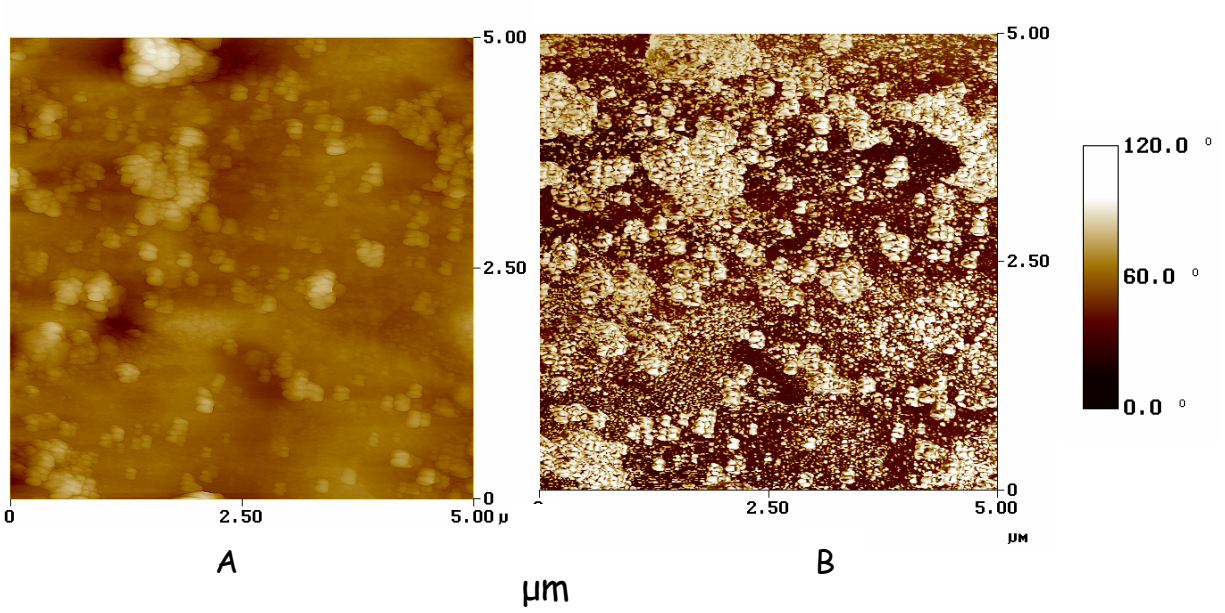

Figure 3-3: (A) Topographical AFM image of coating, 5 μm^2; Z range = 375 nm; roughness (rms) = 32 nm (B) AFM phase image

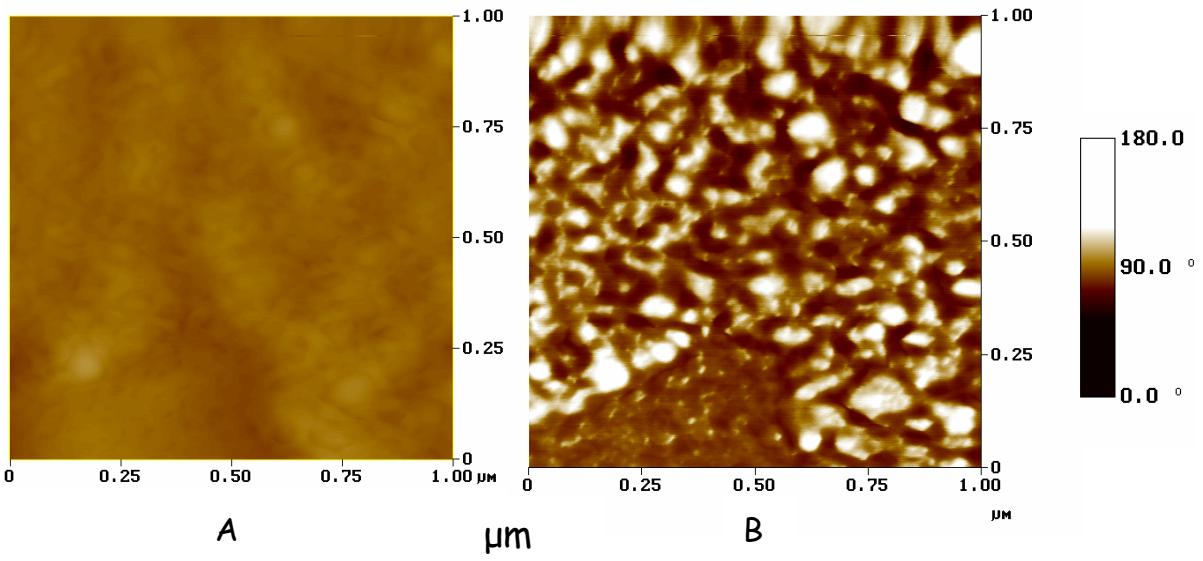

Figure 3-4: (A) Topographical AFM image of coating, 1 μm^2; Z range = 15 nm; roughness (rms) = 1.5 nm (B) AFM phase image

3.3 Release of Tripropylene Glycol and Glycerol

The coating design relied on the presence of sub-micron sized phase domains of melt-point depressant as shown above. The 'melt-point depressant' added to the coating was designed to undergo condensation reactions as shown in figure 1-14, resulting in the slow release of tripropylene glycol (TPG) and glycerol to the coating surface. The chemistry of the melt-point depressant is discussed in more detail in subsequent chapters.

Both TPG and glycerol are water-soluble. Surface concentrations of these molecules are necessary for effective prevention of the nucleation and adhesion of ice; however, these concentrations are depleted upon exposure to water. Therefore, the release of TPG and glycerol to the surface is crucial to the coating lifetime. This process was studied using several different techniques.

Figure 3-5 shows data collected while the coating was immersed in water. The coating was removed from the water, patted dry and weighed at various time intervals. Mass loss is plotted as a function of $(\text{time})^{1/2}$. After the initial weight gain associated with water sorption, the mass decreases as TPG and glycerol leach out of the coating. After the experiment was complete, the samples were dried in a dessicator and weighed again indicating the samples

absorbed an average of 20% of their weight in water and exhibited an average mass loss of 21 weight %. Twenty-two percent of the coating mass consisted of TPG and glycerol prior to water immersion.

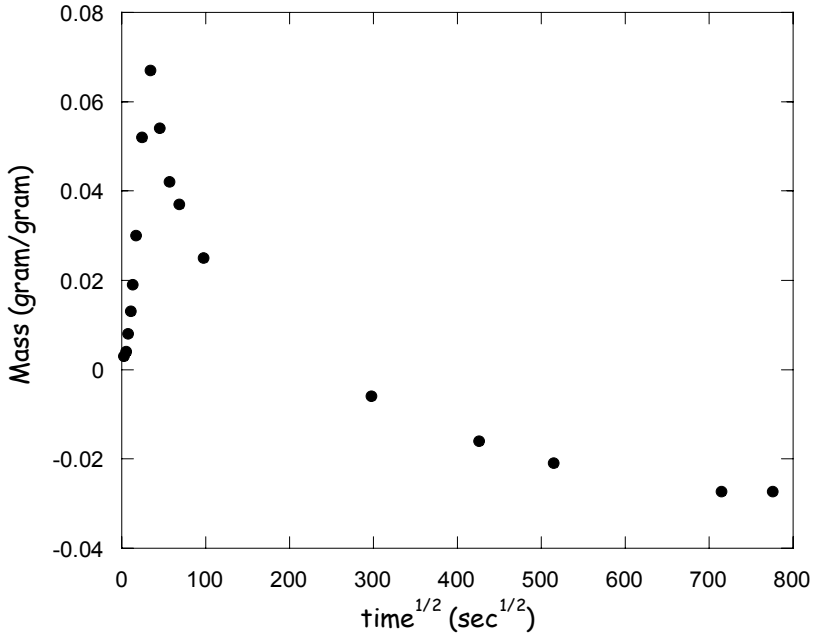

Figure 3-5: Mass loss measurements made during water immersion at 30°C; coating absorbed an average of 20 weight % water, lost an average of 21 weight % TPG and glycerol

Fourier Transform Infrared Spectroscopy (FT-IR) measurements verified that TPG and glycerol were responsible for the mass loss observed in the coating. After water immersion, the coating was removed and the water was evaporated

leaving behind the leachant which was analyzed using FT-IR. Spectra were also obtained for TPG and glycerol. Figure 3-6 shows the leachant spectrum compared to the spectrum of a 3:1 mixture of TPG and glycerol and confirms that TPG and glycerol leached out of the coating in the presence of water.

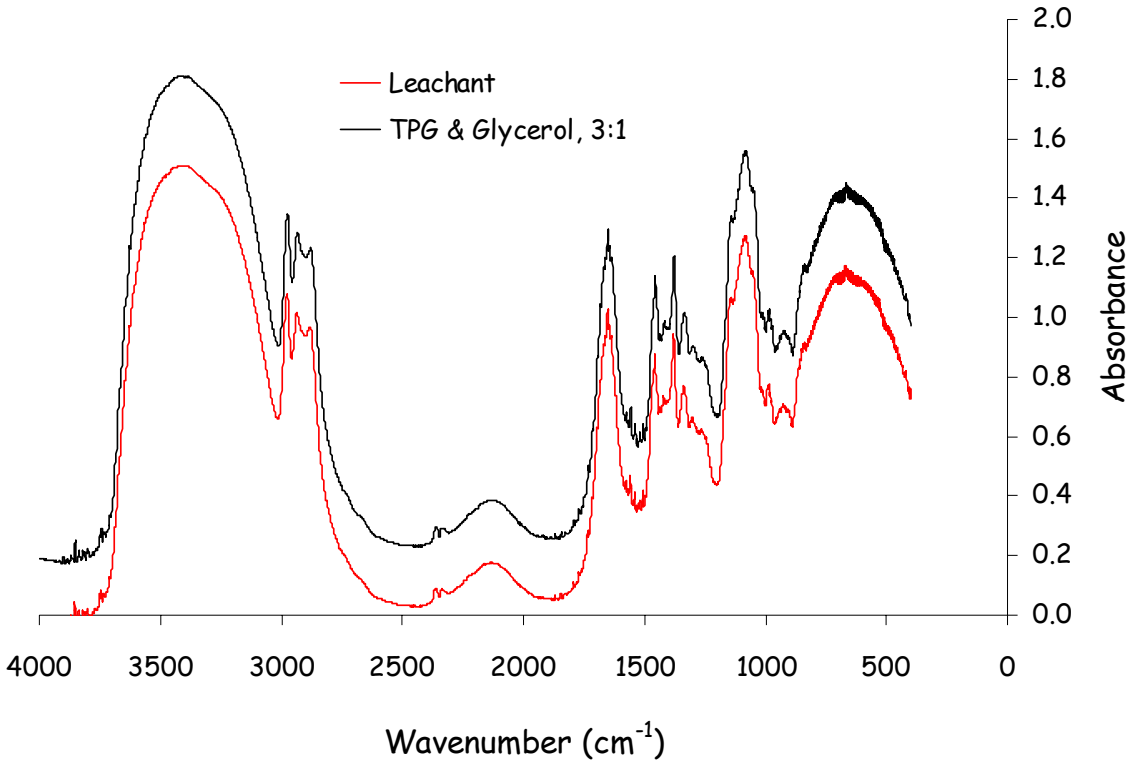

Figure 3-6: FT-IR spectrum of leachant obtained during water immersion

Optical microscopy confirmed that the condensation reaction shown in figure 1-14 also occurs in atmospheric conditions resulting in the slow release of TPG and glycerol to the surface. Figure 3-7 shows an image of the coating taken

after the surface had been wiped clean and an image of the same area taken 20 hours later showing small droplets of TPG and glycerol on the surface.

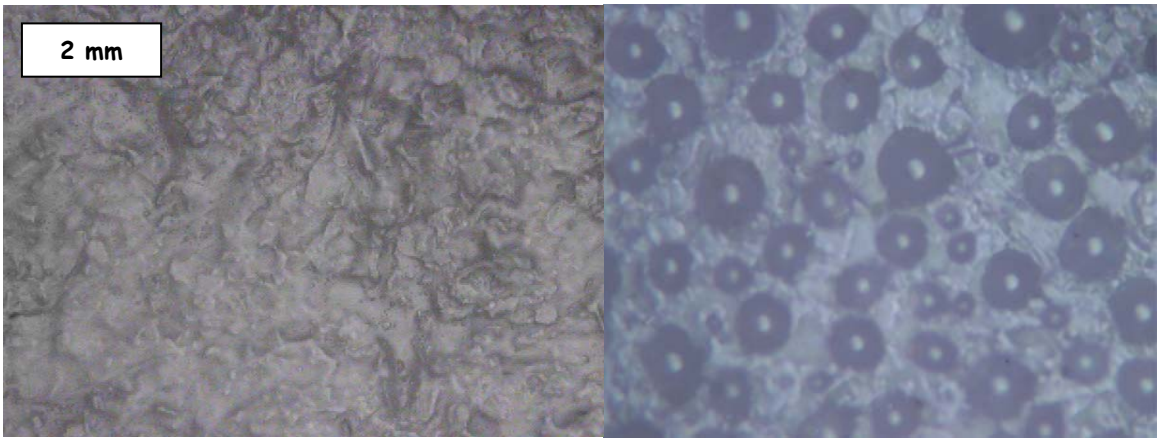

A B

Figure 3-7: Optical images of coating taken at room temperature (A) after the surface was wiped clean and (B) 20 hours later; small droplets of TPG and glycerol are visible on the coating surface

Subsequently, mass loss measurements were collected for the coating in atmospheric conditions. Figure 3-8 shows mass loss plotted as a function of $(\text{time})^{1/2}$ for a coating sample in an oven at 50°C and again indicates an ultimate mass loss of 21%. Despite the higher temperature, mass loss in atmospheric conditions took more than twice as long as that measured during water immersion. This is due to the fact that the sol-gel reaction requires water as indicated in figure 1-14. The sol-gel reaction is therefore dependent on the

amount of water available for reaction, which is obviously greater in the water immersion experiments.

Similar mass loss measurements are presented in later chapters for several different coating formulations at several different temperatures; these were used to estimate the length of time required to deplete concentrations of TPG and glycerol. While no direct correlations were made, this value was taken as an indication of the coating's expected performance lifetime.

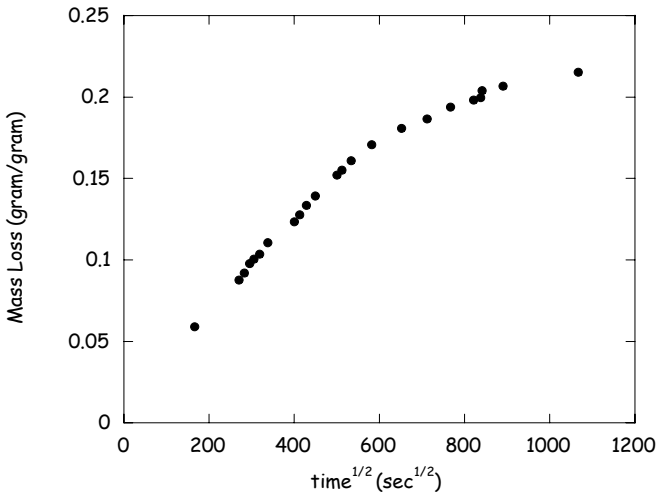

Figure 3-8: Mass loss measurements made in an oven at 50°C; coating lost approximately 21 weight % TPG and glycerol

3.4 Coating Morphology after Water Immersion

SEM and AFM measurements were conducted on coating samples after the loss of TPG and glycerol during water immersion to observe any effects this might have had on the coating morphology. Figure 3-9 shows SEM images taken (A) before and (B) after water immersion and indicates that the surface roughness increases significantly upon the loss of TPG and glycerol. However, AFM images presented in figure 3-10 indicate that sub-micron sized phase domains remain after water immersion despite the larger-scale surface roughness. While the distribution of these domains appears less uniform in the image taken after water immersion, figure 3-3 shows a non-uniform distribution of phase domains before water immersion. Because the images in figure 3-10 represent two different areas on the sample, no conclusions can be drawn about the effect of the sol-gel process on the regularity of the phase domains. The fact that phase domains remain after the loss of TPG and glycerol indicates that the entire melt-point depressant complex does not leave the coating as a result of the sol-gel reaction. These findings are explained in subsequent chapters.

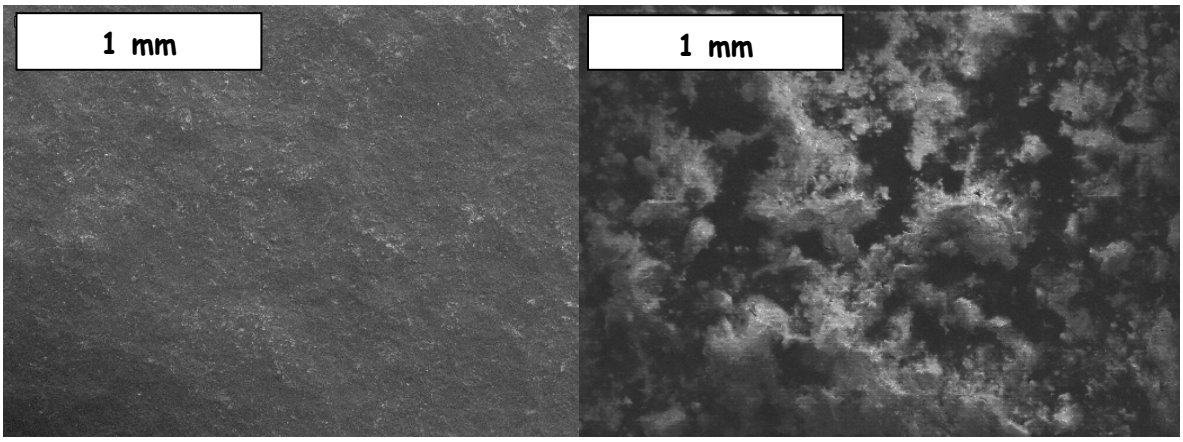

Figure 3-9: SEM images (A) before and (B) after water immersion indicate an increase in surface roughness with the loss of TPG and glycerol

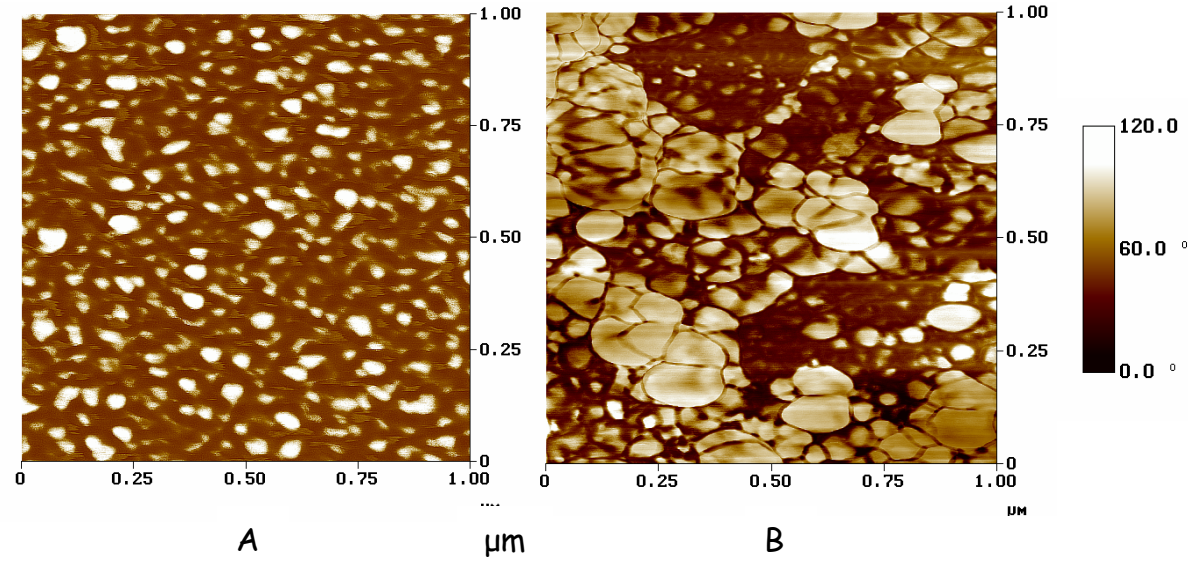

Figure 3-10: AFM images (A) before and (B) after water immersion indicate the presence of sub-micron sized phase domains

3.5 Coating Performance

The coating's ability to prevent the nucleation and adhesion of ice was tested in an icing wind tunnel. These tests were conducted by Microphase Coatings, Inc. Structures were built to emulate vortex generators and an airfoil on the B2 bomber, the aircraft for which the coating was initially designed. Air speed in the tunnel was 150 mph for all of the runs with humidity at 91.4%, a liquid water content of 0.76 g/m^3 and a mean droplet size of 18 μm.

Figure 3-11 shows a vortex generator after being in the icing wind tunnel for approximately 20 minutes at -2°C. The uncoated steel surface exhibited significant ice build-up at the leading edge and on the horizontal surfaces. The coated surface (orange) exhibits only a small amount of ice build up on the leading edge. However, this fell off at the conclusion of the run when the wind speed was reduced.

Figure 3-12 shows another vortex generator after being in the icing wind tunnel for only a few minutes at -9°C. Again, the coated surface exhibits negligible ice build up relative to the uncoated steel surface.

Figure 3-11: Vortex generator after being in the icing wind tunnel for approximately 20 minutes at -2°C; the coated surface (orange) exhibited negligible ice build-up relative to the uncoated steel surface

Figure 3-12: Vortex generator after being in the icing wind tunnel for only a few minutes at -9°C; the coated surface (orange) exhibited negligible ice build-up relative to the uncoated steel surface.

Figure 3-13 shows an airfoil after being in the icing wind tunnel for approximately 12 minutes at -15°C. While the image is less clear than those shown in figures 3-11 and 3-12, ice build-up on the coated surface (black) was much less than that observed on the uncoated steel surface. As the airfoil was rotated, ice adhered to the uncoated portion while the coated section shed most of its ice.

Figure 3-13: Airfoil after being in the icing wind tunnel for approximately 12 minutes at -15°C; the coated surface (black) exhibited negligible ice build-up relative to the uncoated steel surface.

3.6 Summary and Conclusions

The coating design, consisting of sub-micron sized phase domains of a hydrophobic matrix and a sol-gel melt-point depressant complex, was verified using contact angle goniometry, SEM, EDS and AFM techniques.

Mass loss measurements made on the coating both in water at 30°C and in an oven at 50°C, optical microscopy and FT-IR analysis confirmed the slow release of TPG and glycerol to the coating surface.

The combination of these properties proved effective in preventing the nucleation and adhesion of ice in icing wind tunnel tests.

4. Mass Loss Behavior of the Coating and the Melt-Point Depressant Complex

As described in earlier chapters, the coating incorporates sub-micron sized domains of melt-point depressant within a hydrophobic matrix in order to prevent the nucleation and adhesion of ice. The melt-point depressant complex was synthesized from tripropylene glycol (TPG) and glycerol to form the sol-gel complex shown in figure 1-13. This complex then undergoes a condensation reaction resulting in the slow release of TPG and glycerol to the coating surface. The presence of these molecules on the surface is necessary for effective prevention of the nucleation and adhesion of ice; however, their concentrations are depleted with time and exposure to water. The rate at which TPG and glycerol diffuse to the coating surface affects both the coating's performance and its lifetime. This chapter addresses kinetics of mass loss in a few different coating formulations and in the isolated melt-point depressant complex.

Mass loss in the coating is due to the loss of IPA, TPG and glycerol and is the result of two different processes. IPA is released through precursor substitution reactions involving titanium isopropoxide (TIP); TPG and glycerol are released through subsequent condensation reactions. Reaction kinetics

determine the rate at which these molecules are released from the sol-gel complex. Once mobile, these molecules diffuse through the coating to its surface. Mass loss kinetics are therefore dependent on the rates of both reaction and diffusion. In this study, diffusion was assumed to be the slower of these two processes and therefore rate-determining. Data presented in this chapter and the following chapter support this initial assumption .

4.1 Mass Loss in Coating

Mass loss in the coatings was assumed to be diffusion-limited. Therefore, attempts to control the mass loss kinetics consisted of choosing coating additives that would control the diffusion of TPG and glycerol out of the coating. While no direct correlation has been made between the rate of diffusion and coating performance or lifetime, slower diffusion is expected to increase the time that the coating is effective. However, diffusion should be fast enough that surface concentrations of TPG and glycerol are not depleted faster than they can be replaced.

Mass loss data is reported for two different coating formulations to determine additive effects on diffusion behavior. The additives for both formulations are

outlined in table 4-1. Both coating matrices contained both poly(diethoxysiloxane) (12.8%) for its hydrophobic properties and 3-glycidoxypropyltrimethoxysilane (8.7%), a crosslinked epoxy mixture included for physical hardness. Other details of the coatings are outlined in U.S. Patent # 6,702,953.

Table 4-1: Additives in Two Coating Formulations

Formulation	Melt-Point Depressant*	Additives
A	26 %	20 μm mica filler (25%)
B	36 %	8 μm hollow glass spheres (3.6%) polytetrafluroethylene (Teflon®) powder (7.3%) silicone reacted with hexadecane (2.7%)

* All percentages were calculated based on weight

The 20 μm mica flakes were included in formulation A to slow down the diffusion of TPG and glycerol. Figure 3-8 shows mass loss measured for formulation A due to the release of TPG and glycerol under atmospheric conditions at 50°C. The same experiment, measuring mass as a function of time, was performed at temperatures ranging from 30 to 90°C. The results are shown in figure 4-1. The coating exhibits typical Fickian diffusion; mass loss increases linearly as a function of $(\text{time})^{1/2}$ and then levels off as the concentrations of TPG and glycerol are depleted. Figure 4-1 also indicates

that diffusion rates increase drastically with temperature. At 40°C, mass loss levels out at approximately 4000 $sec^{1/2}$ (~26 weeks) while at 90°C, mass loss levels out at approximately 250 $sec^{1/2}$ (~17 hours). Measurements at 30°C may not have reached equilibrium.

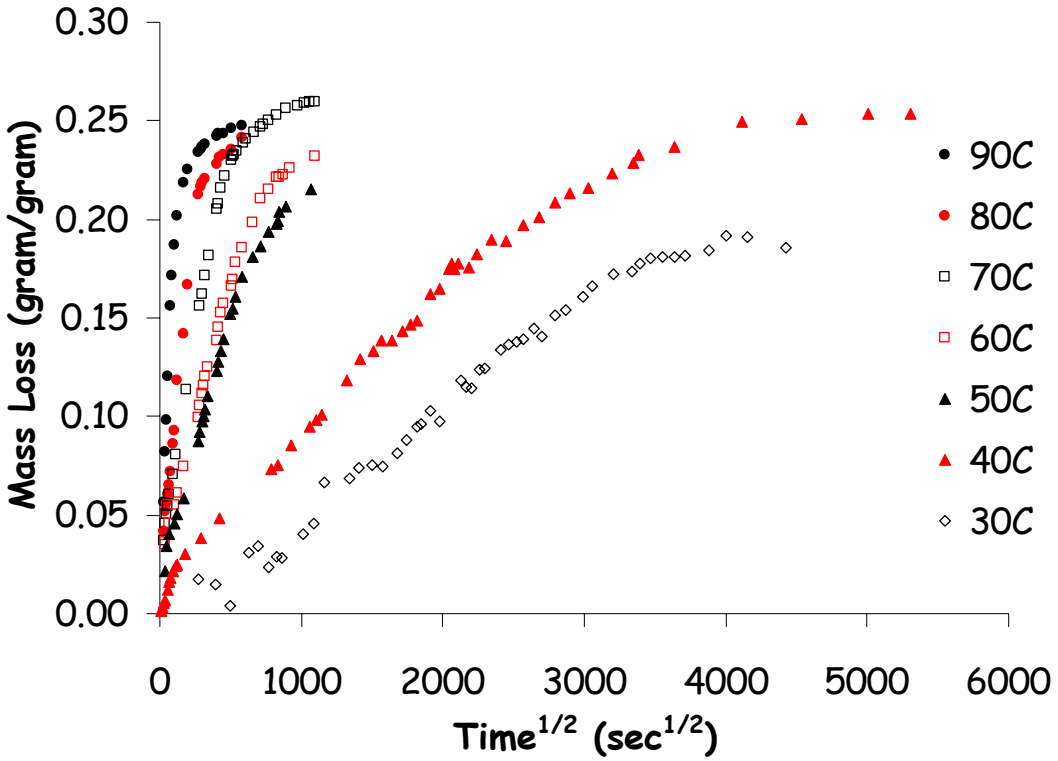

Figure 4-1: Mass loss behavior for coating formulation A

Figure 4-2 shows data taken for coating formulation B. Both the hollow glass spheres and polytetrafluorethylene (Teflon®) powder were added to limit the diffusion of TPG and glycerol.

While limiting diffusion of TPG and glycerol increases the coating lifetime, the release of these chemicals is essential for effective prevention of the nucleation and adhesion of ice. This coating formulation also contains low molecular-weight silicone pre-reacted with hexadecane. The silicone bonds to the siloxane in the matrix while hexadecane is incompatible with both TPG and glycerol and serves as a driving force for removal of these components from the coating.

Ideally, these variables would have been altered systematically in order to determine the combination of additives that maximizes both coating performance and lifetime. Due to time constraints, several factors were altered simultaneously. Changes applied to formulation B include additives designed to both inhibit and promote diffusion of TPG and glycerol. Data presented in this section only attempts to establish that coating additives can affect the mass loss kinetics. Again, figure 4-2 indicates Fickian diffusion with rates that drastically increase with temperature.

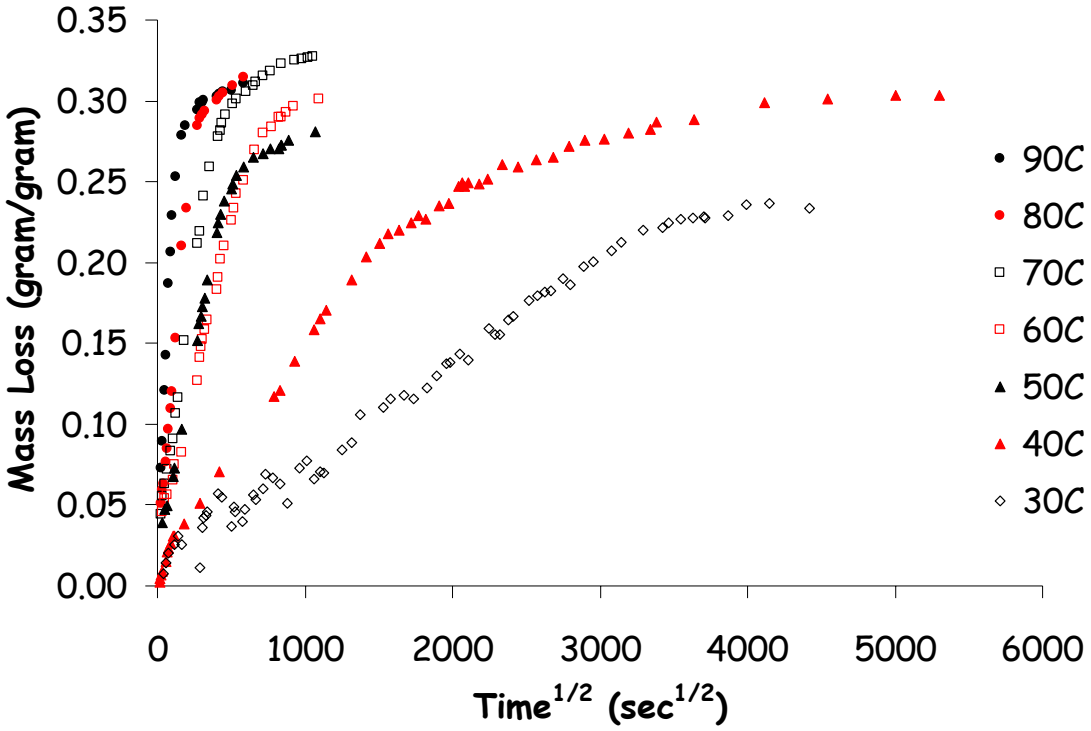

Figure 4-2: Mass loss behavior for coating formulation B

Mass loss kinetics were assumed to be diffusion-limited, and the data collected at each temperature was fit to a diffusion model to determine a diffusion coefficient. A typical example of a curve fit is shown in figure 4-3. This data was taken for formulation A at 90°C and yielded a diffusion coefficient of $8.91 * 10^{-9}$ cm^2/sec.

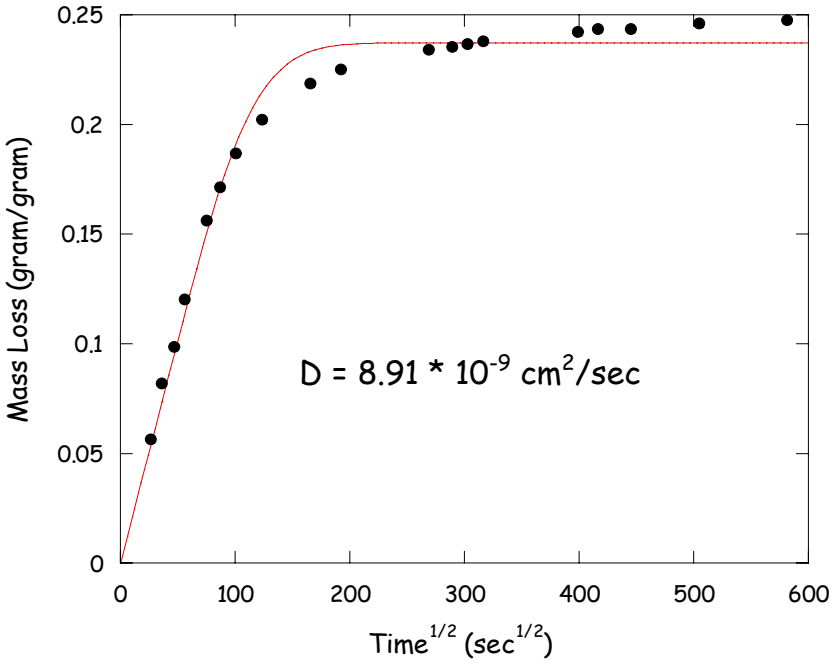

Figure 4-3: Diffusion model curve fit for mass loss data collected for formulation A at 90°C

Table 4-2 lists the diffusion coefficients for both coating formulations at temperatures between 30 and 90 °C and indicates that diffusion coefficients are greater for formulation B by approximately a factor of two.

Table 4-2: Diffusion Coefficients for Coating Formulations A and B

Temperature (°C)	Formulation A		Formulation B	
	10^{11} * D (cm^2/sec)	Mass Loss (gram/gram)	10^{11} * D (cm^2/sec)	Mass Loss (gram/gram)
30	1.93	0.21	3.29	0.25
40	22.9	0.22	44.5	0.28
50	28.4	0.21	58.6	0.27
60	71.4	0.24	129	0.30
70	304	0.26	692	0.30
80	441	0.24	833	0.31
90	891	0.24	2070	0.27

The temperature dependence of diffusion is described by the Arrhenius equation:

$$D = D_0 e^{\frac{-E}{RT}}$$

where D_0 is a pre-exponential factor and E is the activation energy for diffusion. This equation can be rearranged to:

$$\log(D) = \log(D_0) - \frac{E}{2.3 * RT}$$

so that a plot of log (D) vs. 1/T yields a straight line with a slope of $\frac{-E}{2.3 * R}$ and an intercept of $\log(D_0)$. A plot for both formulations is shown in figure 4-4. Activation energies of 21.3 and 22.4 kcal/mol were calculated respectively for coating formulations A and B.

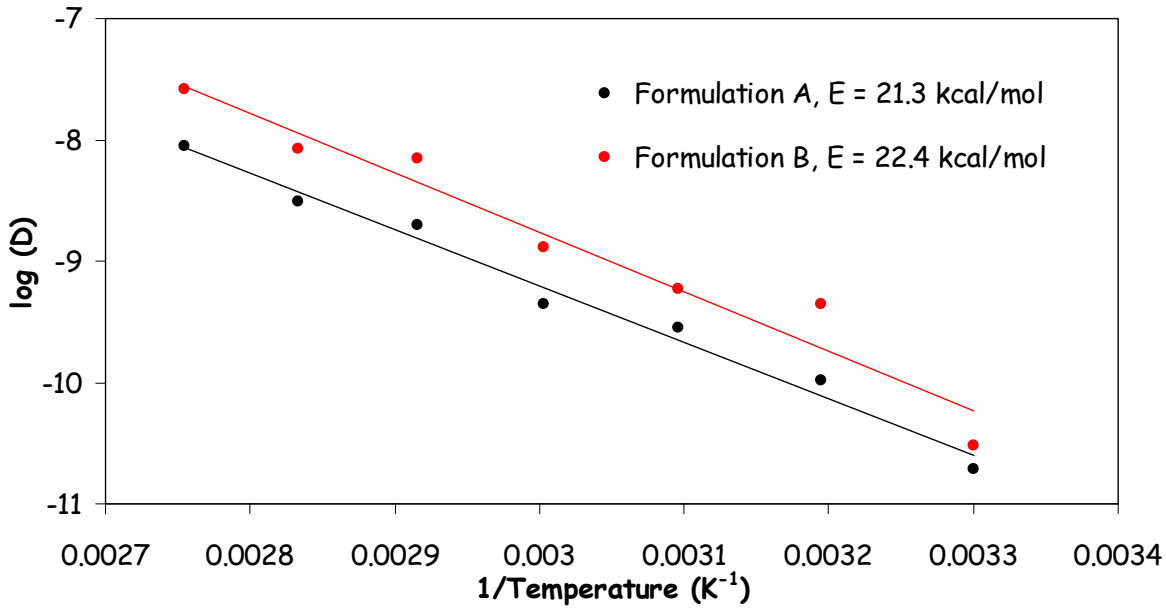

Figure 4-4: Arrhenius plots for coating formulations A and B

While the diffusion coefficients are greater for formulation B, minimal differences are observed in the activation energies for the two coatings. Formulation B exhibits only a slightly larger activation energy, and deviations from the curve fit create some uncertainty in these values.

While no conclusions were drawn regarding the effects of each individual additive, data indicate that the coating formulation can be altered to optimize the mass loss properties of the coating and consequently its performance and lifetime. Formulation B performed better during product testing.

4.2 Mass Loss in the Melt-Point Depressant

In order to better understand the mass loss kinetics in the coating, mass loss measurements were made on the neat melt-point depressant system immediately after mixing. Titanium isopropoxide (TIP) was added to a 3:1 stoichiometric mixture of TPG and glycerol. The heat generated upon the addition of TIP and the odor of isopropyl alcohol (IPA) indicated an immediate reaction occurred. After mixing at high speed for a minute, a measured volume of the reaction mixture was transferred to a Petri dish. The layer of viscous liquid was then treated as a thin film and mass loss measurements were performed in the same manner described for the coating formulations. Figure 4-5 shows mass loss data for the melt-point depressant collected at temperatures ranging from 22 to 90°C.

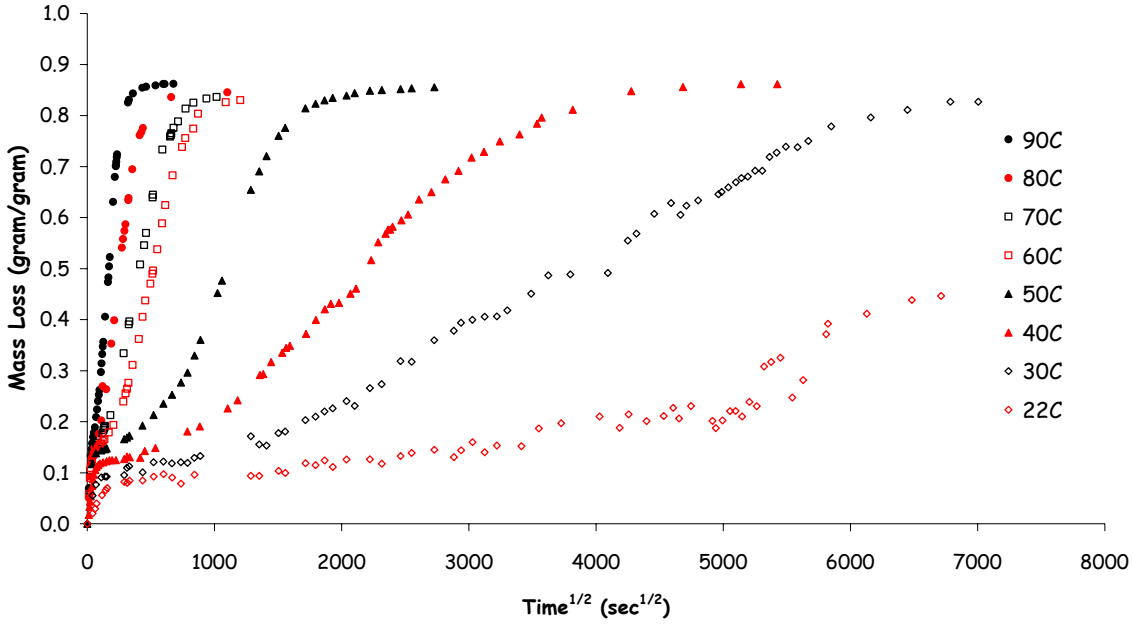

Figure 4-5: Mass loss behavior for the melt-point depressant

In contrast to the mass loss data collected for the full coating formulations, which was easily fit to a diffusion model, mass loss does not appear to exhibit simple Fickian diffusion. Mass loss increases sharply before leveling off between ten and fifteen percent and then increases again. This behavior was compared to a general model for mass loss in sol-gel systems. This model is shown in figure 4-6 and then applied to data obtained for the melt-depressant in figure 4-7.

Figure 4-6 correlates weight loss and volume loss for three different stages of the sol gel reaction, which occur with time or increasing temperature. Wright

and Sommerdijk attribute the first region of mass loss to the loss of alcohol.[11] In this case, isopropyl alcohol (IPA), formed during the reaction of TIP with TPG and glycerol, diffuses out of the gel. Minimal shrinkage is observed in this region, because IPA leaves from pores already present in the gel.

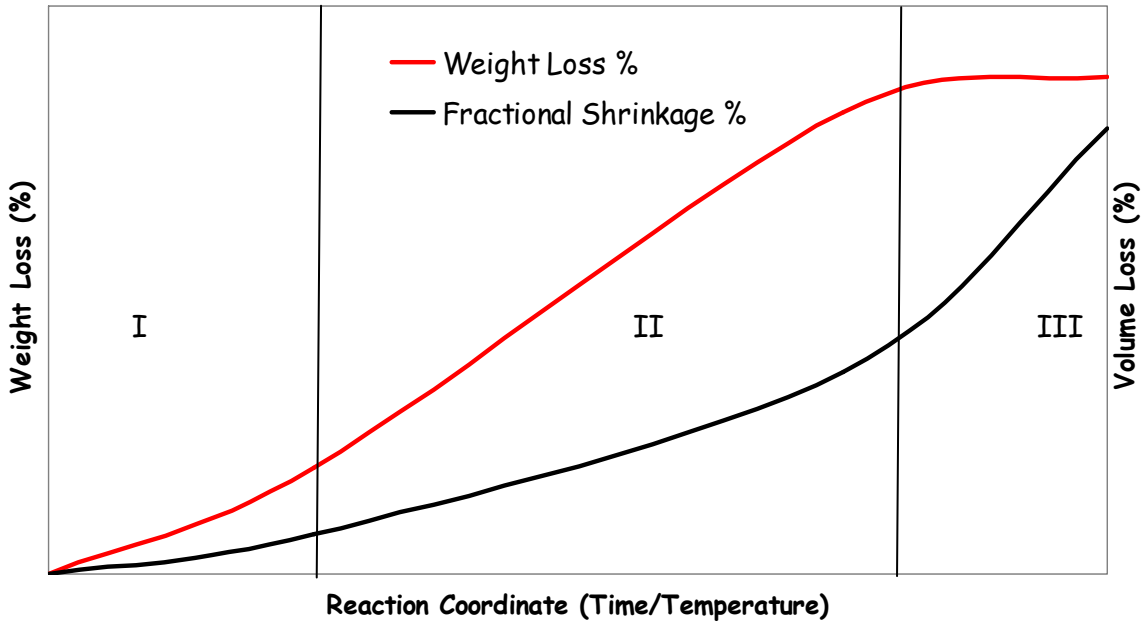

Figure 4-6: Three regions of mass loss in a sol-gel

The second region is attributed to the loss of organics, in particular TPG and glycerol released during condensation reactions. Both weight loss and shrinkage occur in this region. The gel cracks as Ti-O-Ti crosslinks are formed. The extent of cracking depends on the reaction rate, the thermal history and the pore density and size within the gel.

The third region is attributed to structural relaxation within the gel. Pores were formed during condensation reaction and the subsequent release of TPG and glycerol. The sol-gel rearranges to minimize its surface area (Ostwald ripening). As a result, shrinkage is observed with minimal weight loss. The mass loss that occurs in this region is attributed to the release of entrapped molecules with structural rearrangement.

Figure 4-7 shows mass loss data obtained for the melt-point depressant at 70°C. The letters along the curve correspond to images of the sample displayed in Figure 4-8.

Immediately after mixing, the components of the melt-point depressant produced a clear viscous liquid. 3 ml of the reaction mixture was coated on the bottom of a Petri dish as shown in figure 4-8a. The first region of mass loss is attributed to diffusion of IPA out of the gel following alcohol exchange. During this process, the viscosity of the liquid increased to a gel consistency. At this point, the sample contained regions of reacted precursor molecules. The anticipated composition of these molecules is shown in figure 1-13. The sample also contains regions of unreacted TIP and TPG and regions where Ti-O-Ti

crosslinks had formed as a result of condensation reactions. The many different phase regions within the gel scattered light and made the gel appear white and opaque as shown in figure 4-8b.

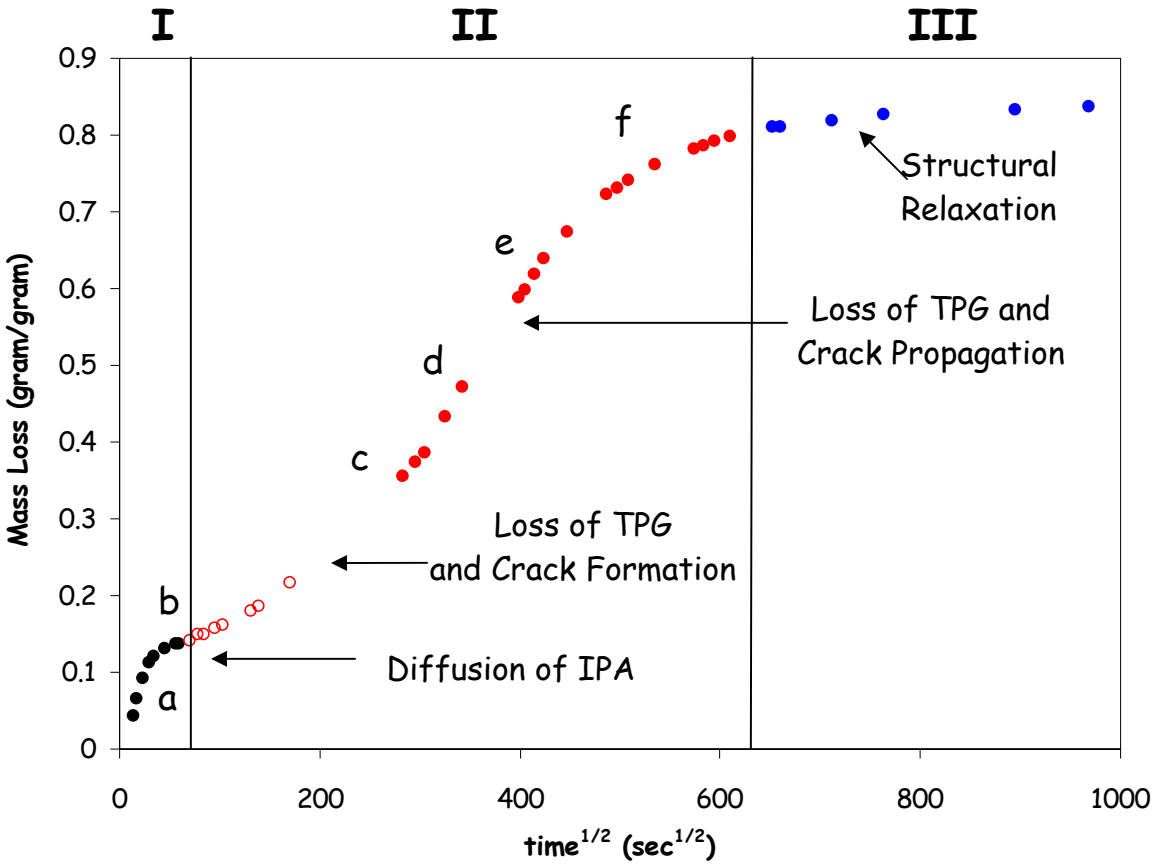

Figure 4-7: Three regions of mass loss observed for the melt-point depressant at 70°C

black data points indicate loss of IPA (region 1)
open **red** data points indicate slow loss of TPG before crack formation (region 2)
closed **red** data points indicate loss of TPG after crack formation (region 2)
blue data points indicate structural relaxation (region 3)

Mass loss continued as the condensation reactions proceeded, accompanied by the release of TPG and glycerol. Cracks formed as Ti-O-Ti crosslinks increased the density of the gel; this mechanism is represented in figure 1- 5. As cracks

formed (figure 4-8c), the rate of diffusion increased. This region is marked with solid red circles in figure 4-7.

As the crosslink density increased, the composition of the gel became more uniform, which was indicated by the increasingly transparent appearance of the gel. The third region of mass loss was associated with structural relaxation and exhibited minimal mass loss.

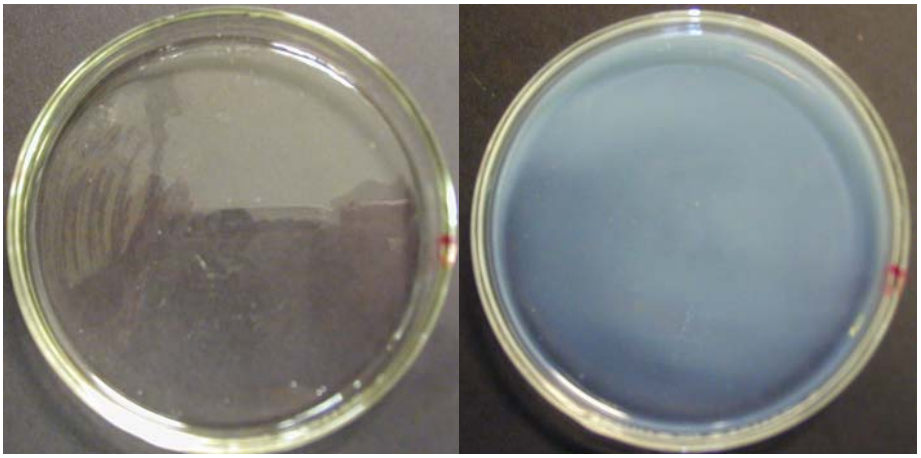

a (time = 0)

b (time = 35 minutes, 70°C)

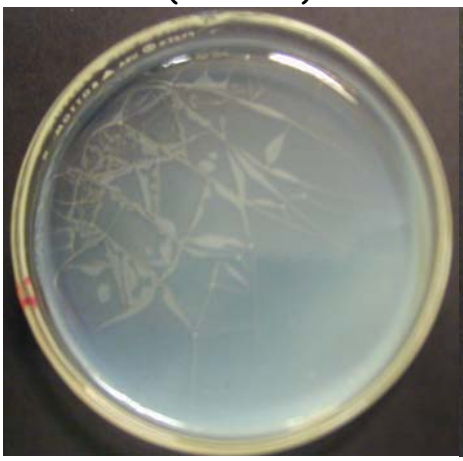

c (time = 22 hours, 70°C)

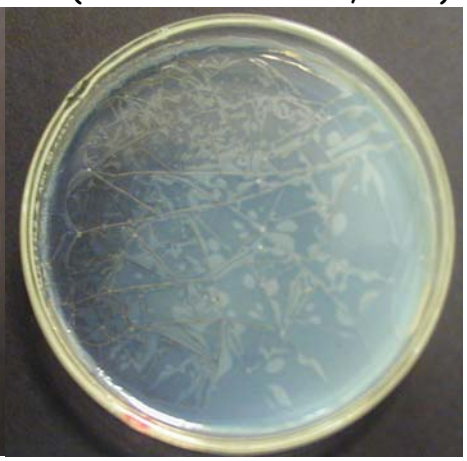

d (time = 29 hours, 70°C)

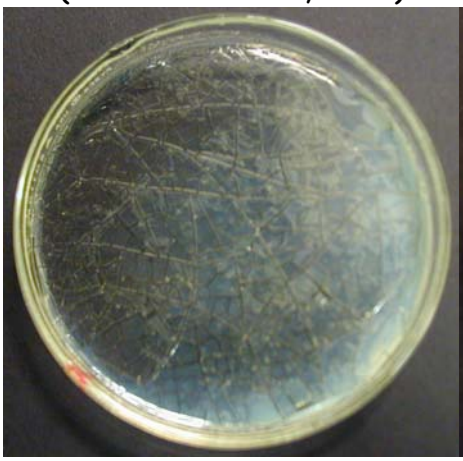

e (time = 2 days, 70°C)

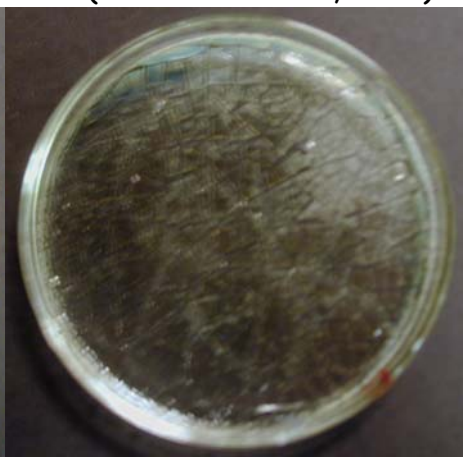

f (time = 3 days, 70°C)

Figure 4-8: Physical changes in the melt-point depressant during mass loss at 70°C

As described earlier, the nature of the cracks formed depends on the rate of reaction. Figure 4-9 shows mass loss data obtained for the melt-point depressant at 22°C. While the data did not reach equilibrium, the initial regions of mass loss are evident.

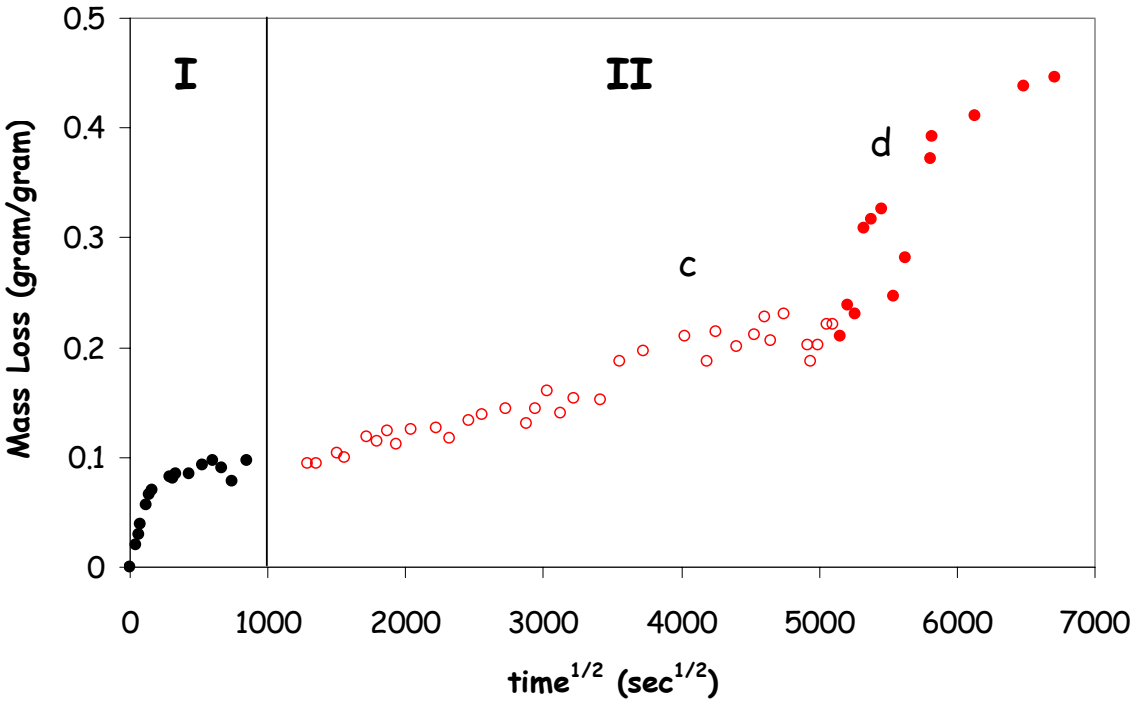

Figure 4-9: Three regions of mass loss observed for the melt-point depressant at 22°C

black data points indicate loss of IPA (region 1)
open **red** data points indicate slow loss of TPG before crack formation (region 2)
closed **red** data points indicate loss of TPG after crack formation (region 2)

Figure 4-10 shows images corresponding to points (c) and (d) on the mass loss curve. While mass loss occurs more slowly at 22°C than at 70°C, points (c) and (d) in figure 4-9 occur at similar points along the mass loss curve as the

corresponding points in figure 4-7. Figure 4-10c shows cracks, which have propagated in figure 4-10d. The cracks appear much larger than those observed at 70°C. The slower reaction rate at low temperatures allows for additional Ostwald ripening and structural rearrangement that minimizes the surface area of the gel. As described in the introduction, this process is favored thermodynamically, but limited by kinetics. In addition, the viscosity increase of the pore liquid with temperature is generally not proportional to the increase in reaction rate. This creates a build-up of pressure in the pores of the gel, which leads to additional cracking. Both of these phenomena describe the increased crack density at higher temperatures.

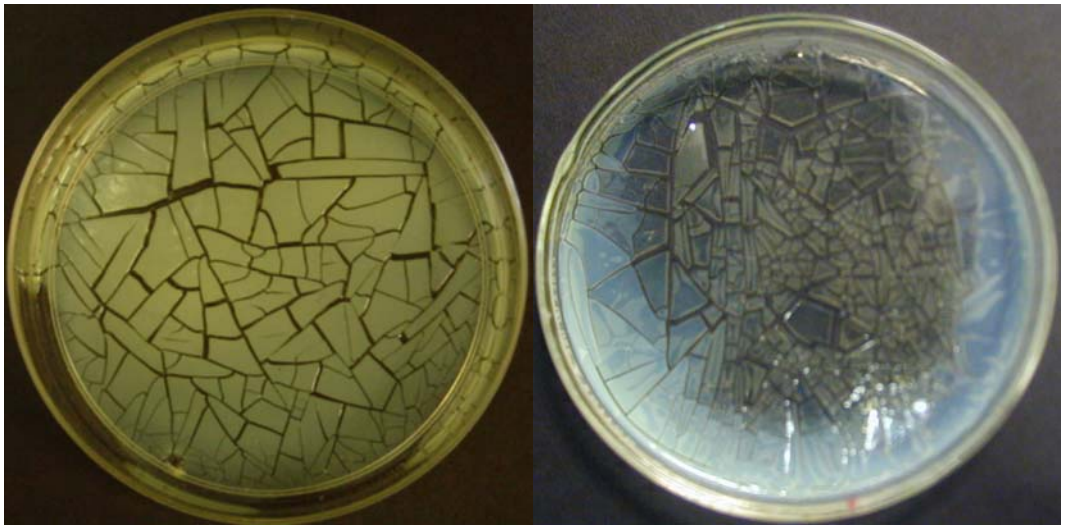

c (32 weeks, 22°C) d (49 weeks, 22°C)

Figure 4-10: Physical changes in melt-point depressant during mass loss at 22°C

The mass loss of the melt-point depressant was also analyzed using thermogravimetric analysis (TGA), a technique capable of separating mass loss due to IPA, TPG and glycerol. A TGA scan from 25 to 400°C is shown in figure 4-11. In contrast to the isothermal measurements which track mass loss, TGA scans track the mass remaining at each temperature during the scan. The second axis shows the derivative of mass loss, which indicates the rate of mass loss at each temperature. The first region is again attributed to the loss of IPA. The derivative plot supports this, showing a maximum rate of mass loss occurs at approximately 72°C, slightly below the boiling point for IPA (82°C). The second region of mass loss is due to the loss of TPG and glycerol released during condensation reactions. The derivative curve shows two peaks in this region at 200 and 245°C, respectively for TPG and glycerol. These regions of mass loss were identified by the size of each peak and their proximity to the boiling points for each species, 273 and 290°C, respectively for TPG and glycerol.

Mass loss levels off in the third region corresponding to structural relaxation as indicated in figure 4-6. The last region in the TGA spectrum indicates

decomposition of organics remaining within the gel after condensation is complete. This process is described in more detail in the next chapter.

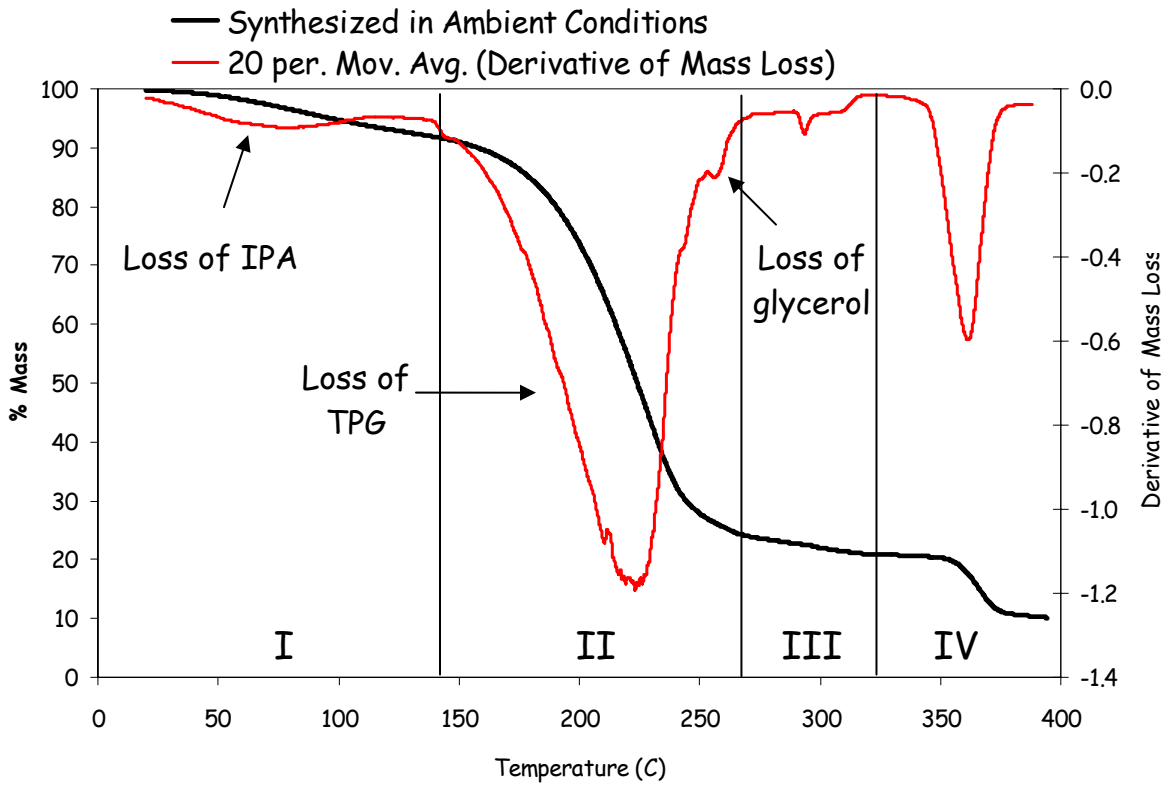

Figure 4-11: TGA scan of the melt-point depressant from 25 to 400°C
The notation, '20 per. Mov. Avg.' indicates the data has been smoothed.

4.3 Mass Loss Kinetics for the Melt-Point Depressant

The sol-gel process involves many different reactions that are dependent on several different factors, and consequently the kinetics are extremely difficult to describe. The first region of mass loss associated with the loss of IPA was assumed to be diffusion-limited and fit to a diffusion model. Figure 4-12 shows

an example curve fit for data in at 70°C and table 4-3 lists the diffusion coefficients measured in this first region of mass loss for samples between 22 and 90°.

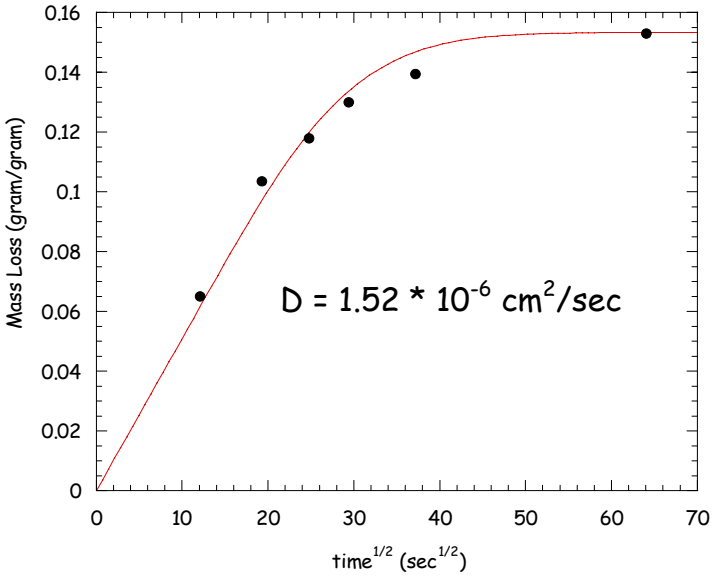

Figure 4-12: Curve fit for diffusion of IPA out of the melt-pointdepressant at 70°C

Table 4-3: Diffusion Coefficients for IPA out of the Melt-Point Depressant

Temperature (°C)	10^8 * D (cm^2/sec)	Mass Loss (gram/gram)
22	5.68	0.09
30	19.4	0.11
40	52.8	0.12
50	80.8	0.14
60	135	0.15
70	152	0.14
80	175	0.16
90	134	0.16

Figure 4-13 shows the logarithmic plot for mass loss in this region, which does not appear to exhibit Arrhenius behavior. The rate of mass loss increases with temperature up to approximately 50°C, then levels off. There are a few possible explanations for this behavior. The diffusion behavior may be different for the liquid and gas phases of IPA. It is also possible that kinetics are diffusion-limited at low temperature and reaction-limited at higher temperatures. An Arrhenius curve fit was applied to the data below 50°C and yielded an activation energy of 18 kcal/mol.

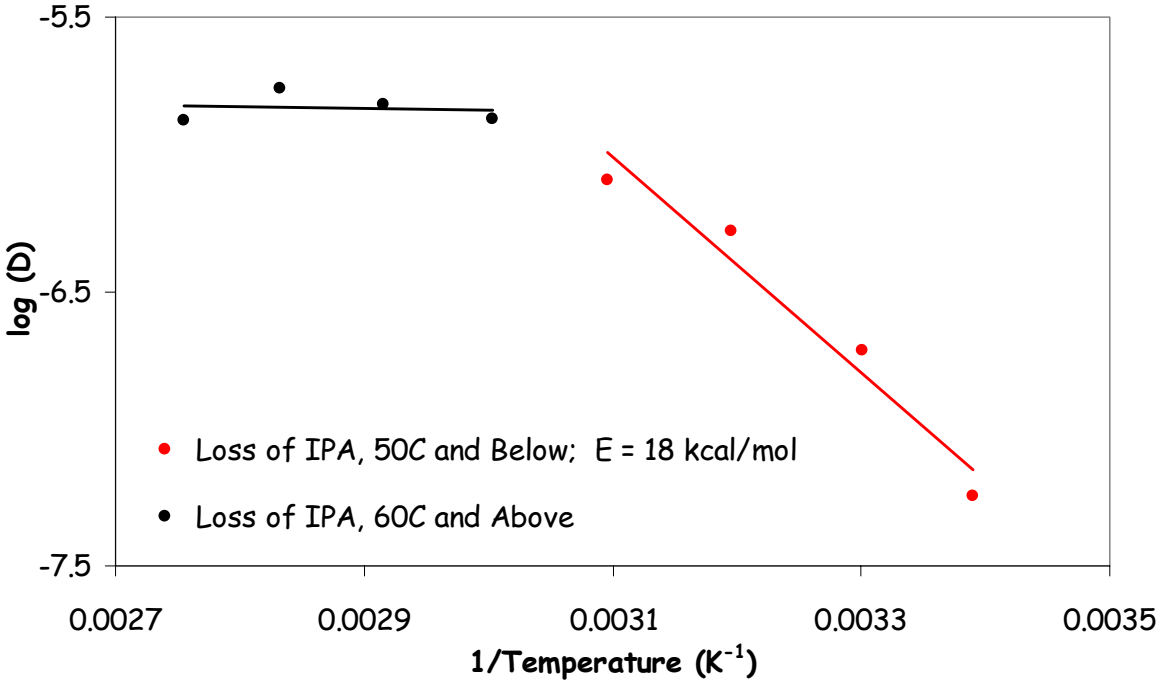

Figure 4-13: Arrhenius plot for diffusion of IPA out of the melt-point depressant

After diffusion of IPA out of the sample, there is a region of gradual mass loss marked with open circles in figure 4-7. In this region, condensation reactions slowly produce TPG and glycerol and mass loss kinetics were assumed to be reaction-limited. As the concentrations of free TPG and glycerol increase and cracks form in the sol-gel, the rate of mass loss increases.

The second part of region II, marked with closed red circles in figure 4-6, was attributed to the loss of TPG released through condensation reactions. Condensation rate constants for reactions involving transition metal oxides have not been reported in the literature, because reactions are rapid and difficult to measure.[20] Reaction rates on the order of 10^{-4} sec^{-1} have been reported for the condensation of TEOS in solution (figure 1-3).[20] Reactions involving similar compounds in which the reactants contain titanium instead of silicon are reported to be even faster.[20] The melt-point depressant complex was not synthesized in solution; the system transformed from a high viscosity liquid to a gel-like solid. Reaction rates for this system could therefore not be directly compared with TEOS rates measured in solution. However, based on a conservative estimate, reaction rates for the melt-point depressant were expected to be at least three orders of magnitude greater than the observed

rates of mass loss. It was therefore assumed that mass loss in this region is limited by diffusion rather than by chemical reaction and data was fit to a diffusion model. It is believed that TPG and glycerol released via condensation are entrapped by the sol-gel network as indicated in figure 1-10. Diffusion of TPG and glycerol from the network results in a slow release of these molecules to the coating surface. Figure 4-14 shows a typical curve fit for the 70°C data and table 4-4 lists the diffusion coefficients obtained for this region of mass loss at temperatures between 30 and 90°C.

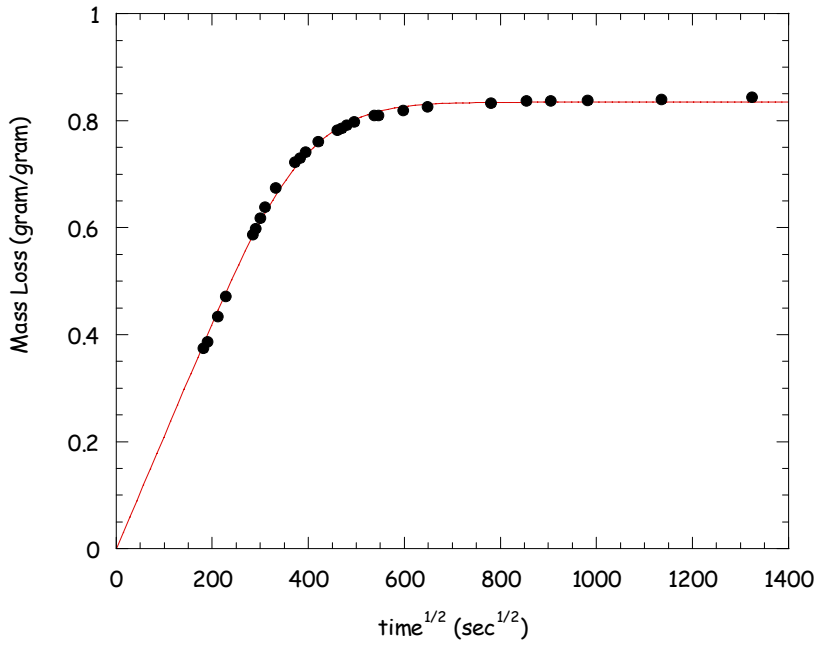

Figure 4-14: Curve fit for diffusion of TPG and glycerol out of melt-point depressant at 70°C

Table 4-4: Diffusion Coefficients for TPG and Glycerol out of the Melt-Point Depressant

Temperature (°C)	10^{11} * D (cm^2/sec)	Mass Loss (gram/gram)
30	5.50	0.91
40	15.5	0.90
50	133	0.86
60	287	0.91
70	504	0.86
80	1780	0.88
90	6520	0.83

The logarithmic plot in figure 4-15 indicates Arrhenius behavior for mass loss in this region with an activation energy of 25.1 kcal/mol. Both the diffusion coefficients and the activation energy for this process are greater than those observed for IPA. This is expected, because TPG and glycerol are larger molecules and the presence of Ti-O-Ti crosslinks inhibits diffusion in this region.

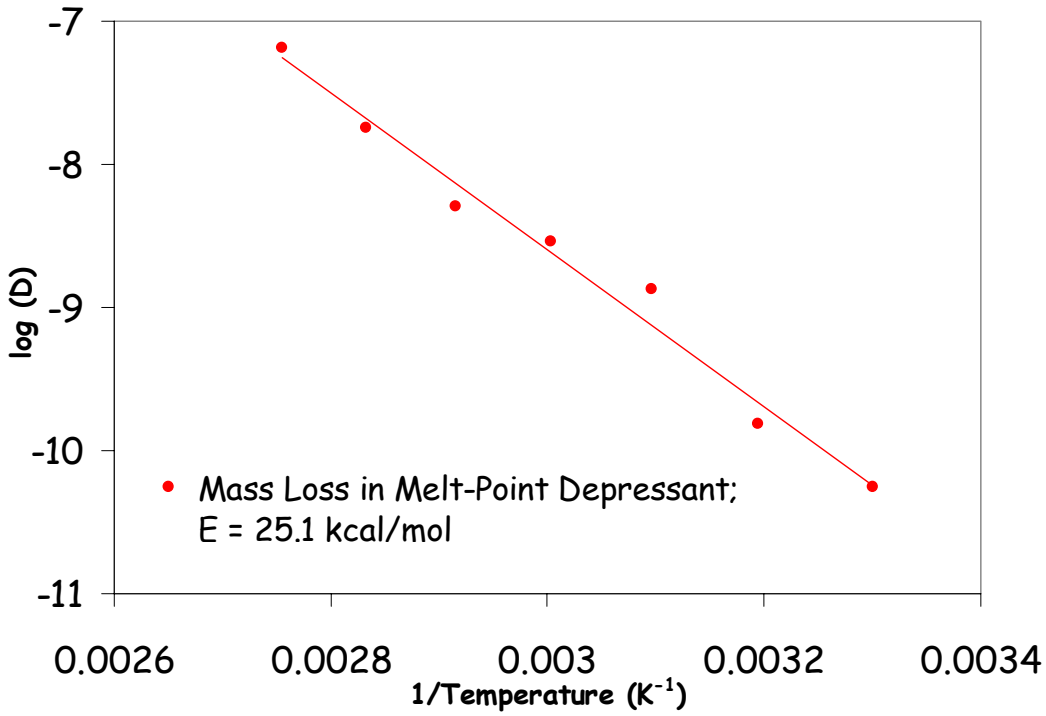

Figure 4-15: Arrhenius plot for diffusion of TPG and glycerol out of the melt-point depressant

As mentioned above, the third region of mass loss associated with structural relaxation and exhibits minimal mass loss. It was, therefore, not analyzed for this system.

4.4 Coating Formulations Compared to the Melt-Point Depressant

Figure 4-16 compares the Arrhenius curve fits for both coating formulations with the second region of mass loss in the melt-point depressant. Because the majority of mass loss occurred in this region, it was determined to be most

significant to the mass loss properties of the sol-gel system. At low temperatures, the diffusion coefficient for the melt-point depressant is comparable to that obtained for the coatings. However, the melt-point depressant exhibits faster diffusion at higher temperatures and a slightly greater activation energy. This is attributed to the large degree of cracking in the isolated melt-point depressant at higher temperatures which adds additional surface area. The coating matrix inhibits cracking, resulting in a less dramatic increase in the diffusion behavior with temperature for the coatings.

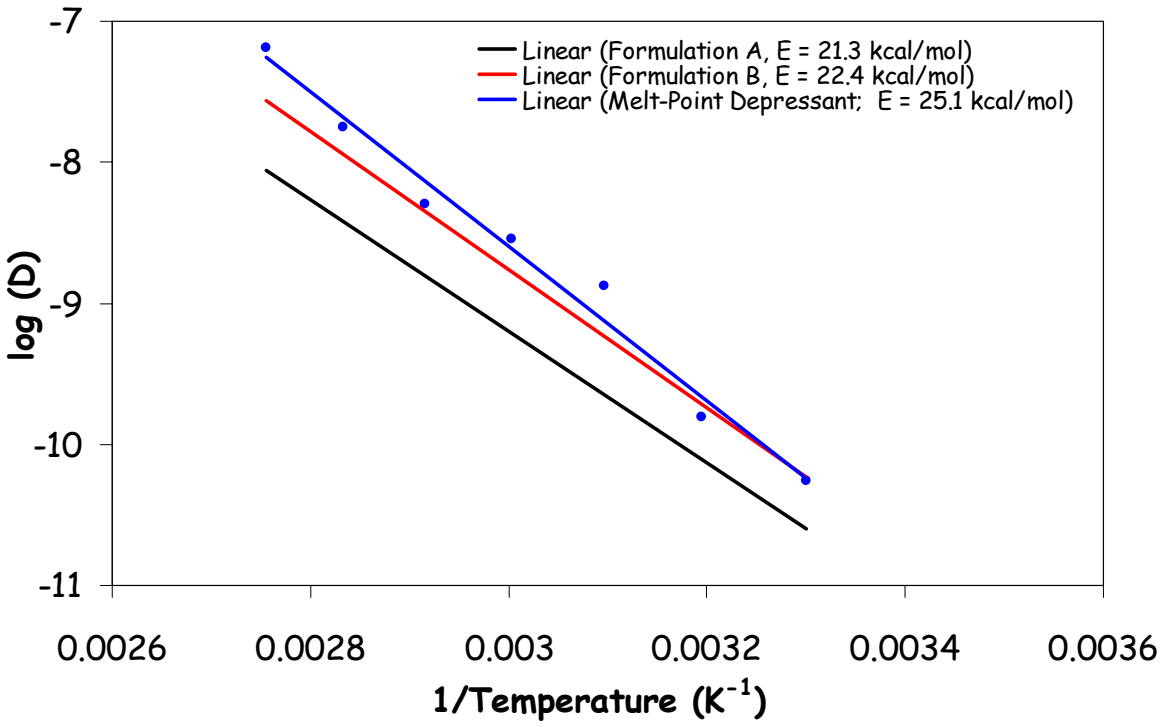

Figure 4-16: Arrhenius plots for coating formulations compared to that for the isolated melt-point depressant.

4.5 Summary and Conclusions

Mass loss data was obtained for two different coating formulations and for the isolated melt-point depressant. The two coatings consisted of a similar matrix with different additives included to control the mass loss behavior. While formulation A exhibited diffusion coefficients greater than those obtained for formulation B by approximately a factor of two, the activation energies for the two coatings were comparable, 21.3 and 22.4 kcal/mol respectively for formulations A and B. Although the differences in diffusion behavior were not significant, these data indicate that additives can be used to control the mass loss behavior in the coatings.

Mass loss data obtained for the melt-point depressant exhibited three regions corresponding to the loss of IPA, the loss of TPG and glycerol, and then structural relaxation of the gel. TGA indicates a fourth region of mass loss at high temperatures associated with the decomposition of organics remaining in the sol-gel network. Data presented in chapter 5 suggest that some glycerol remains bound to the network and explains the high-temperature mass loss in the TGA data.

Because the majority of mass loss occurred in the second region, it was determined to be most significant to the mass loss properties of the coating. Diffusion coefficients obtained for this region of mass loss were comparable to those obtained for the coating formulations. However, the melt-point depressant exhibited faster diffusion at high temperatures and a slightly larger activation energy compared to the coatings. This is attributed to greater crack density at high temperatures observed for the isolated melt-point depressant.

5. Chemistry of the Melt-Point Depressant

As described in earlier chapters, the coating included a sol-gel system designed to slowly release tripropylene glycol (TPG) and glycerol to the coating surface. This design was based on the assumption that in the presence of a 3:1 molar ratio of TPG and glycerol, titanium isopropoxide (TIP) undergoes complete substitution to form the metal-organic precursor $Ti(C_9H_{19}O_4)_3(C_3H_7O_3)$ according to the reaction shown in figure 5-1.

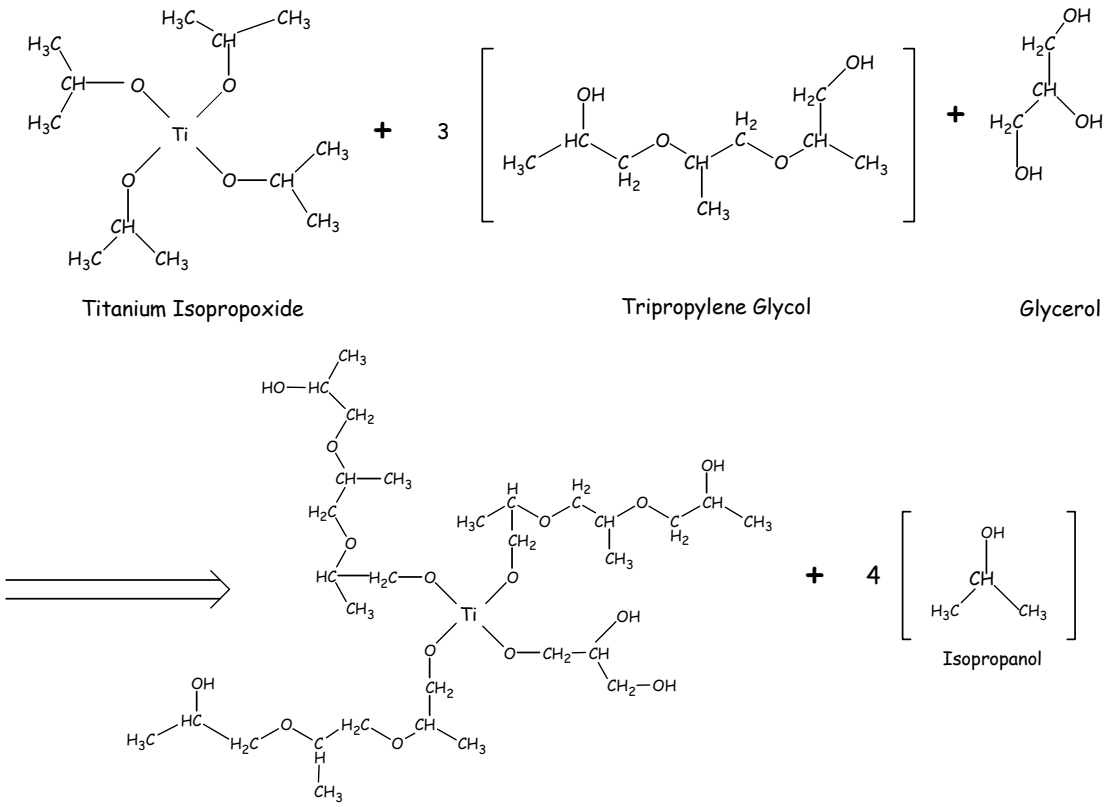

Figure 5-1: Reaction of titanium isopropoxide with tripropylene glycol and glycerol

It was then predicted that in the presence of water, this monomeric precursor would undergo condensation reactions resulting in the release of TPG and glycerol and the formation of a pure Ti-O-Ti network as shown in figure 5-2.

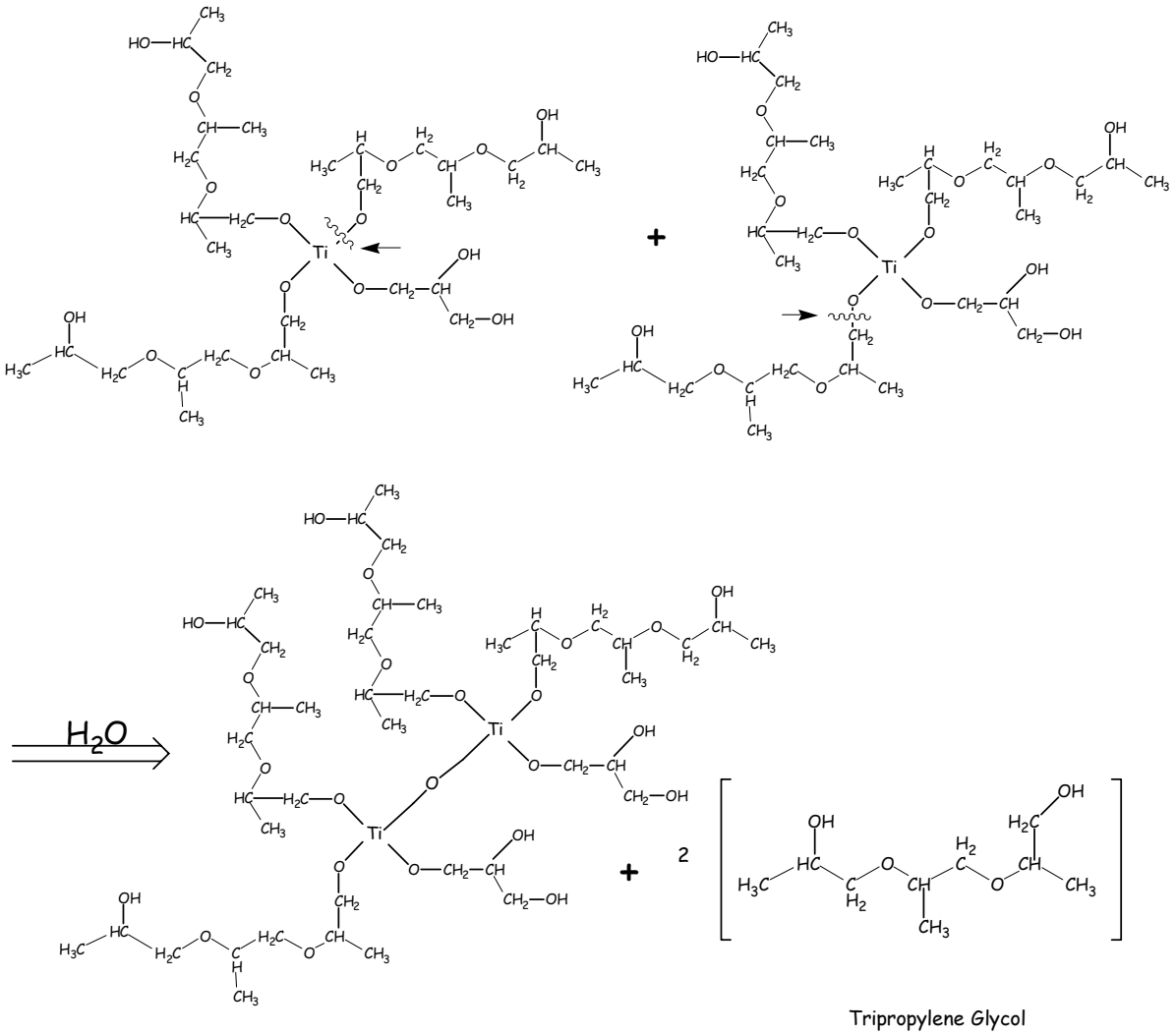

Figure 5-2: Sol-gel reaction

5.1 Fourier Transform-Infrared Spectroscopy

FT-IR Spectroscopy was used in an attempt to verify this chemistry. Spectra were obtained for each of the three reactants, TIP, TPG and glycerol, and for the melt-point depressant complex shortly after synthesis. The melt-point depressant was synthesized by first mixing a 3:1 stoichiometric ratio of TPG: glycerol with a high-speed mixer and then slowly adding an equivalent of TIP. The resulting exothermic reaction produced a clear viscous liquid, which gelled and turned white with condensation as shown in figure 4-8. Upon reaction, the solution emitted the distinct odor of isopropyl alcohol (IPA), confirming some degree of substitution occurs as shown in Figure 5-1. All spectra were obtained using transmission FT-IR. A composite spectrum was generated by adding the individual TIP:TPG:glycerol spectra in a 3:1:1 stoichiometric ratio which was compared to the spectrum of the reacted complex displayed in figure 5-3. Differences in the two spectra should reflect vibrational changes due to free IPA, the addition of both TPG and glycerol to titanium, and Ti-O-Ti bonds formed through the condensation reactions.

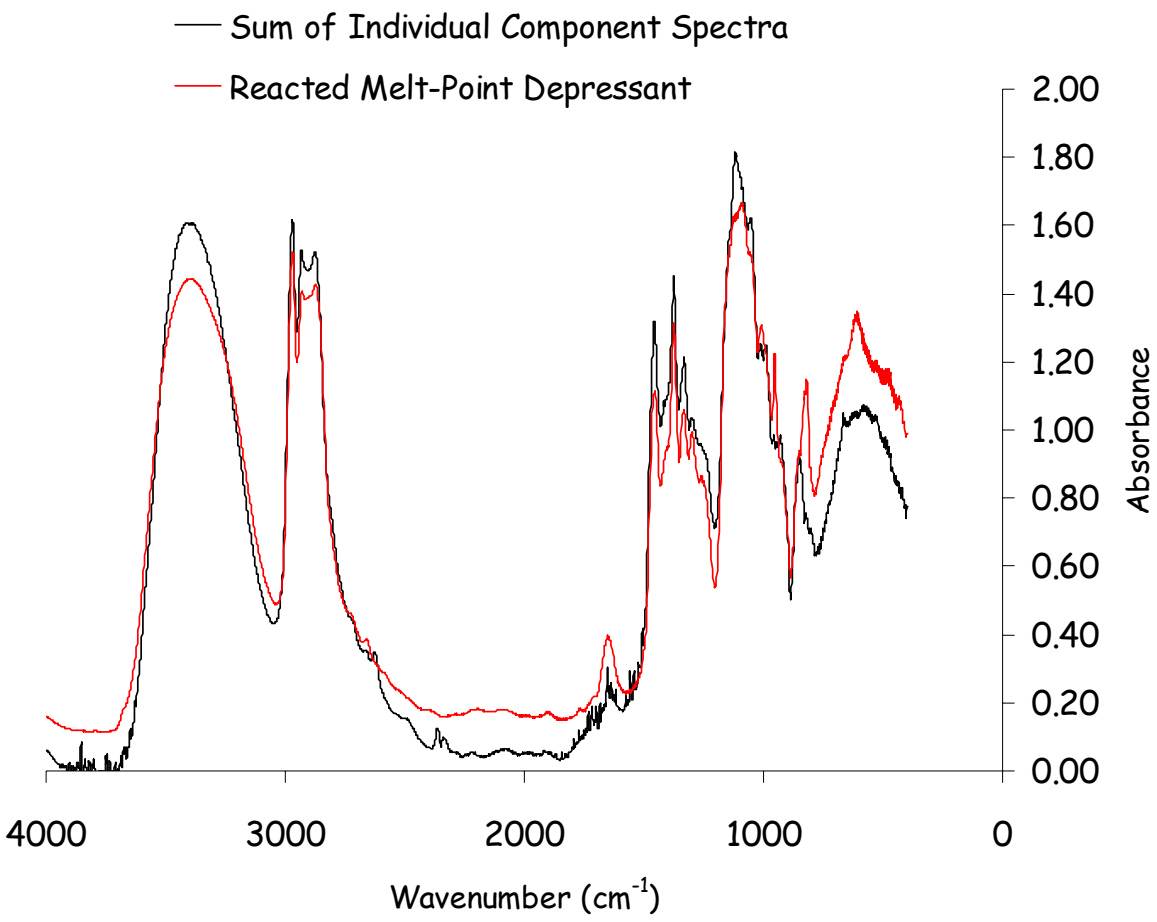

Figure 5-3: FT-IR spectrum of reacted melt-point depressant compared to the sum of the individual reactants

In addition to the peaks present in the reactant spectra, the spectrum of the melt-point depressant shows two additional peaks at 953 and 820 cm^{-1}. This region is expanded in figure 5-4 and compared to the spectrum for IPA. The FT-IR spectrum for IPA shows peaks at both 953 and 820 cm^{-1}, suggesting the peaks that appear in the melt-point depressant spectrum could be due to free IPA. The exact mode of vibration associated with these peaks is not known.

However, because these peaks are not discernable in the component spectra, they can be attributed to the C-OH bond formed when isopropyl alcohol dissociates from the titanium complex.

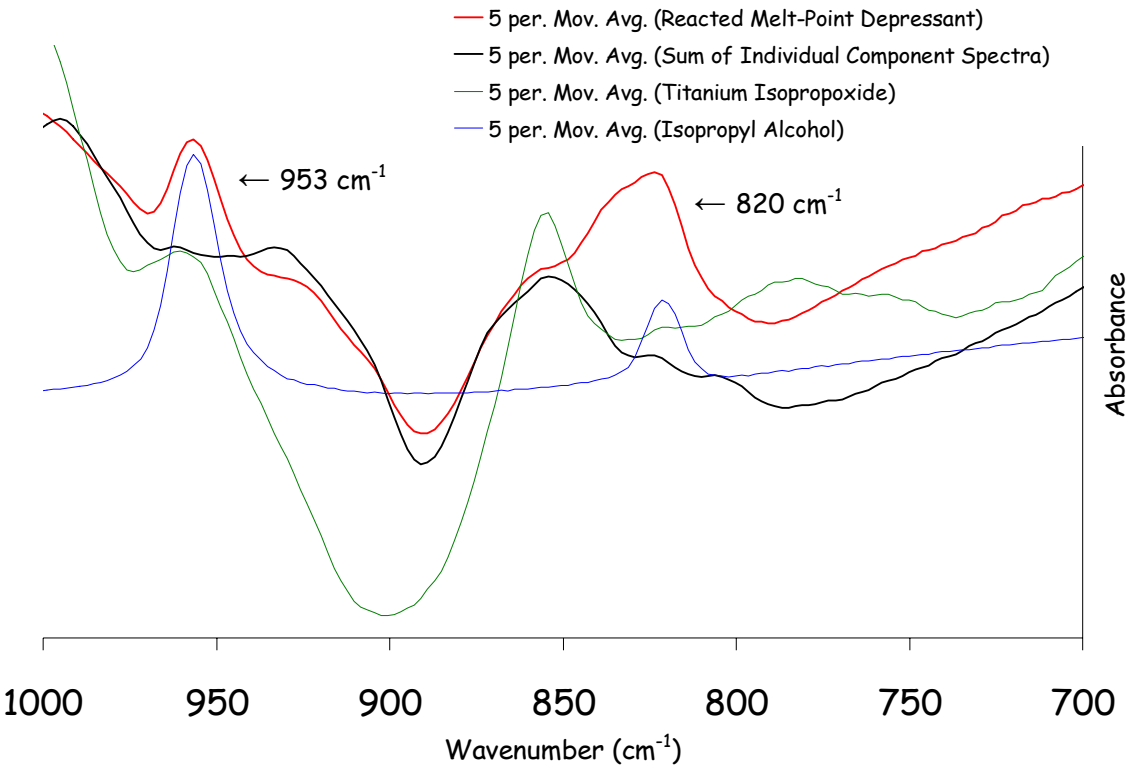

Figure 5-4: FT-IR spectrum of the reacted melt-point depressant compared to IPA and TIP*

* the notation '5 per. Mov. Avg.' indicates data has been smoothed

Figure 5-4 also compares the spectrum of the melt-point depressant to that for pure TIP. TIP does exhibit a small peak in the region of 953 cm^{-1}, which can be attributed to a small amount of free IPA formed as the result of partial hydrolysis that occurs when TIP is exposed to the atmosphere. However, the spectrum for TIP does not exhibit a corresponding peak at 820 cm^{-1}.

The peak at 820 cm^{-1} associated with the reacted melt-point depressant in figure 5-4 also appears much broader than the corresponding peak in the IPA spectrum. The irregular shape of this peak suggests its appearance could be due to the presence of two overlapping signals. Additional references were consulted in attempt to identify this peak.

The current literature does not report FT-IR stretching frequencies for titanium sol-gel reactions, but values have been reported for silicone-based systems. These are listed in Table 5-1. As the sol-gel network forms, peaks appear as a result of Si-O-R, Si-O-Si and Si-R-Si bonds. Similar behavior is therefore expected for systems containing Ti-O-R bonds and could explain the peak formed at 820 cm^{-1}. If this peak were due to the formation of Ti-TPG or Ti-Glycerol bonds (Ti-O-R), its intensity would decrease as condensation continued and TPG and glycerol were released. On the other hand, if this peak were associated with the formation of Ti-O-Ti bonds, its intensity would increase throughout the sol-gel reaction. Assuming the peak at 953 cm^{-1} is associated with free IPA, its intensity would decrease throughout the sol-gel reaction.

Table 5-1: Reported Vibrational Frequencies for Silica Gels[20]

Group		Vibrational Mode	Frequency Range (cm^{-1})
Si-O-R	$Si-O-CH_3$	Asymmetric –CH stretch	2880-2860
		-CH rock	1190
		Antisymmetric Si-O-C stretch	1100-1080
		Symmetric Si-O-C Stretch	850-800
	$Si-(OCH_3)_2$	Symmetric Si-O-C Deformation	390-360
	$Si-(OCH_3)_3$		480-440
Si-O-Si		Asymmetric Si-O-Si Stretch	1300-1000 peak broadens with length of siloxane chain
		Symmetric Si-O-Si Stretch	625-480
Si-R-Si	$Si-CH_2-Si$	CH_2 twist	1100-1000
		Si-C-Si stretch	~ 758
	$Si-(CH_2)_2-Si$	Unknown	1250-1100

A spectrum was obtained the melt-point depressant after it was dried at 50°C for approximately 12 weeks and had incurred a mass loss of 85%, indicating the sol-gel process was complete. This spectrum was obtained using attenuated reflectance spectroscopy (ATR). Figure 5-5 shows that the peak at 953 cm^{-1} disappears as expected while the peak at 820 cm^{-1} remains, confirming this peak is associated with the titania system. Because ATR generated a different baseline than transmission FT-IR at low wavenumbers, the intensities of the 820 cm^{-1} peaks in the spectra of the melt-point depressant before and after drying could not be directly compared. Additional experiments were required to determine if this peak was due to Ti-O-R or Ti-O-Ti bond formation.

A spectrum was also obtained for hydrolyzed TIP. When TIP is exposed to the atmosphere, it hydrolyzes forming a white powder consisting of TiO_2. If a Ti-O-Ti stretch were present, it would have been observed in this spectrum as well. However, hydrolyzed TIP exhibits no peak in this region. Therefore, the peak at 820 cm^{-1} was attributed to either the formation of Ti-O-R or Ti-O-R-O-Ti bonds. Silicone-based systems show peaks for corresponding stretches in the range of 1100-1000 cm^{-1}. Because titanium is greater in mass than silicon, it is expected it will exhibit lower frequency vibrations. However, it is difficult to discern which vibration causes this peak. Data presented later in this chapter suggest that Ti-O-R-O-Ti bonds create this absorbance.

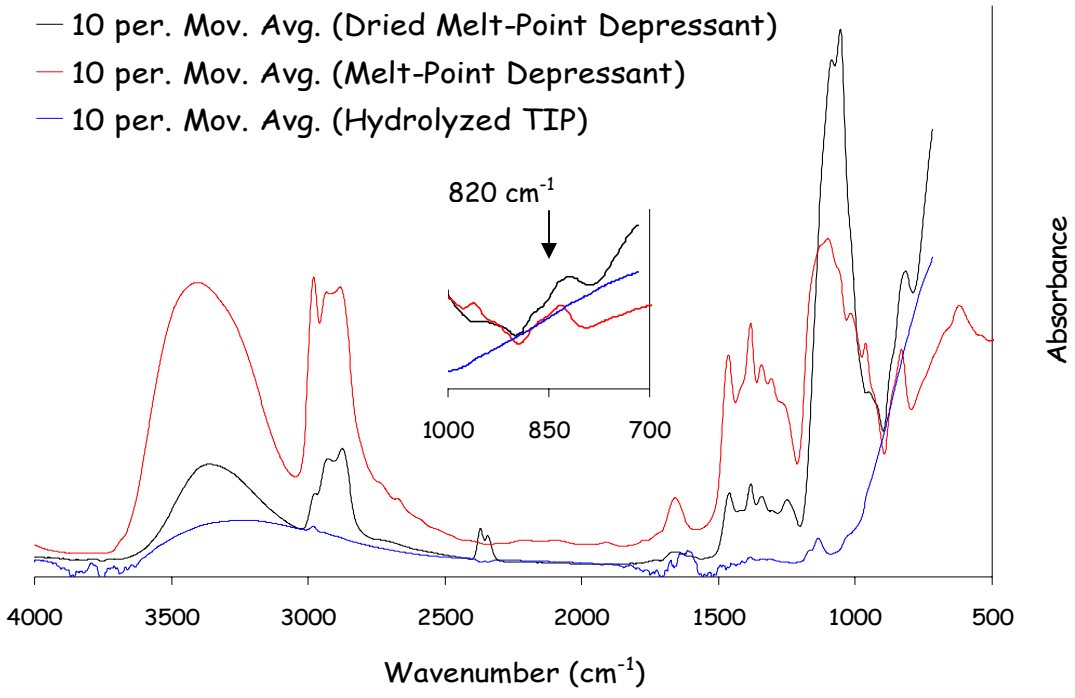

Figure 5-5: FT-IR spectra of dried melt-point depressant and hydrolyzed TIP*
* the notation '10 per. Mov. Avg.' indicates data has been smoothed

The spectrum obtained for the dried melt-point depressant also indicates that complete hydrolysis does not occur in this sol-gel system. If this were the case, the spectra for the dried melt-point depressant and hydrolyzed TIP would be identical, whereas figure 5-5 clearly shows they are not. The spectrum for hydrolyzed TIP exhibits very few peaks; the broad peak in the region of 3200 cm^{-1} and the small peak at 1650 cm^{-1} indicate the presence of water, which is expected because hydroxyl groups generally absorb on the surface of TiO_2.[20] Depending on the isotopic composition, Ti-O-Ti stretches fall between 135 and 610 cm^{-1} with the Ti-O-Pr stretch in TIP falling just outside that range, 620 cm^{-1}.[10, 20] The germanium crystal used for the ATR measurements absorbs at these frequencies so peaks in this region could not be observed. While the spectrum for hydrolyzed TIP is relatively featureless, many peaks are observed for the dried melt-point depressant above 700 cm^{-1} indicating that it does not completely condense to produce a pure TiO_2 network.

The spectrum of the dried melt-depressant indicates glycerol remains bonded within the titanium complex after TPG and IPA have been released. This was determined from the substantial decrease in $-CH_3$ stretching (2972 cm^{-1}) relative to $-CH_2$ (2935 cm^{-1}) and -CH stretches (2883 cm^{-1}), and the much

greater intensity of C-O stretches in both primary and secondary alcohols (1050 cm^{-1} and 1084 cm^{-1}, respectively) relative to the –CH stretches. The spectrum also indicates a decrease in the 1464 and 1377 cm^{-1} peak intensities associated with both $-CH_3$ and $-CH_2$ vibrational modes, supporting this conclusion. The peak at 1464 cm^{-1} shows overlapping signals from both $-CH_2$ scissor vibrations and the anti-symmetric deformation of $-CH_3$ while the peak at 1377 cm^{-1} reflects symmetric deformation of $-CH_3$ groups.

As the sol-gel reaction proceeded at room temperature, a clear liquid was released from the gel and collected on its surface. This liquid was collected and analyzed using transmission FT-IR. The resulting spectrum is shown in figure 5-6. The spectrum for the liquid released from the melt-point depressant strongly resembles that for TPG with the exception of the two peaks at 820 and 953 cm^{-1}. The peak at 953 cm^{-1} is expected as IPA is released from the system. The peak at 820 cm^{-1} could indicate that a few oligomeric species containing Ti-O-R-O-Ti crosslinks were released from the sol-gel network, but it is much narrower and less intense than the peak observed for the melt-point depressant and is more likely associated with free IPA. This

peak is most likely present in the reacted melt-point depressant, but obscured by the larger Ti-O-R-O-Ti absorbance.

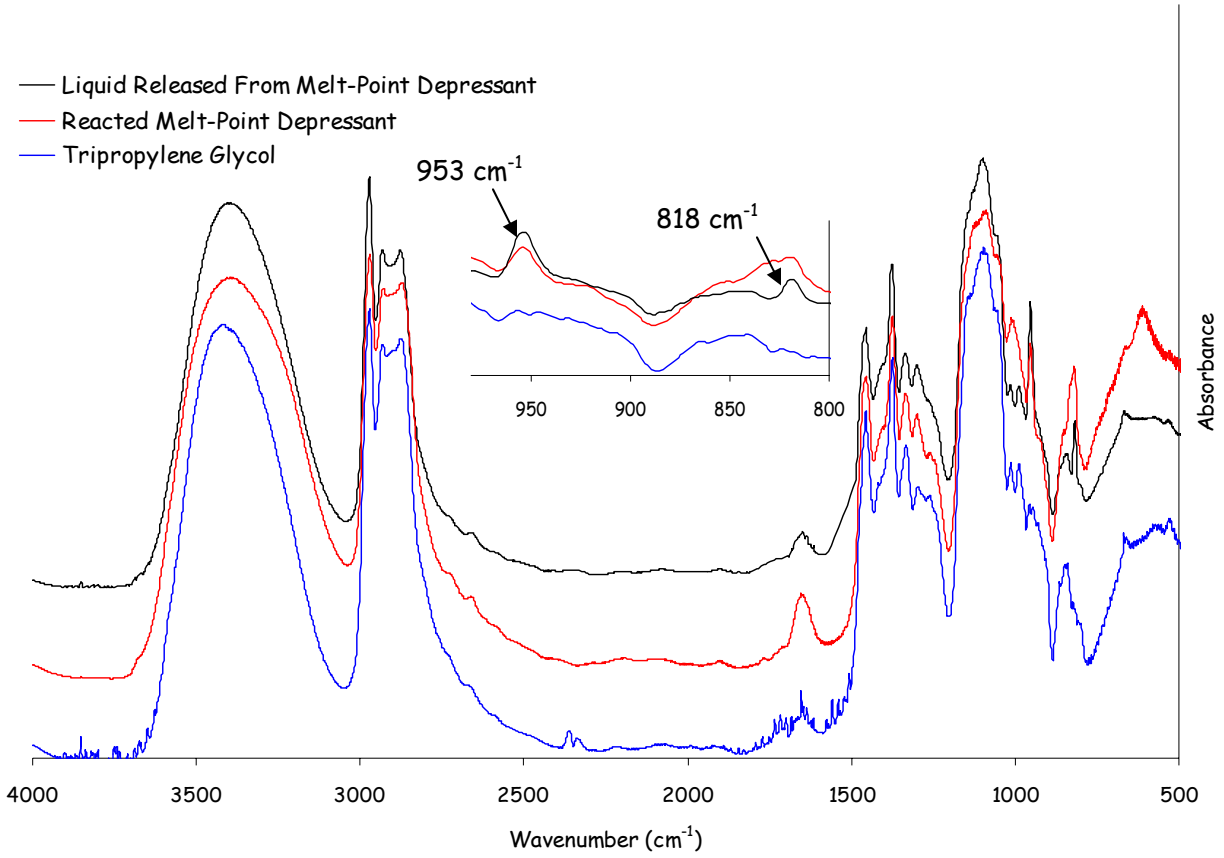

Figure 5-6: FT-IR spectrum of the liquid released from the melt-point depressant

In summary, FT-IR data indicate that glycerol remains in the system and that Ti-O-R-O-Ti bonds form. This suggests that both primary alcohol groups on glycerol bond to titanium groups as shown in figure 5-7.

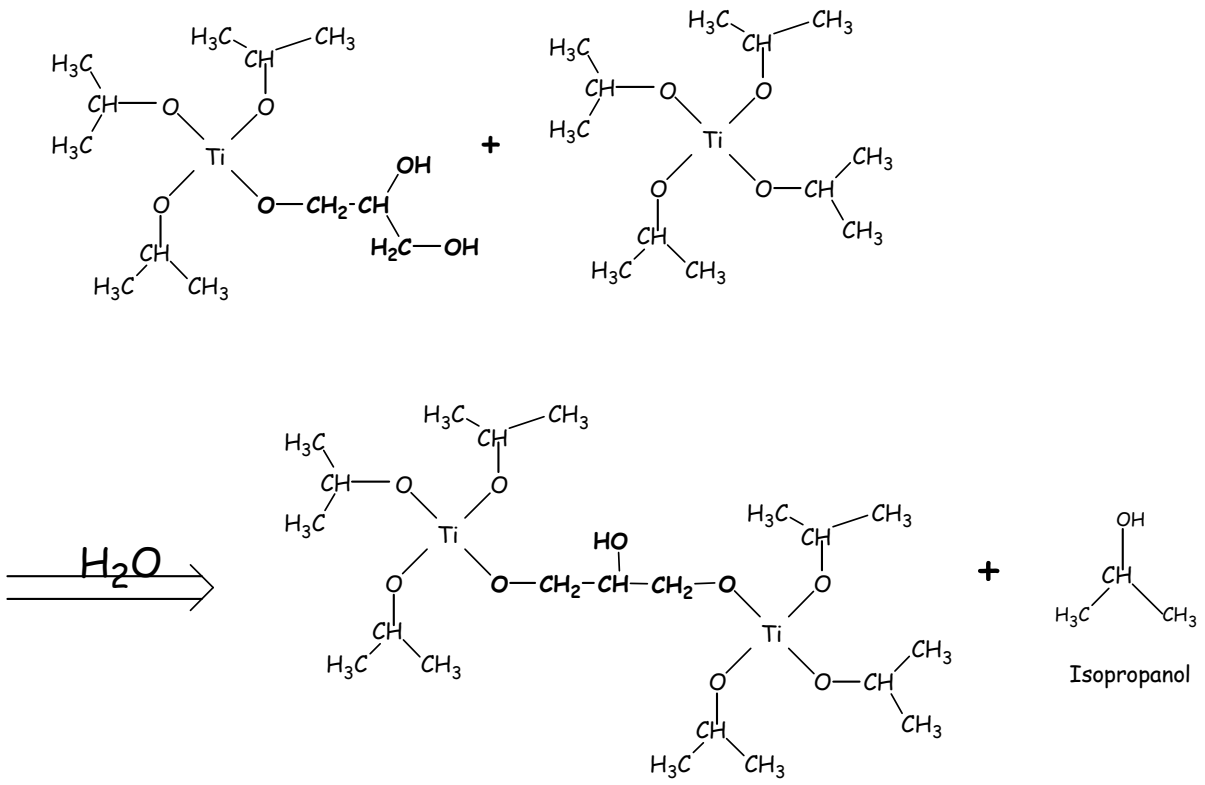

Figure 5-7: Chemistry resulting in Ti-O-R-O-Ti infrared band

This contradicts the predicted sol-gel behavior shown in figure 5-2. However, this behavior has been observed in other systems. One study reports the presence of both organic (Ti-glycerol-Ti) and inorganic (Ti-O-Ti) crosslinks in systems containing glycerol and acetic acid. [21] In order to explain this phenomenon, the precursor sol-gel chemistry was examined more closely.

5.2 Predictive Model for the Sol-Gel Reaction

A 'Predictive Model for Inorganic Polymerization Reactions' described by Jacques Livage and Marc Henry[22] was used to analyze the driving forces for the above reactions. According to this model, metal alkoxides, $M(OR)_4$, react with X-OH (X = R', H or M) species according to:

$$M(OR)_n + mXOH \rightarrow M(OR)_{n-m}(OX)_m + mROH$$

This reaction proceeds via an SN2 nucleophilic substitution mechanism, which is broken down into three steps as indicated below.[21-23] Certain conditions are necessary at each step in order for the reaction to occur. If any of these conditions are not met, the reaction does not proceed.[22]

(1) The nucleophilic addition of an –OH group to a positively charged metal atom only occurs only if the partial charge on the hydroxyl group, δ(OH), is negative and the partial charge on the metal, δ(M), is positive as indicated below.

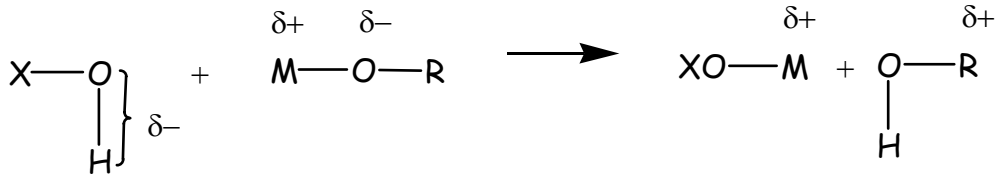

Depending on the chemical nature of X, this reaction describes all aspects of the sol-gel process: chemical modification of the precursor, hydrolysis and condensation.

Chemical Modification (X=R')

$$M\text{-}OR + HO\text{-}R' \rightarrow M\text{-}OR' + ROH$$

Hydrolysis (X=H)

$$M\text{-}OR + HO\text{-}H \rightarrow M\text{-}OH + ROH$$

Condensation (X=M)

$$M\text{-}OR + HO\text{-}M \rightarrow M\text{-}O\text{-}M + ROH$$

(2) δ(OR) must be less than δ(H) in order for the proton to transfer from the attacking ligand to the –OR group.

(3) δ(ROH) must be greater than zero in order for the protonated species to successfully depart.

A means for calculating the partial charges on each molecular species is required in order to apply Livage and Henry's model. This is done based on R.T. Sanderson's principle of electronegativity equalization and Pearson's hardness model. R.T. Sanderson describes his principle of electronegativity equalization with the statement "when two or more atoms initially different in electronegativity combine, they adjust to the same intermediate electronegativity of the compound".[24] Thermodynamically, this corresponds to

the equalization of chemical potential between two atoms in contact with each other. According to this principle, the effective electronegativity of an atom varies with its environment, specifically its partial charge. The relationship is described in the following equation:

$$\chi_i = \chi_i^o + \eta_i \delta_i \quad (1)$$

χ_i^o = electronegativity of neutral atom

δ_i = partial charge on atom

η_i = Pearson's hardness of atom = $k\sqrt{\chi_i^o}$ where k is a constant

For Pauling Electronegativies, k=1.36.

Livage and Henry calculated softness, S(G) (~$1/n_i$), of groups (G) with the formula $C_nO_mH_p$ according to:

$$S(G) = \frac{\frac{n}{\sqrt{X_C^o}} + \frac{m}{\sqrt{X_O^o}} + \frac{p}{\sqrt{X_H^o}}}{1.36} \quad (2)$$

The effective electronegativity of the group, X(G), was then calculated according to:

$$X(G) = \frac{\sum_i t_i \sqrt{x_i^o + kz}}{\sum_i \frac{t_i}{\sqrt{x_i^o}}} = \frac{(n\sqrt{X_C^o} + m\sqrt{X_O^o} + p\sqrt{X_H^o})}{1.36\ S(G)} \quad (3)$$

t_i = stoichiometry of the i^{th} atom

z = total charge of ionic species

and the partial charge of a group within a molecule according to:

$$\delta(G) = S(G)[X - \chi(G)] \qquad (4)$$

X = effective electronegativity of entire molecule

Once calculated, the partial charges on all groups in the precursor reaction can be compared to Livage and Henry's criteria for reaction in order to predict whether the reaction will occur.

Before this model was applied to the melt-point depressant complex, it was tested by on a similar reaction for which the products were known: that of titanium isopropoxide with acetic acid. Birnie and Bendzko[25] demonstrated with NMR data that when titanium isopropoxide is exposed to an excess of acetic acid, only two isopropyl groups are replaced with acetate groups as shown in figure 5-8.

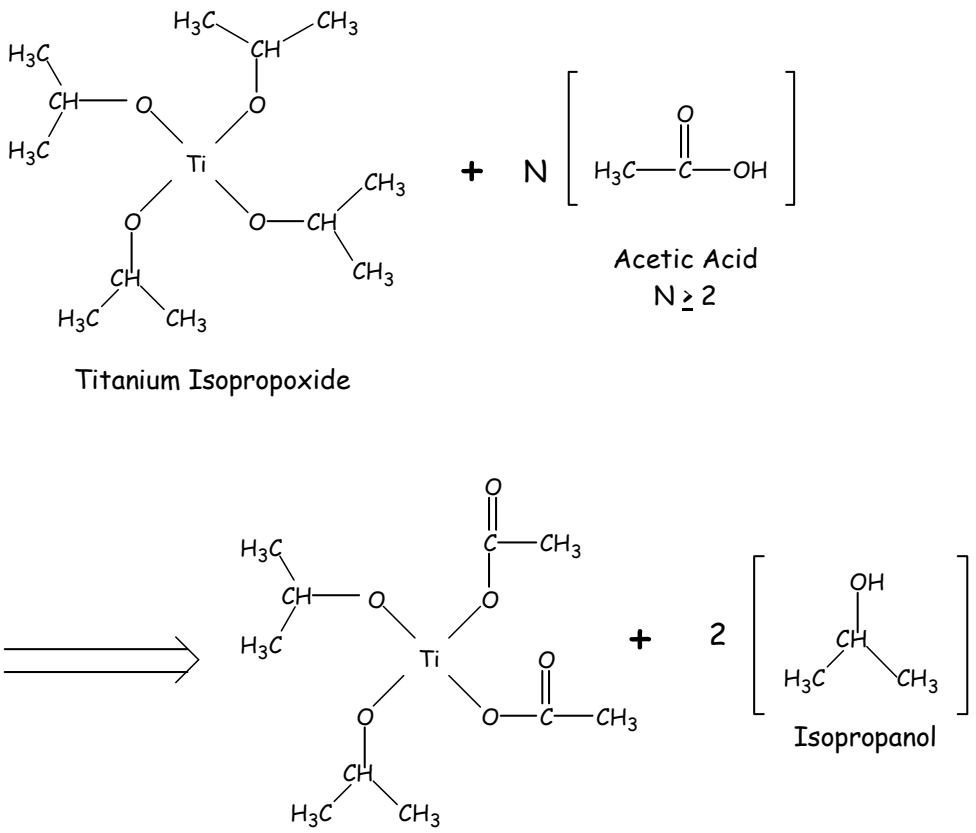

Figure 5-8: Reaction of TIP with acetic acid

Livage and Henry's model was applied to this system to see if it could predict this result. The partial charges on all species involved were calculated and then used to predict the reaction behavior. Table 5-2 lists the softness and effective electronegativity values for all of the molecular species involved in this reaction.

Table 5-2: Partial Charge Calculations for TIP Reacted with Acetic Acid

Compound	S	X	δ(Ti)	Isopropyl $\delta(C_3H_70)$	Acetate $\delta(C_2H_3O_2)$	δ(OH)	δ(H)
$Ti(C_3H_70)_4$ (TIP)	21.58	2.36	+0.49	-0.13			
$C_2H_4O_2$ (Acetic Acid)	3.70	**2.55**				-0.18	+0.23
$C_3H_7O_4$ (IPA)	5.74	**2.37**				-0.34	+0.08
$Ti(C_3H_70)_3(C_2H_3O_2)$	19.54	2.40	+0.51	+0.06	-0.56		
$Ti(C_3H_70)_2(C_2H_3O_2)_2$	17.49	2.44	+0.53	+0.29	-0.41		

X_{Ti} = 1.54, χ_C = 2.55, χ_O = 3.44, χ_H=2.20

For substitution of the first acetate ion, the conditions for the first two steps of the nucleophilic substitution were considered as outlined in Livage and Henry's model. These conditions are listed below next to the partial charge data, which confirms that these conditions were met for the addition of the first acetate group to TIP. It was assumed that δ(ROH) ~ 0 and the conditions for the third reaction step were ignored.

(1) $\delta(OH)_{Acetic\ Acid}$ = -0.18, δ(Ti) = +0.49; δ(OH) < 0 and δ(M) > 0

(2) $\delta(OR)_{Isopropyl}$ = -0.13, $\delta(H)_{Acetic\ Acid}$ = +0.23; δ(OR) < δ(H)

The reaction criteria are satisfied indicating that acetic acid will add to titanium isopropoxide. The partial charges were calculated for the new molecule (shown in row 4 of table 5-2) and the process was repeated.

After the first isopropyl group on the titanium alkoxide was replaced with a more electronegative acetate group, the electron density surrounding the remaining isopropyl groups decreases, leaving them with a partial positive charge (+0.06) as indicated in row 4 of table 5-2. The electron density surrounding the isopropyl groups decreases again with the addition of a second acetate group (row 5 of table 5-2). At this point, $\delta(OR)_{isopropyl}$ (+0.29) is greater than $\delta(H)_{acetate}$ (+0.23), prohibiting electron transfer and preventing the substitution of additional acetate groups.

The relative driving forces for each of the reactions above were analyzed by looking at bond dissociation energies. Several estimates of bond strength based on electronegativity values have been reported. Pauling's Bond Energy Equation gives the bond dissociation energy of a diatomic species according to:

$$D(A-B) = \frac{1}{2}\left[D(A-A) + D(B-B)\right] + 23(\chi_A - \chi_B)^2 \qquad (5)$$

D(A-B) = bond dissociation energy in kcal/mol
D(A-A) and D(B-B) = bond dissociation energies for individual species
χ_A, χ_B = electronegativities of each species

Several versions of this equation have appeared in the literature, generally with different constants. One study reported the ionic nature of the bond energy varied with electronegativity according to:

$$E_{ionic} = C(\chi_A - \chi_B)^2 + D \qquad (6)$$

where C and D are empirical constants that vary depending upon the nature of the system. [26]

This study does not attempt to assign quantitative values of bond energy to the reactions in the sol-gel system, but does note that bond strength increases with the square of the electronegativity difference between the two species, $\Delta^2 = (\chi_{alkoxide} - \chi_{ligand})^2$. The greater the electronegativity of the attacking ligand, the greater the driving force for the reaction.[26-31]

Table 5-3 lists Δ^2 values associated with each step in the reaction of TIP with acetic acid. Each column represents the substitution of one acetic acid molecule, and the Δ^2 value indicates the driving force for that reaction. Table 5-3 indicates that the driving force for this reaction decreases with the second substitution and that a third substitution does not occur, because $\delta(OR)_{isopropyl}$ is greater than $\delta(H)_{acetate}$, preventing the substitution of additional acetate groups as indicated above.

Table 5-3: Reaction of TIP with Acetic Acid

Product	$(\Delta^2)_1$	$(\Delta^2)_2$
$Ti(C_3H_70)_2(C_2H_3O_2)_2$	0.036	0.022

$(\Delta^2) = (X_{alkoxide} - X_{ligand})^2$

The information presented in table 5-3 is also illustrated by the flowchart in figure 5-9. While this additional illustration is not necessary for the simple reaction of TIP with acetic acid, it explains the more complicated flowcharts presented later for reactions involving TPG and glycerol.

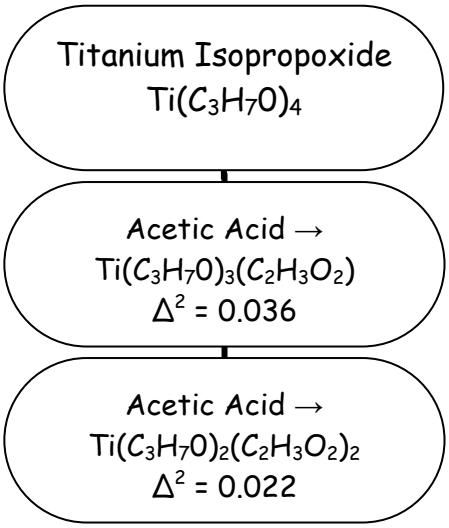

Figure 5-9: Flowchart showing reaction of TIP with acetic acid

Livage and Henry's model predicts that the reaction stops after the addition of two acetate ions as described above. This agrees with the experimental results Birnie and Bendzko observed through both ^1H and ^{13}C NMR.[24] The authors did not explain their results, but suggested that the free acetic acid underwent a

competing reaction with free IPA, limiting the stoichiometric amount of acetic acid available for substitution on the alkoxide. This predictive model provides an alternate explanation for their results. In addition, the model's agreement with Birnie and Bendzko's experimental data supports the model's ability to predict the extent of substitution in sol-gel reactions.

The model was next applied to the reaction of TPG and glycerol with TIP. The same procedure was used, calculating the softness and electronegativity values for all the reactants in both their neutral and deprotonated forms. These values are listed in table 5-4. Because initial synthesis of this sol-gel system was conducted in ambient conditions, it was assumed that atmospheric water vapor would play a part in the reaction and the effects of hydrolysis were also considered. As mentioned previously, hydrolysis leads to the formation of Ti-O-Ti bonds as shown in the reaction scheme below.

Hydrolysis: $Ti\text{-}OR + HO\text{-}H \rightarrow Ti\text{-}OH + ROH$

The hydrolyzed alkoxide can then react with another functionalized alkoxide

Condensation: $Ti\text{-}OR + HO\text{-}Ti \rightarrow Ti\text{-}O\text{-}Ti + ROH$

This adds significant complexity to the system and creates many additional reaction pathways. The calculations performed here predict the behavior of

only monomeric species. Hydrolysis is considered and assumed to result in condensation. However, the condensation reactions are not shown. A more sophisticated computer modeling system would be required to account for this.

Table 5-4: Partial Charge Calculations for Reactants Involved in Sol-Gel Reaction

Group		**S**	**X**	**δ(OH)**	**δ(H)**
Water	**H_2O**	1.39	***2.55***	-0.18	+0.18
Hydroxide Ion	**OH**	0.89	2.75		
Titanium ion	**Ti**	0.59	1.54		
Isopropyl Alcohol (IPA)	**C_3H_7OH**	5.74	***2.37***	-0.34	+0.08
De-protonated IPA	**C_3H_7O**	5.25	2.39		
Glycerol	**$C_3H_7O_3H$**	6.54	***2.50***	-0.27	+0.15
De-protonated Glycerol	**$C_3H_7O_3$**	6.04	2.52		
Tripropylene Glycol (TPG)	**$C_9H_{19}O_4H$**	15.64	***2.42***	-0.30	+0.11
De-protonated TPG	**$C_9H_{19}O_4$**	15.15	2.43		

X_{Ti} = 1.54, χ_C = 2.55, χ_O = 3.44, χ_H=2.20

Table 5-4 shows that both glycerol and tripropylene glycol are more electronegative than the isopropyl groups associated with the titanium isopropoxide ($\delta(C_3H_7O)$ = -0.13, table 5-2) making them suitable nucleophiles in the proposed SN2 reaction and satisfying the requirement that $\delta(OH)_{substituting\ ligand}$ must be negative . Therefore, the requirement for proton transfer, $\delta(OR)_{alkoxide} < \delta(H)_{substituting\ ligand}$, dictates whether substitution occurs. This condition is met for all of the reactants in their initial states, but limits the reactivity of several of the intermediate products as shown in table 5-5.

Table 5-5: Charge Distributions for All Possible Reaction Intermediates of Sol-Gel System Synthesized in Ambient Conditions

Compound	S	X	δ(Ti)	IPA δ(C_3H_70)	Glycerol δ($C_3H_7O_3$)	TPG δ($C_9H_{19}O_4$)	Water δ(OH)
$Ti(C_3H_70)_4$	21.58	2.36	+0.49	-0.13			
$Ti(C_3H_70)_3(C_9H_{19}O_4)$	31.48	2.39	+0.50	+0.02		-0.55	
$Ti(C_3H_70)_3(C_3H_7O_3)$	22.38	2.40	+0.51	+0.07	-0.75		
$Ti(C_3H_70)_3OH$	17.22	2.38	+0.49	-0.05			-0.33
$Ti(C_3H_70)_2(C_9H_{19}O_4)_2$	41.39	2.40	+0.51	+0.09		-0.34	
$Ti(C_3H_70)_2$ $(C_9H_{19}O_4)(C_3H_7O_3)$	32.28	2.41	+0.52	+0.15	-0.66	-0.05	
$Ti(C_3H_70)_2(C_9H_{19}O_4)OH$	27.13	2.40	+0.51	+0.07		-0.45	-0.31
$Ti(C_3H_70)_2(C_3H_7O_3)_2$	23.17	2.44	+0.53	+0.27	-0.53		
$Ti(C_3H_70)_2(C_3H_7O_3)OH$	18.02	2.42	+0.52	+0.18	-0.60		-0.29
$Ti(C_3H_70)_2(OH)_2$	12.87	2.40	+0.51	+0.06			-0.31
$Ti(C_3H_70\ )(C_9H_{19}O_4)_3$	51.29	2.41	+0.51	+0.13		-0.22	
$Ti(C_3H_70)$ $(C_9H_{19}O_4)_2(C_3H_7O_3)$	42.18	2.42	+0.52	+0.20	-0.60	-0.03	
$Ti(C_3H_70)(C_9H_{19}O_4)_2OH$	41.39	2.40	+0.51	+0.09		-0.34	
$Ti(C_3H_70)$ $(C_9H_{19}O_4)(OH)_2$	22.77	2.42	+0.52	+0.18		-0.15	-0.29
$Ti(C_3H_70\ )$ $(C_9H_{19}O_4)(C_3H_7O_3)_2$	33.07	2.44	+0.53	+0.28	-0.51	+0.20	
$Ti(C_3H_70)(\ C_9H_{19}O_4)$ $(C_3H_7O_3)OH$	27.92	2.43	+0.53	+0.23	-0.54	+0.09	-0.28
$Ti(C_3H_70)(C_3H_7O_3)_2OH$	18.81	2.47	+0.55	+0.44	-0.36		-0.25
$Ti(C_3H_70)(C_3H_7O_3)(OH)_2$	13.66	2.46	+0.54	+0.39	-0.36		-0.26
$Ti(C_3H_70)(OH)_3$	8.52	2.44	+0.53	+0.28			-0.28
$Ti(C_9H_{19}O_4)$ $(C_3H_7O_3)_2OH$	28.72	2.46	+0.54		-0.36	+0.45	-0.26
$Ti(C_9H_{19}O_4)$ $(C_3H_7O_3)(OH)_2$	23.57	2.45	+0.54		-0.42	+0.30	-0.27
$Ti(C_9H_{19}O_4)(OH)_3$	18.42	2.45	+0.54			+0.30	-0.26
$Ti(C_9H_{19}O_4)_2(C_3H_7O_3)_2$	42.97	2.44	+0.53	+0.28	-0.51	+0.20	
$Ti(C_9H_{19}O_4)_2$ $(C_3H_7O_3)OH$	37.82	2.44	+0.52		-0.52	+0.19	-0.29
$Ti(C_9H_{19}O_4)_2(OH)_2$	32.67	2.43	+0.53			+0.02	-0.28
$Ti(C_9H_{19}O_4)_3(C_3H_7O_3)$	52.08	2.43	+0.53		-0.59	+0.02	
$Ti(C_9H_{19}O_4)_3OH$	46.93	2.43	+0.53			-0.07	-0.30

S = caclulated softness, X = effective electronegativity, δ = partial charge

Table 5-5 shows partial charge calculations for all possible reaction intermediates in the sol-gel reaction. Appendix 1 displays the reaction paths predicted by these calculations in flowcharts similar to the one shown in figure 5-9 for the reaction of acetic acid with TIP. Because of the complexity of the system, several flowcharts were created to show the possible reaction paths. Again, each step is accompanied by a Δ^2 value as an indication of the driving force for the given reaction. Assuming the alkoxide is in equal proximity to all three substituting ligands, TPG, glycerol and water, the reaction with the greatest Δ^2 value is most likely to occur. Generally, the three substituting ligands will not be in equal proximity due to the 3:1 stoichiometric ratio of TPG: glycerol and the uncharacterized amount of water in the atmosphere. This is not considered in predicting possible reaction paths.

The flow charts in Appendix 1 show 56 possible reaction paths with ten possible monomeric products, which are summarized in tables 5-6 and 5-7. Just as in table 5-3, each column represents an additional substitution reaction.

Table 5-6: Predicted Reaction Products for Melt-Point Depressant Synthesized in Ambient Conditions

Product	$(\Delta^2)_1$	$(\Delta^2)_2$	$(\Delta^2)_3$	$(\Delta^2)_4$	$(\Delta^2)_5$
$Ti(C_3H_70)_2(C_3H_7O_3)_2$	**0.026**	**0.014**			
	0.026	0.001	**0.012**		
	0.005	**0.017**	**0.012**		
$Ti(C_3H_70)(C_3H_7O_3)_2OH$	**0.152**	0.003	**0.014**	**0.008**	
	0.026	**0.123**	**0.010**		
	0.026	0.001	**0.116**	**0.008**	
	0.005	**0.130**	**0.014**	**0.008**	
	0.005	**0.017**	**0.116**	**0.008**	
	0.005	0.002	0.014	**0.109**	0.008
$Ti(C_3H_70)(C_3H_7O_3)(OH)_2$	**0.152**	**0.020**	**0.109**		
	0.152	0.003	**0.014**	**0.102**	
	0.026	**0.123**	**0.109**		
	0.026	0.001	**0.116**	**0.109**	
	0.005	**0.130**	**0.014**	**0.102**	
	0.005	**0.130**	0.001	**0.123**	**0.008**
	0.005	**0.017**	**0.116**	**0.109**	
	0.005	0.002	**0.014**	**0.109**	**0.102**
$Ti(C_3H_70)(OH)_3$	**0.152**	**0.137**	**0.123**		
	0.152	**0.137**	**0.014**	**0.102**	
	0.152	**0.137**	0.001	**0.109**	
	0.152	0.003	**0.123**	**0.109**	
	0.005	**0.130**	**0.123**	**0.109**	
$Ti(C_3H_70)(C_9H_{19}O_4)(C_3H_7O_3)_2$	**0.026**	0.001	**0.012**		
	0.005	**0.017**	**0.012**		
	0.005	0.002	**0.014**	**0.010**	

$(\Delta^2) = (\chi_{alkoxide} - \chi_{ligand})^2$

Red indicates substitution reactions involving water.

Blue indicates substitution reactions involving glycerol.

Black indicates substitution reactions involving TPG.

Table 5-7: Predicted Reaction Products for Melt-Point Depressant Synthesized in Ambient Conditions, Continued

Product	$(\Delta^2)_1$	$(\Delta^2)_2$	$(\Delta^2)_3$	$(\Delta^2)_4$	$(\Delta^2)_5$	$(\Delta^2)_6$
$Ti(C_9H_{19}O_4)(OH)_3$	0.152	0.137	0.001	0.109		
	0.152	0.003	0.123	0.109		
	0.152	0.003	0.001	0.103		
	0.152	0.003	0.001	0.001	0.102	0.102
	0.005	0.130	0.123	0.109		
	0.005	0.130	0.001	0.123	0.102	
	0.005	0.130	0.001	0.001	0.102	0.102
	0.005	0.002	0.123	0.123	0.102	
	0.005	0.002	0.123	0.001	0.102	0.102
	0.005	0.002	0.001	0.116	0.102	0.102
$Ti(C_9H_{19}O_4)(C_3H_7O_3)_2OH$	0.152	0.003	0.001	0.014	0.006	
	0.152	0.003	0.001	0.001	0.008	0.006
	0.005	0.130	0.001	0.014	0.006	
	0.005	0.130	0.001	0.001	0.008	0.006
	0.005	0.002	0.123	0.014	0.006	
	0.005	0.002	0.001	0.116	0.008	0.006
$Ti(C_9H_{19}O_4)(C_3H_7O_3)(OH)_2$	0.152	0.137	0.001	0.010		
	0.152	0.003	0.123	0.010		
	0.152	0.003	0.001	0.123	0.008	
	0.152	0.003	0.001	0.014	0.096	
	0.152	0.003	0.001	0.001	0.102	0.008
	0.152	0.003	0.001	0.001	0.008	0.096
	0.005	0.130	0.123	0.010		
	0.005	0.130	0.001	0.014	0.096	
	0.005	0.130	0.001	0.001	0.102	0.008
	0.005	0.002	0.123	0.123	0.008	
	0.005	0.002	0.123	0.014	0.096	
	0.005	0.002	0.123	0.001	0.120	0.008
$Ti(C_9H_{19}O_4)_2(C_3H_7O_3)OH$	0.005	0.002	0.123	0.001	0.008	
	0.005	0.002	0.001	0.012	0.102	
$Ti(C_9H_{19}O_4)_2(C_3H_7O_3)_2$	0.005	0.002	0.001	0.012	0.008	

$(\Delta^2) = (\chi_{alkoxide} - \chi_{ligand})^2$

Red indicates substitution reactions involving water.

Blue indicates substitution reactions involving glycerol.

Black indicates substitution reactions involving TPG.

The (Δ^2) parameters in tables 5-6 and 5-7 are color-coded to indicate the substituting ligand in each reaction step; red indicates the addition of water, blue indicates glycerol and black indicates TPG. The tables show much larger driving forces for water and glycerol than for TPG. Based on values listed in table 5-6 for the first reaction step, the ionic component of the bond energy was approximated using Pauling's bond energy equation, equation (5). These values are listed in table 5-8 and assign quantitative values to the differences in the reactive driving forces associated with each of the substituting ligands. As mentioned earlier, this study does not claim these values are absolute. Pauling's bond energy equation was developed for diatomic species, much less complicated than the sol-gel system presented here. Table 5-8 merely attempts to claim that the differences in driving forces are significant.

Table 5-8: Ionic Components of Bond Energy Approximated Using Pauling's Bond Energy Equation

Substituting Ligand	(Δ^2)	E (kcal/mol)
Water	0.152	3.5
Glycerol	0.026	0.6
TPG	0.005	0.1

$(\Delta^2) = (X_{alkoxide} - X_{ligand})^2$

$E = 23(\Delta^2)$ in kcal/mol

Tables 5-6 and 5-7 also show that the magnitude of these driving forces decreases with each substitution reaction involving the same species (same color in tables 5-6 and 5-7)

It was also noted that when added to the alkoxide, highly electronegative species attract electrons from the remainder of the alkoxide, preventing additional reactions once $\delta(OR)_{alkoxide}$ exceeds $\delta(H)_{substituting\ ligand}$. Tables 5-6 and 5-7 show complete substitution does not occur when the initial reaction steps involve the more electronegative species, water and glycerol. For instance, the first row in table 5-6 indicates that no further reactions occur after the substitution of only two glycerol molecules. Similarly, reactions cease after the addition of three water molecules. The reaction pathways represented in table 5-6 involve substitution of several water and glycerol molecules. Consequently, none of these products reflect complete substitution; at least one isopropyl group remains. The products in table 5-7 are the result of substitution with the less electronegative species, TPG, and undergo complete substitution.

The model indicates much greater driving forces for the reaction of TIP with glycerol and water and substitution of these species prevents additional

reactions. If an excess of water and glycerol were present in the system, TPG would most likely not react. However, the reaction involved a 3:1 ratio of TPG: glycerol and the concentration of water was limited to vapor present in the atmosphere. Consequently, significant amounts of TPG did react in this system. However, the substitution of three TPG groups per TIP molecule, the stoichiometry upon which the coating was designed, does not occur (figure 5-1). The only path that will create the desired product, $Ti(C_9H_{19}O_4)_3(C_3H_7O_3)$, requires the addition of three TPG groups before the addition of the glycerol group, which is unlikely due to the high reactivity of glycerol compared to TPG. All other reaction schemes result in a significant amount of unreacted TPG within the gel.

The model also shows that glycerol is an unlikely leaving group once it is bound, which could explain why glycerol peaks were evident in the FT-IR spectrum of the dried melt-point depressant. TPG groups leave via condensation reactions while glycerol groups do not.

Livage and Henry's model predicts the formation of Ti-O-R-O-Ti crosslinks. These structures are not reported in the predicted reaction paths, because

these paths only attempt to predict monomeric species. As described earlier, the model illustrates that when an electronegative ligand adds to an alkoxide, it draws additional electron density from the complex, which increases its negative charge. The partial charge distribution that occurs when glycerol adds to TIP is listed in Table 5-8. The partial charge of glycerol is more negative after substitution (-0.75 < -0.27) making it a suitable nucleophile for addition to another titanium complex despite steric factors. Many of the monomeric products listed in Tables 5 and 6 contain isopropyl or TPG groups, which could be substituted by an attached glycerol ligand as shown in Figure 5-7. Because isopropyl groups are extremely susceptible to substitution, Ti-O-R-O-Ti crosslinks are more prevalent in systems with incomplete TIP substitution.

Table 5-9: Charge Distribution of $Ti(C_3H_70)_3(C_3H_7O_3)$

Compound	**S**	**X**	**δ(Ti)**	**Isopropyl δ(C_3H_70)**	**Glycerol δ($C_3H_7O_3$)**
$Ti(C_3H_70)_3(C_3H_7O_3)$	22.38	2.40	+0.51	+0.07	-0.75

5.3 Extension of Predictive Model

The predictive model indicates a limited amount of $Ti(C_9H_{19}O_4)_3(C_3H_7O_3)$ is formed during the precursor sol-gel reactions and incomplete precursor

substitution results in a greater concentration of Ti-O-R-O-Ti crosslinks. This is due to the extreme reactivity of both glycerol and water with TIP. The amount of $Ti(C_9H_{19}O_4)_3(C_3H_7O_3)$ formed would likely increase if glycerol were added after the TIP was allowed to react with TPG and without competing hydrolysis reactions due to atmospheric conditions. In order to test this theory, Livage and Henry's model was also applied to three additional systems:

(1) melt-point depressant synthesized under ambient conditions; glycerol added after TPG was allowed to react for approximately one minute

(2) melt-point depressant synthesized under N_2 to limit hydrolysis

(3) melt-point depressant synthesized under N_2; glycerol added after TPG was allowed to react for approximately one minute

The first system was synthesized similarly to the initial melt-point depressant complex. TPG was added to TIP in ambient conditions and mixed at high speed. Again, this reaction was exothermic and the smell of IPA indicated that the isopropyl groups were leaving the titanium alkoxide. After approximately one minute, glycerol was added and allowed to react. The time of one minute was arbitrarily chosen in order to give TPG sufficient time to react while limiting the extent of polymerization due to condensation reactions. Upon mixing the

reactants, the viscosity gradually increases and a gel is formed after only a few minutes.

Appendix 2 contains flowcharts showing the possible reaction paths for the system synthesized in ambient conditions with glycerol added last. These flow charts are based on partial charge calculations listed in Table 5-5 and are divided into reactions that occur before glycerol is added to the system and reactions that occur afterward. The net result is seven possible monomeric products which occur through 28 possible reaction paths, half the number of reaction paths presented for the initial system. These monomeric products are summarized in Table 5-10. Not only does this system result in a more controlled, less diverse reaction scheme, but significantly more reactions reflect the substitution of TPG. As described previously, when both glycerol and TPG are added simultaneously, glycerol dominates the initial reactions and limits the substitution of TPG.

Table 5-10: Summary of Reaction Paths for Sol-Gel System Synthesized in Ambient Conditions, Glycerol Added Last

	TPG Added in Atmosphere						Glycerol Added		
Product	$(\Delta^2)_1$	$(\Delta^2)_2$	$(\Delta^2)_3$	$(\Delta^2)_4$	$(\Delta^2)_5$	$(\Delta^2)_6$	$(\Delta^2)_1$	$(\Delta^2)_2$	$(\Delta^2)_3$
$Ti(C_3H_70)(OH)_3$	**0.152**	**0.137**	**0.123**						
	0.152	**0.137**	0.001	**0.109**					
	0.152	0.003	**0.123**	**0.109**					
	0.005	**0.130**	**0.123**	**0.109**					
$Ti(C_3H_70)(C_3H_703)(OH)_2$	**0.152**	0.003					**0.014**	**0.102**	
	0.005	0.002	0.001				**0.008**	**0.109**	**0.103**
$Ti(C_3H_70)(C_3H_703)_2(OH)$	**0.152**	0.003					**0.014**	**0.008**	
	0.005	0.002	0.001				**0.008**	**0.019**	**0.008**
$Ti(C_3H_70)(C_9H_{19}O_4)(C_3H_703)_2$	0.005	0.002	0.001				**0.008**	**0.010**	
$Ti(C_9H_{19}O_4)(OH)_3$	**0.152**	**0.137**	0.001	0.109					
	0.152	0.003	**0.123**	0.109					
	0.152	0.003	0.001	**0.123**	**0.102**				
	0.152	0.003	0.001	0.001	**0.102**	**0.102**			
	0.005	**0.130**	**0.123**	**0.109**					
	0.005	**0.130**	0.001	**0.123**	**0.102**				
	0.005	**0.130**	0.001	0.001	**0.102**	**0.102**			
	0.005	0.002	**0.123**	**0.123**	**0.123**				
	0.005	0.002	0.001	**0.116**	**0.102**	**0.102**			
$Ti(C_9H_{19}O_4)(C_3H_703)(OH)_2$	**0.152**	0.003	0.123				**0.010**		
	0.152	0.003	0.001	0.001	**0.102**		**0.008**		
	0.152	0.003	0.001	0.001			**0.008**	**0.096**	
	0.005	**0.130**	0.001	0.001	**0.102**		**0.008**		
	0.005	**0.130**	0.001	0.001			**0.008**	**0.096**	
	0.005	0.002	0.001	**0.116**	**0.102**		**0.008**		
	0.005	0.002	0.001	**0.116**			**0.008**	**0.096**	
$Ti(C_9H_{19}O_4)(C_3H_703)_2(OH)$	**0.152**	0.003	0.001	0.001			**0.008**	**0.006**	
	0.005	**0.130**	0.001	0.001			**0.008**	**0.006**	
	0.005	0.002	0.001	**0.116**			**0.008**	**0.006**	

$(\Delta^2) = (\chi_{alkoxide} - \chi_{ligand})^2$

Red indicates substitution reactions involving water.

Blue indicates substitution reactions involving glycerol.

Black indicates substitution reactions involving TPG.

While Table 5-10 indicates much fewer reaction products are achieved by adding glycerol last, there are still many reactions involving water as indicated by the (Δ^2) values in red. Synthesizing the melt-point depressant under nitrogen should significantly reduce the number of possible reaction paths by limiting condensation reactions during precursor formation. The previous reaction schemes show substitution reactions involving the hydroxyl groups which compete with the substitution of glycerol and TPG. Eliminating hydroxyl groups from the reaction conditions should increase the degree of precursor substitution prior to condensation reactions. This gel was synthesized by first mixing the 3:1 stoichiometric ratio of TPG and glycerol in an oven-dried flask under the flow of nitrogen and then slowly injecting TIP into the system using a syringe. This reaction was stirred at high speed under nitrogen before being exposed to atmospheric conditions. Appendix 3 shows the reaction paths predicted for this system while it is under nitrogen and then afterwards when exposed to the atmosphere. Five products are predicted via ten possible reaction paths as summarized in table 5-11.

Table 5-11: Summary of Reaction Paths for Sol-Gel System Synthesized Under Nitrogen

	Reacted Under Nitrogen				Exposure to Atmosphere		
Product	$(\Delta^2)_1$	$(\Delta^2)_2$	$(\Delta^2)_3$	$(\Delta^2)_4$	$(\Delta^2)_1$	$(\Delta^2)_2$	$(\Delta^2)_3$
$Ti(C_3H_7O)(C_3H_7O_3)_2(C_9H_{19}O_4)$	**0.026**	0.001	**0.012**				
	0.005	**0.017**	**0.012**				
$Ti(C_3H_7O)(C_3H_7O_3)(C_9H_{19}O_4)_2$	0.005	0.002	**0.014**				
$Ti(C_3H_7O_3)_2(C_9H_{19}O_4)_2$	**0.026**	**0.014**					
$Ti(C_3H_7O_3)(C_9H_{19}O_4)(OH)_2$	0.005	0.002	**0.014**		**0.109**	**0.102**	
	0.005	0.002	0.001	**0.012**	**0.102**	**0.096**	
	0.005	**0.017**	0.012		**0.109**	**0.102**	
	0.005	**0.017**			**0.116**	**0.084**	
	0.026	0.001			**0.116**	**0.084**	
$Ti(C_9H_{19}O_4)(OH)_3$	0.005	0.002	0.001		**0.116**	**0.102**	**0.102**

$(\Delta^2) = (\chi_{alkoxide} - \chi_{ligand})^2$

Red indicates substitution reactions involving water.
Blue indicates substitution reactions involving glycerol.
Black indicates substitution reactions involving TPG.

The final system explored attempts to maximize the substitution of TPG, providing more control over the reaction chemistry. This is achieved by synthesizing the melt-point depressant under nitrogen allowing TPG to react for a few minutes before the addition of glycerol. The model predicts only three reaction products achieved through three possible paths. Reaction paths are shown in Appendix 4 and summarized in table 5-12. Table 5-12 shows that under these reaction conditions, three TPG groups add to TIP, as intended by the original design of the coating.

Table 5-12: Summary of Reaction Paths for Sol-Gel System Synthesized Under Nitrogen with Glycerol Added Last

	Reacted Under Nitrogen					Exposure to Atmosphere			
	Only TPG			Glycerol					
Product	$(\Delta^2)_1$	$(\Delta^2)_2$	$(\Delta^2)_3$	$(\Delta^2)_4$	$(\Delta^2)_5$	$(\Delta^2)_1$	$(\Delta^2)_2$	$(\Delta^2)_3$	$(\Delta^2)_4$
$Ti(C_9H_{19}O_4)_2(C_3H_7O_3)_2$	0.005	0.002	0.001	**0.012**	**0.008**				
$Ti(C_9H_{19}O_4)_2(C_3H_7O_3)OH$	0.005	0.002	0.001	**0.012**		**0.096**			
$Ti(OH)_4$	0.005	0.002	0.001			**0.116**	**0.102**	**0.102**	**0.090**

$(\Delta^2) = (\chi_{alkoxide} - \chi_{ligand})^2$

Red indicates substitution reactions involving water.
Blue indicates substitution reactions involving glycerol.
Black indicates substitution reactions involving TPG.

Table 5-13 summarizes the predictions generated for each system and illustrates the role reaction conditions play in controlling the sol-gel chemistry. Limiting condensation reactions by synthesizing the gel under nitrogen is predicted to have a greater effect than adding glycerol last and maximum control is demonstrated for a system synthesized under nitrogen with glycerol added last. Not only does this model predict a decreasing number of final products, but more importantly the possible reaction paths decrease by a factor of greater than 18 as the reaction conditions are changed. This reflects a much more controlled process with fewer competing reactions and, in this case, increased substitution of TPG. This is desired in the synthesis of a melt-point depressant designed to slowly release TPG into the coating matrix.

Table 5-13: Summary of Predicted Reactions

Reaction Conditions	Predicted Products	Predicted Reaction Paths
Ambient	10	56
Ambient, Glycerol Added Last	7	28
Nitrogen	5	10
Nitrogen, Glycerol Added Last	3	3

Livage and Henry's model was used to predict the reaction chemistry for the four different systems. The remainder of this chapter tests these predictions through FT-IR, NMR and TGA analysis.

5.4 Verification of Model

Infrared Spectroscopy

First, infrared spectroscopy was used to compare the melt-point depressant synthesized under varying reaction conditions. Figure 5-10 shows FT-IR spectra for all four systems taken shortly after synthesis and figure 5-11 shows these same samples after drying at 70°C for 23 days and approximate mass losses of 85%. The mass loss data is described in more detail later in the chapter. Again, there is very little difference in these spectra with the exception of peaks located at 953 and 820 cm^{-1}.

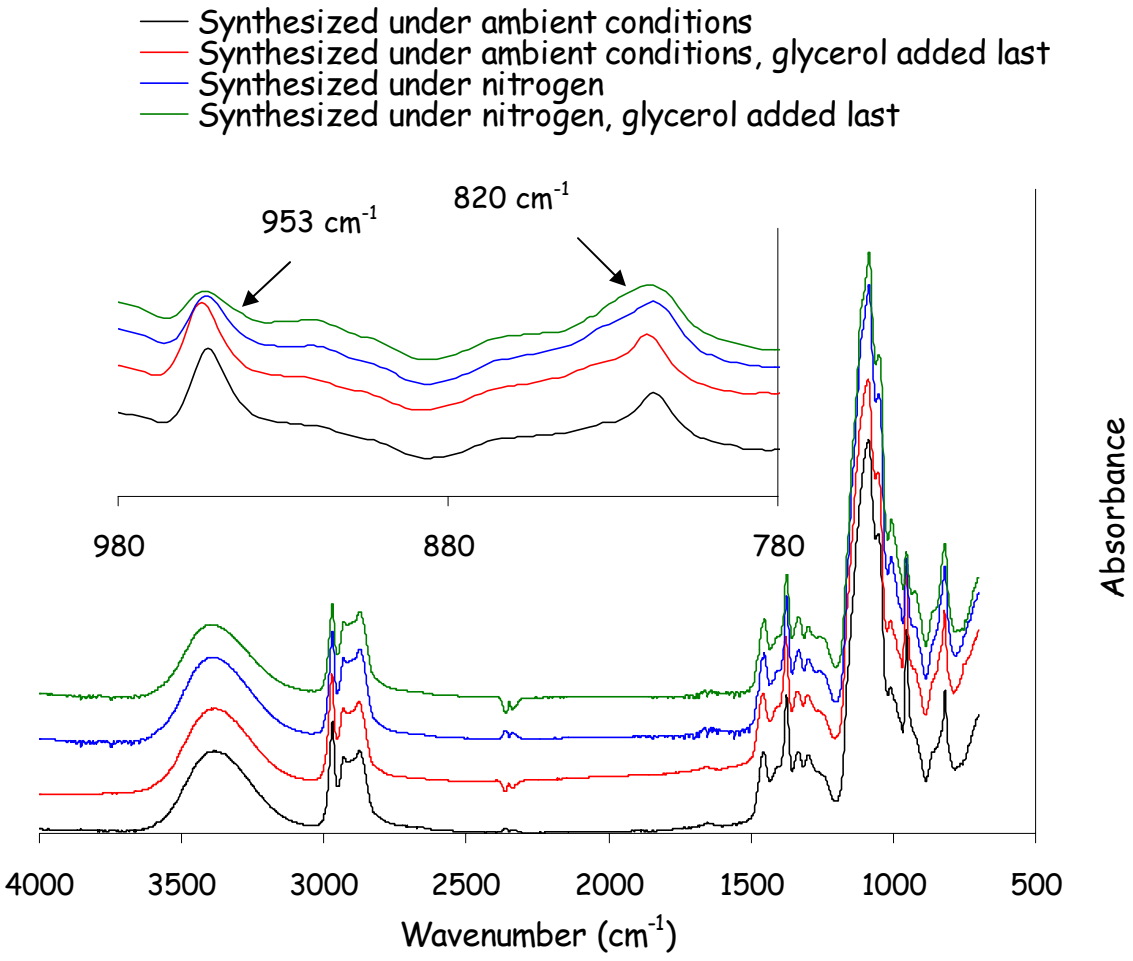

Figure 5-10: FT-IR spectra of sol-gel system reacted under different conditions

The peak at 953 cm^{-1}, associated with free IPA, decreases in intensity as the reaction conditions become more controlled; this peak is significantly smaller in the spectra of systems synthesized under nitrogen. This suggests that less free IPA is present in the system at the time of analysis. This is explained

according to the model, which predicts more substitution of TIP in systems with limited exposure to glycerol and water. Substitution reactions result in the release of IPA during precursor formation while the average titanium alkoxide composition is monomeric.

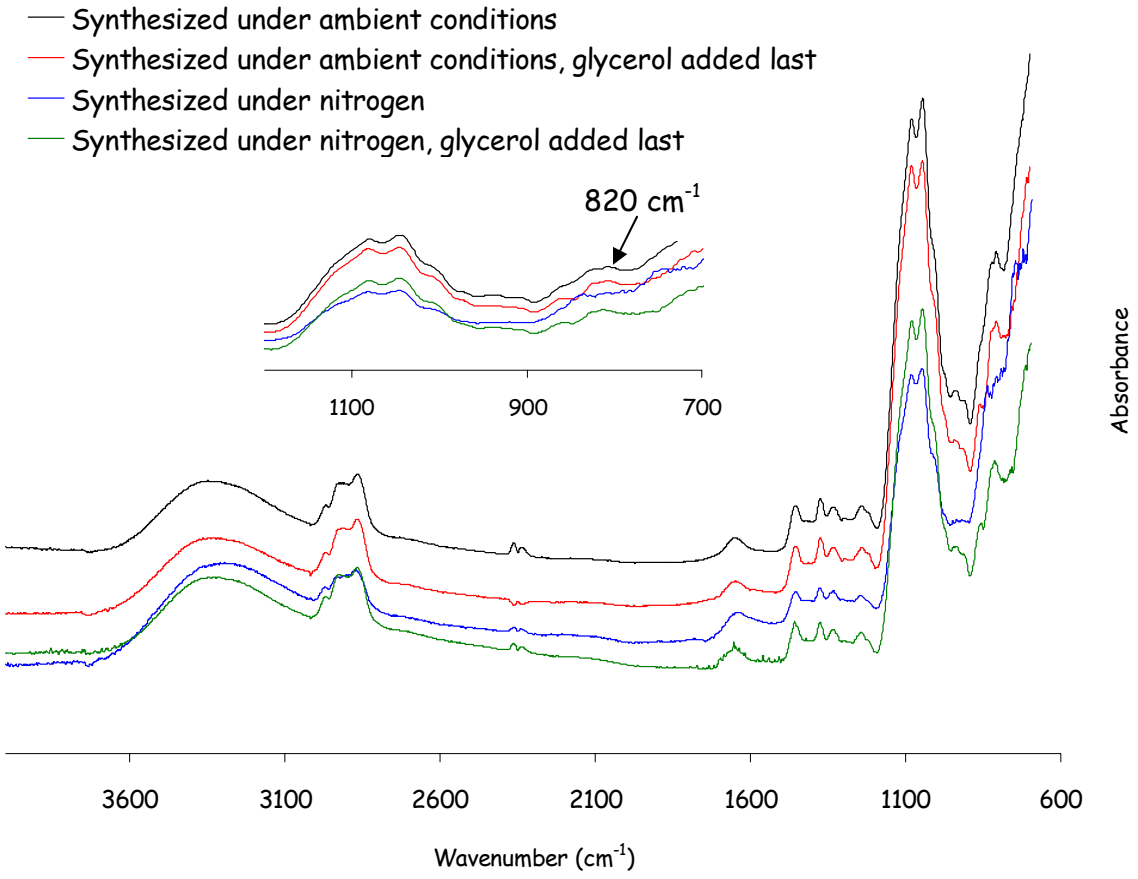

Figure 5-11: FT-IR spectra of dried sol-gel systems reacted under different conditions

In the less controlled reaction schemes, substitution reactions are limited and a significant amount of IPA is released via condensation reactions. Condensation reactions occur at a slower rate depending on the concentration of water in the

atmosphere and the resulting oligomeric and polymeric structures limit the diffusion rate of IPA out of the gel. It is therefore expected that a larger concentration of free IPA would be present in the less controlled reaction schemes at the time of analysis as the spectra indicate. This is supported by mass loss data shown later in this chapter. Observation of a larger IPA peak at 953 cm^{-1} could be achieved if FT-IR analysis was performed immediately upon mixing the reactants under nitrogen. The intensity of this peak should decrease with time. In contrast, systems mixed under ambient conditions produce a peak at 953 cm^{-1} which slowly increases in intensity before dropping off.

The peak at 820 cm^{-1} was attributed to a broad Ti-O-R-O-Ti absorption overlapping a narrower one at the same frequency associated with free IPA. While the difference is less evident, the samples synthesized under ambient conditions appear to have a stronger absorbance in this region. This is expected due to both the higher concentration of free IPA in these systems and the greater occurrence of Ti-O-R-O-Ti crosslinks in less substituted systems. Because two peaks overlap in this region, it is impossible to discern

which absorption dominates; this peak is analyzed more accurately in the spectra of the dried melt-point depressants where IPA is absent.

The spectra of the dried melt-point depressant do show a slightly smaller absorption in the region of 820 cm^{-1} for systems reacted under nitrogen, indicating a smaller concentration of Ti-O-R-O-Ti bonds. However, this difference is extremely subtle. This trend is confirmed by the less intense –CO stetch peaks associated with both primary and secondary alcohols at 1065 and 1100 cm^{-1} respectively. This suggests a smaller concentration of glycerol remains in systems synthesized under nitrogen.

The FT-IR spectra indicate that Ti-O-R-O-Ti crosslinks are more prevalent in systems where precursor substitution is limited. However, reaction conditions were controlled for only the first few minutes during precursor formation. All subsequent condensation reactions proceeded in atmospheric conditions in the presence of water vapor. If the system were not exposed to water vapor, hydrolysis would be limited and additional Ti-O-R-O-Ti linkages would be expected. This effect was further examined by comparing the spectra of the sol-gel reacted under nitrogen for approximately 30 min before being exposed

to the atmosphere with the same system reacted under nitrogen for 24 hours before being exposed to atmosphere. This is shown in figure 5-12.

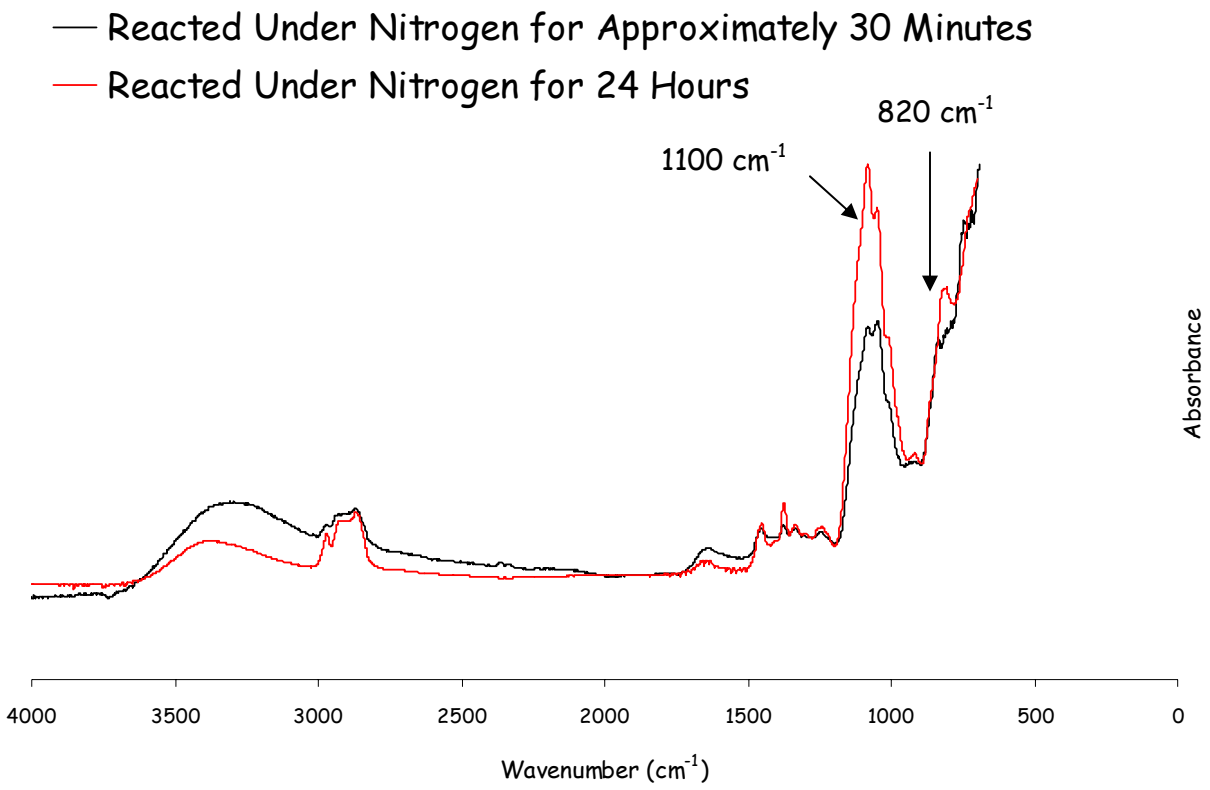

Figure 5-12: FT-IR spectra of dried MPD reacted under nitrogen for different time periods

The spectra shown in figure 5-12 clearly show that in the absence of water, the concentration of Ti-O-R-O-Ti crosslinks increases dramatically. The peak at 1100 cm^{-1} associated with –CO stretching in secondary alcohols is significantly more intense than the corresponding peak for primary alcohols (1045 cm^{-1}) indicating that both primary alcohol sites have reacted with a significant concentration of glycerol molecules, a reaction shown in

figure 5-7. This is also indicated by a narrower, less intense –OH peak in the area of 3400 cm^{-1}. This spectrum also shows a more intense peak at 820 cm^{-1}, supporting the earlier conclusion that this peak is a result of Ti-O-R-O-Ti crosslinks.

The FT-IR data shown supports the model's prediction that a more highly substituted titanium precursor and a more uniform sol-gel reaction with fewer Ti-O-R-O-Ti crosslinks can be synthesized by controlling the pre-cursor reaction conditions. For maximum coating lifetime, it is theorized that a highly-substituted titanium precursor is desirable. In addition, the majority of the TPG and glycerol should be released as the sol-gel reaction progresses.

FT-IR data suggests this is best achieved by synthesizing the melt-point depressant under nitrogen, adding glycerol last and removing the system from nitrogen after just a few minutes, so that maximum precursor substitution is obtained but condensation proceeds via hydrolysis. Additional time under nitrogen results in condensation reactions which form Ti-O-R-O-Ti crosslinks and limit the release of melt-point depressant.

The above conclusions were drawn based on observed FT-IR absorbances. Other techniques were applied to verify these conclusions.

Nuclear Magnetic Resonance Spectroscopy

Nuclear Magnetic Resonance Spectroscopy (NMR) was also employed to study the sol-gel chemistry and the effects of reaction conditions. First, spectra were taken of all three reactants and compared to that of the reacted melt-point depressant. Figure 5-14 shows the full spectra obtained using ^{1}H NMR and figure 5-15 shows an expanded view of the region from 3-5 ppm. All reactants were dissolved in deuterated dimethyl sulfoxide (DMSO) with the exception of TIP, which was dissolved in deuterated toluene.

Just as in the FT-IR measurements, the expected peak differences should correspond to the release of IPA and the bonding of TPG and glycerol groups to the titanium complex. For ^{1}H NMR, this should be reflected by peak shifts of protons alpha to the bonds being formed or broken. The affected protons are highlighted in red in figure 5-13. Protons on groups forming

bonds with the titanium complex are expected to display an increase in resonance frequency while isopropyl protons leaving the complex are expected to display a decrease in resonance frequency.

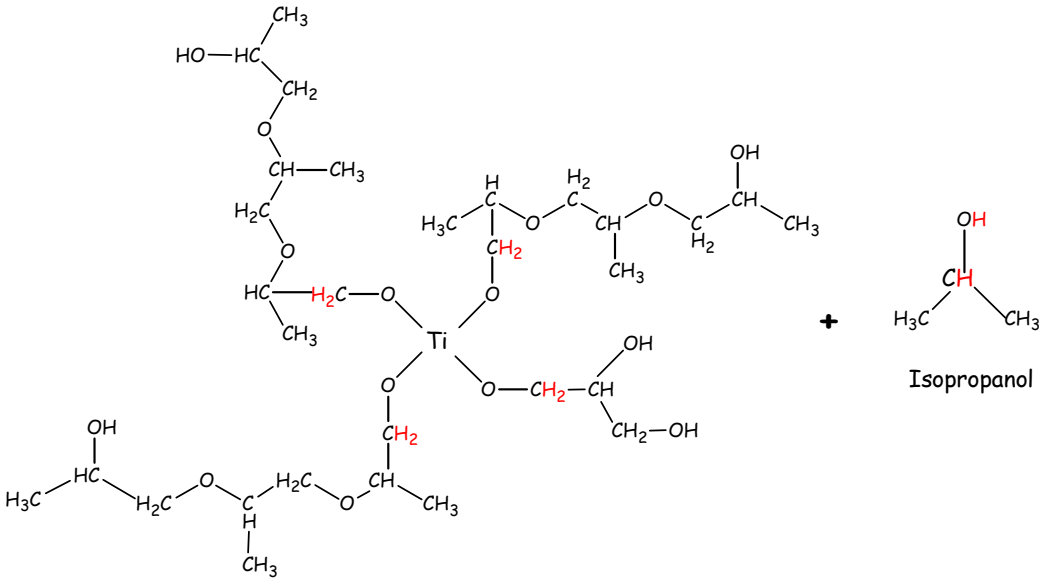

Figure 5-13: Protons affecting 'H NMR chemical shifts

Resonances in the range of 1.0 ppm are due to methyl protons, those in the range of 3.0 - 4.0ppm are due to –CH and –CH_2 protons, and the highest frequency resonances shown in figures 5-14 and 5-15 are –OH protons and protons alpha to a titanium – oxygen bond. Peaks in the melt-point depressant were grouped together and assigned a percentage of the signal.

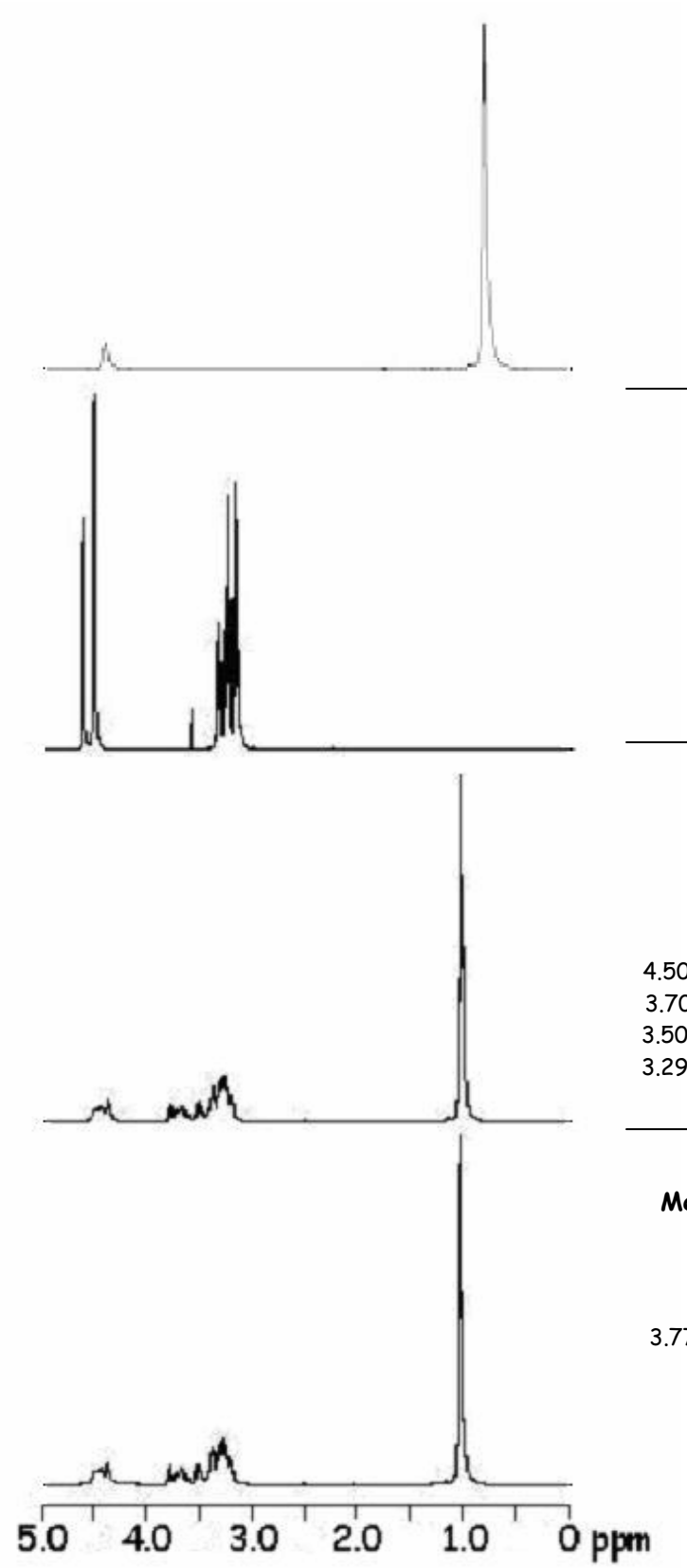

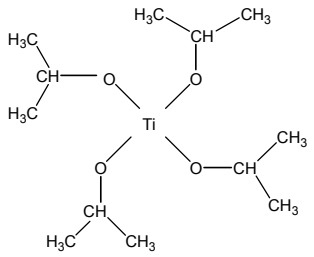

Titanium Isopropoxide

4.49 ppm, 4-H

1.23 ppm, 24-H (J=6.3 Hz)

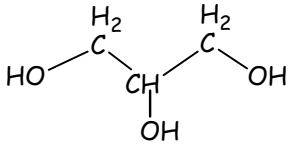

Glycerol

4.54 ppm, 1-H (J_1=5.0 Hz, J_2=1.7 Hz)

4.46 ppm, 2-H (J_1=5.7 Hz, J_2=1.5 Hz)

3.42 ppm, 1-H (J=4.95 Hz)

3.36 ppm, 2-H (J_1=5.5 Hz, J_2=1.3 Hz)

3.28 ppm, 2-H (J_1=5.6 Hz, J_2=1.4 Hz)

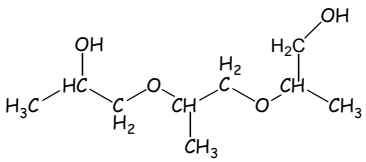

Tripropylene Glycol

4.50 ppm, 1-H (J=4.5 Hz); 4.44 ppm, 1-H (J=3.9 Hz)

3.70 ppm, 1-H (J=5.9 Hz); 3.65 ppm, 1-H (J=5.1 Hz)

3.50 ppm, 1-H (J=6.2 Hz); 3.38 ppm, 2-H (J=2.9 Hz)

3.29 ppm, 2-H (J=4.7 Hz); 3.19 ppm, 2-H (J=3.8 Hz)

1.02 ppm, 9-H (J=3.8 Hz)

Melt-Point Depressant Synthesized in Ambient Conditions

δ (ppm) = 4.49, 4.43, 4.36 (11%)

3.77, 3.71, 3.66, 3.51, 3.37, 3.29, 3.18 (37.5%)

1.05 (51.5%)

Figure 5-14: 'H NMR of melt-point depressant

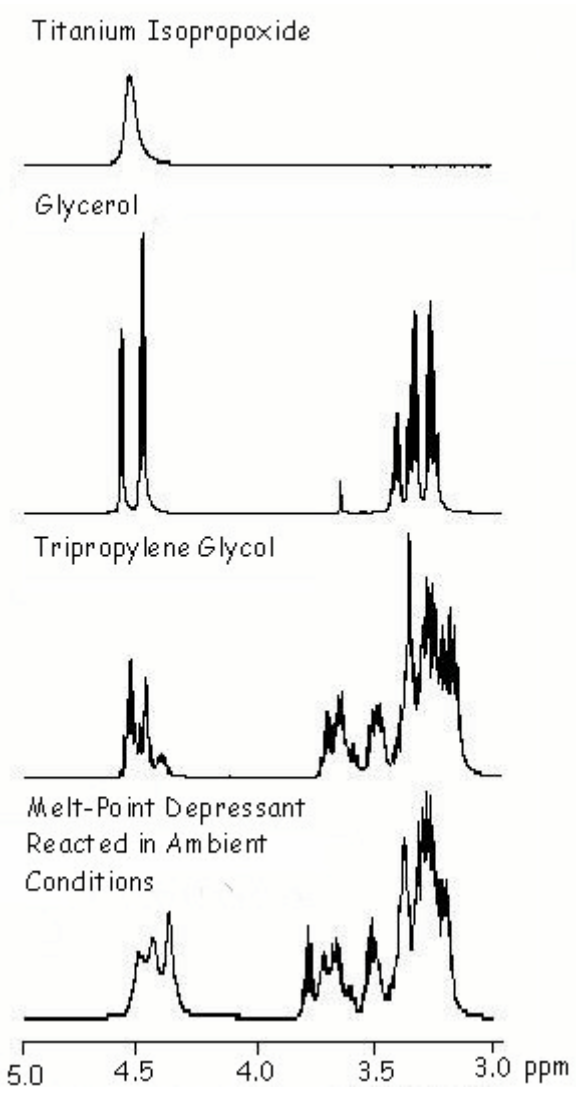

Figure 5-15: Magnified view of ^{1}H NMR of melt-point depressant

Peak overlap makes it difficult to integrate each peak and the total number of protons in the system is unknown. The combined reactants contain 96 protons; however, FT-IR data confirms that IPA leaves the system during the course of the reaction. When all the IPA has left the system, the number of protons

decreases to 64. In addition, hydrolysis requires the absorption of water, which also alters the number of protons in the system. The melt-point depressant was placed in sealed NMR tubes with deuterated solvent immediately after synthesis. Therefore, it is assumed in this study that water does not contribute a significant number of protons. It is also assumed that at this stage of the reaction, all TPG and glycerol remain in the system.

All peaks in the spectrum for the melt-point depressant were also present in at least one of the reactant spectra; thus, the occurrence of a reaction was not immediately apparent. The reactant spectra were used to predict in more detail the changes expected during the reaction of the melt-point depressant. These changes are outlined in figure 5-16.

When isopropyl groups dissociate from TIP, a proton is transferred from the attacking species to the isopropyl group as described in section 5-2. In addition, the adjacent –CH proton experiences a decrease in resonance frequency. Proximity of the titanium complex is expected to deshield the proton from the magnetic field resulting in a higher resonance frequency, which decreases as the group leaves the titanium complex. This phenomenon is

confirmed by a reference spectrum for IPA as shown in figure 5-16. The exact resonances corresponding to the reference spectrum for IPA are not present in the melt-point depressant. However, the reference spectrum does confirm the deshielding effect of the titanium complex. In contrast, when glycerol and TPG groups add to the titanium, they lose an alcoholic proton and the alpha protons are expected to exhibit an increase in resonance frequency due to the deshielding effect of the titanium complex.

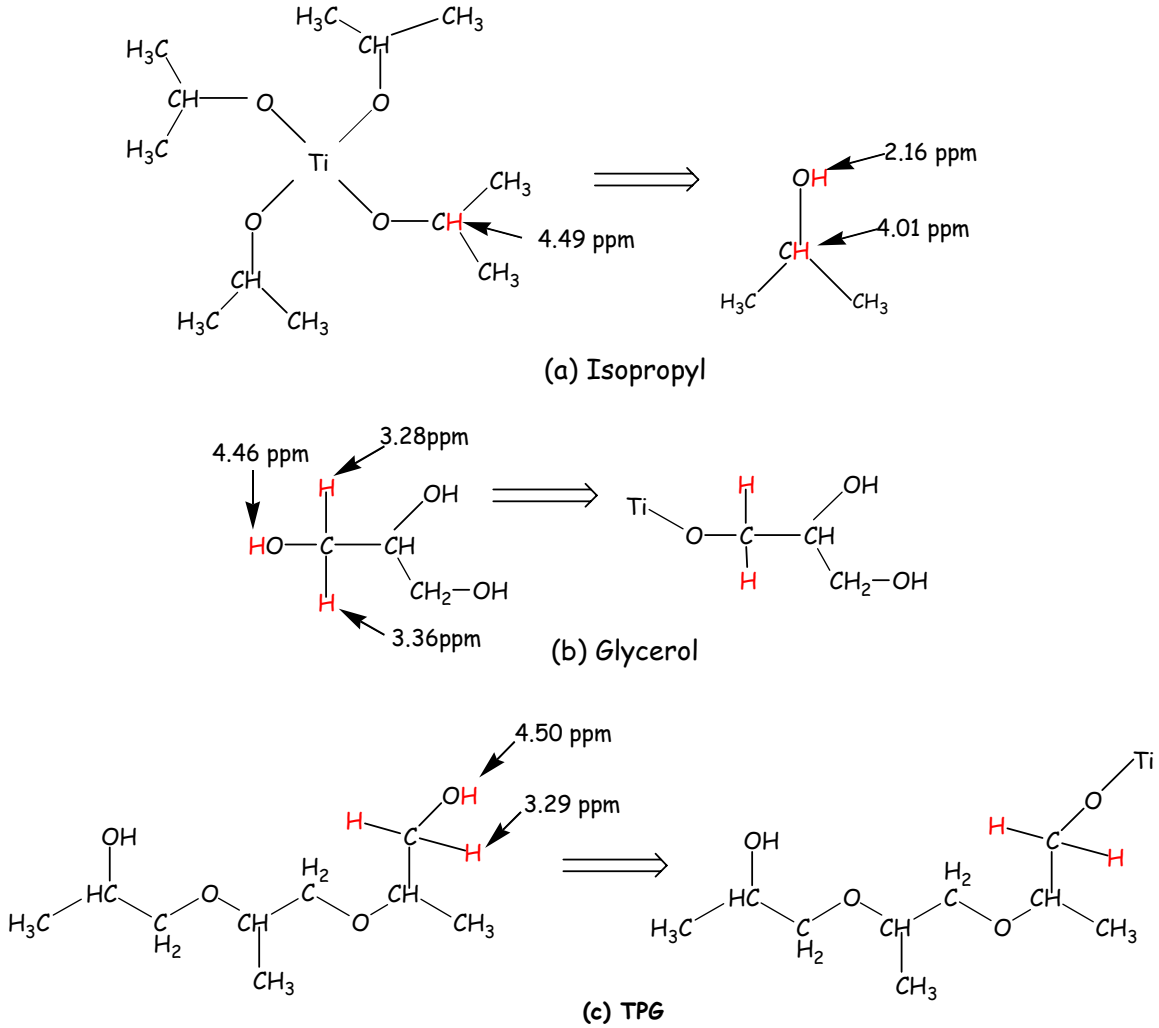

Figure 5-16: Chemical shift changes expected for 'H NMR of sol-gel

With the exception of the -OH on unbound IPA, all alcoholic protons and protons associated with Ti-O-R linkages resonate above 4ppm. Therefore, the most significant changes in the spectrum of the melt-point depressant were expected in this region. The peak at 4.49 ppm in the spectrum for the MPD corresponds to the Ti-O-CH resonance in TIP. There is also an –OH resonance at 4.50ppm associated with TPG, which may overlap with this peak. The intensities of both of these resonances are expected to decrease with the substitution of TPG. The MPD peak which appears at 4.43ppm is most likely due to the secondary alcoholic proton on TPG, which resonates at 4.44ppm with possibly some overlap from the alcoholic proton on glycerol, which resonates at 4.46 ppm. It could also be due to the Ti-O-CH resonance of glycerol as it adds to the titanium. The proton trans to the secondary alcohol resonates at a higher frequency than the proton in the cis position. The peak at 4.36 ppm is not present in any of the reactant spectra (negligible in TPG) and is associated with Ti-R-CH resonances that result from the addition of TPG and glycerol to titanium. The intensity of this peak is expected to increase with the substitution of TPG. These peak assignments were used to identify differences in the spectra obtained for the melt-point depressant synthesized under different conditions.

Spectra for the melt-point depressant synthesized under different conditions are shown in figure 5-17. While peaks overlap and were not integrated separately, the relative intensities of peaks in the region above 4ppm were used to assess differences in the substitution behavior. The peak at 4.49 ppm is much less intense in the spectra where glycerol was added last, reflecting greater substitution of the isopropyl groups in these systems as the model predicts. Little difference is observed in the peak at 4.43 ppm, as expected based on the peak assignments. The intensity of unbonded alcoholic protons did not change and the amount of glycerol bonded in the system was not expected to change. On the other hand, the relative intensity of the peak at 4.36ppm increases as the reaction conditions were changed. Based on the peak assignments, this indicates a greater degree of TPG substitution and supports the model's prediction.

Also considered in these spectra were the relative intensities of peaks in three different regions. As described previously, methyl protons are found in the area of ~ 1ppm, CH and CH_2 protons are found between 3 and 4 ppm, and –OH and Ti-O-CH protons are found above 4ppm.

The number of protons expected in each region varies depending on the nature of the system. Table 5-14 shows the number of protons expected in each of the three regions for multiple systems. The systems described are all extremes. The melt-point depressant samples were expected to contain a mixture of all the described bonds to varying degrees.

Table 5-14 indicates that a noticeable decrease in the $-CH_3$ concentration is expected when IPA has left the system. As discussed in reference to FT-IR data, a decrease in IPA corresponds to a system with a greater degree of precursor modification, i.e. substitution of isopropyl groups with glycerol and TPG. Figure 5-17 shows a marked decrease in the intensity of the methyl protons for the system where glycerol was added last under ambient conditions. This confirms the previous conclusion that greater precursor substitution results in more efficient removal of IPA. The systems synthesized under nitrogen show a similar trend, a decreased concentration of methyl protons for the system where glycerol was added last.

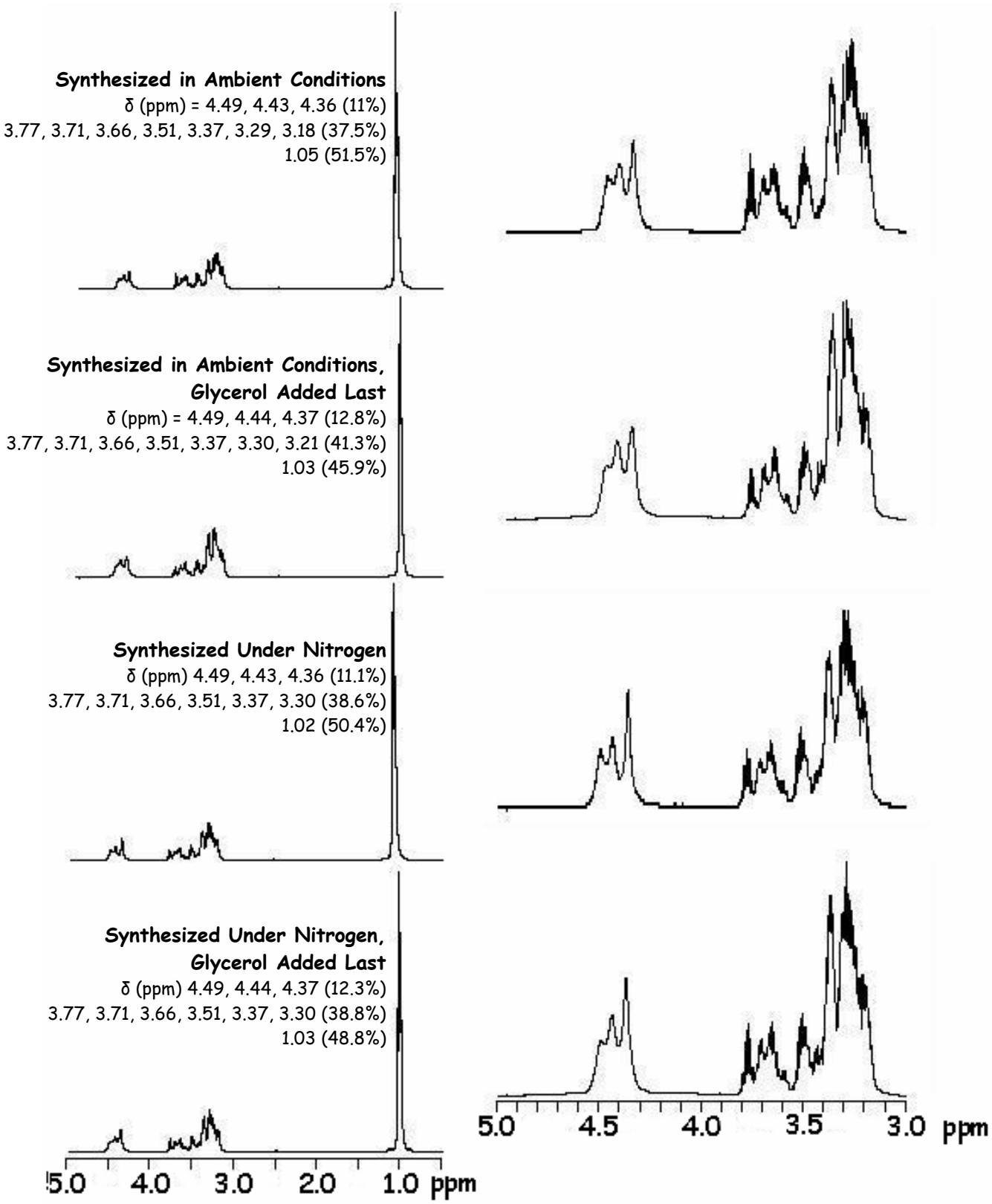

Figure 5-17: ^{1}H NMR spectra for melt-point depressant synthesized under different conditions

Table 5-14: Signals Expected in Various Systems Analyzed with ^1H NMR

System (Number of Protons)	-O**H**	Ti-O-C**H**	Total > 4ppm	- C**H** and $-CH_2$ (3-4ppm)	$-CH_3$ (~ 1ppm)
IPA Bound (96)	9	4	13 (13.5%)	32 (33.3%)	51 (53.1%)
IPA Unbound (96)	5 (+4 IPA)	8	13 (13.5%)	28 (29.1%)	51 (53.1%)
No IPA (64)	5	8	13 (20.3%)	24 (37.5%)	27 **(42.2%)**
All Ti-O-Ti (with IPA) (96)	9 (+4 IPA)	0	9 (9.4%)	32 (33.3%)	51 (53.1%)
All Ti-O-Ti (no IPA) (64)	9	0	9 (14.1%)	28 (33.3%)	27 **(42.2%)**
All Ti-R-Ti (with IPA) (96)	5 (+4 IPA)	8 per Ti	13 (13.5%)	28 (29.1%)	51 (53.1%)
All Ti-R-Ti (no IPA) (64)	5	8 per Ti	13 (20.3%)	24 (37.5%)	27 **(42.2%)**

'IPA Bound' describes a system where the isopropyl groups remain bound to the titanium; TPG and glycerol are in the system, but unreacted

'IPA Unbound' describes a system where TPG and glycerol have substituted the isopropyl groups bound to the titanium; assumes the primary alcohol group on TPG binds preferentially, free IPA remains in the system.

'No IPA' describes a system where TPG and glycerol have substituted the isopropyl groups bound to the titanium; assumed the primary alcohol group on TPG binds preferentially, IPA has diffused out of the system and is no longer present.

'All Ti-O-Ti (with IPA)' describes a system where complete condensation has occured; free IPA remains in the system

'All Ti-O-Ti (no IPA)' describes a system where complete condensation has occurred; IPA has diffused out of the system and is no longer present.

'All Ti-R-Ti (with IPA)' describes a system where complete condensation has occurred resulting in Ti-R-Ti bonds; calculations based on one glycerol and one TPG molecule bound per Ti atom, two free TPG molecules per Ti atom, free IPA remains in the system

'**All Ti-R-Ti (no IPA)'** describes a system where complete condensation has occurred resulting in Ti-R-Ti bonds, calculations based on one glycerol and one TPG molecule bound per Ti atom, two free TPG molecules per Ti atom, free IPA has difused out of the system and is no longer present

A greater degree of substitution was expected for systems synthesized under nitrogen; however, this was not reflected by the concentration of methyl protons. This result could be explained by the fact that the melt-point depressant was never exposed to the atmosphere; the gel was transferred from the flask under nitrogen directly to the NMR tube where it was dissolved in deuterated solvent. Rather than evaporating into the atmosphere, free IPA remained within the gel.

^{13}C NMR was also performed in attempt to gain additional information regarding this sol-gel system. This technique proved less useful, because the intensity of ^{13}C NMR peaks cannot be correlated with the number of carbons associated with them. Spectra were taken in order to identify peak shifts between bound and unbound species. Figure 5-18 shows carbons expected to exhibit a chemical shift when reacted with TIP. However, these chemical shifts were not observed. All of the peaks present in the melt-point depressant spectrum were also present in the reactant spectra with the exception of a peak associated with free IPA.

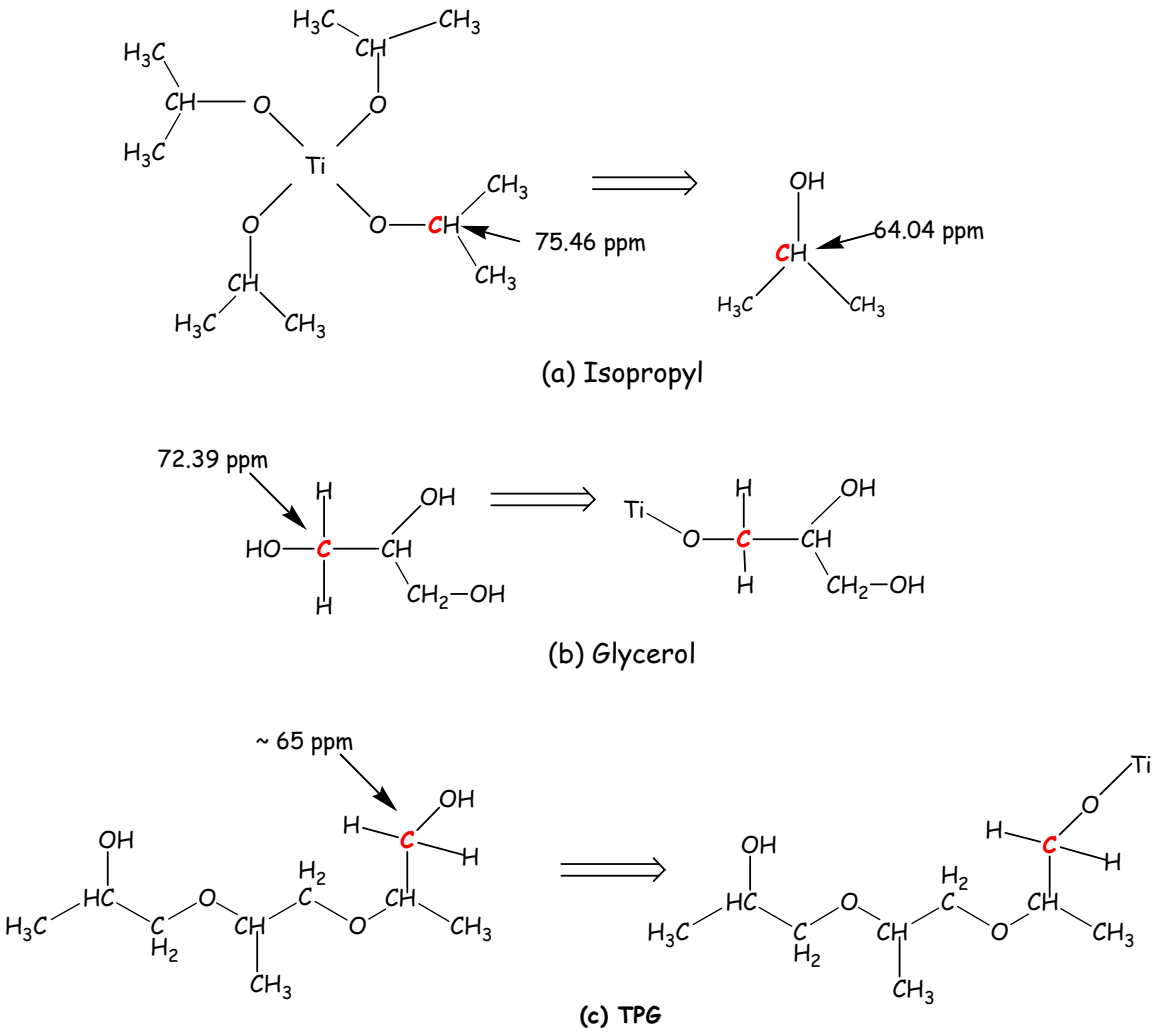

Figure 5-18: Chemical shift changes expected for ^{13}C NMR of sol-gel

Further investigation with NMR techniques such as Heteronuclear Shift Correlation (HETCOR), ^{47}Ti or ^{49}Ti NMR, possibly coupled with ^{17}O NMR would likely provide more information regarding the sol-gel chemistry. A two-dimensional NMR experiment using titanium and oxygen nuclei was proposed in order to track changes in the Ti-O bonds. However, the probes needed for this

experiment were not available. Because ^{13}C NMR did not yield any additional information, the spectra are not shown.

5.4 Mass Loss Kinetics

Mass loss measurements were performed on the melt-point depressant synthesized under different conditions in order to determine what effects, if any, chemistry had on the mass loss behavior. Figure 5-19 shows initial data for the four systems presented earlier:

(1) Melt-point depressant synthesized under ambient conditions

(2) Melt-point depressant synthesized under ambient conditions; glycerol added after TPG allowed to react for approximately one minute

(3) Melt-point depressant synthesized under N_2 to limit hydrolysis; system exposed to atmosphere after approximately 30 minutes

(4) Melt-point depressant synthesized under N_2; glycerol added after TPG allowed to react for approximately one minute; system exposed to atmosphere after approximately 30 minutes

In addition, data obtained for two other systems are presented:

(5) Melt-point depressant synthesized under N_2 to limit hydrolysis; system exposed to atmosphere after approximately 24 hours

(6) Melt-point depressant synthesized under N_2, glycerol added after TPG allowed to react for approximately one minute; system exposed to atmosphere after approximately 24 hours.

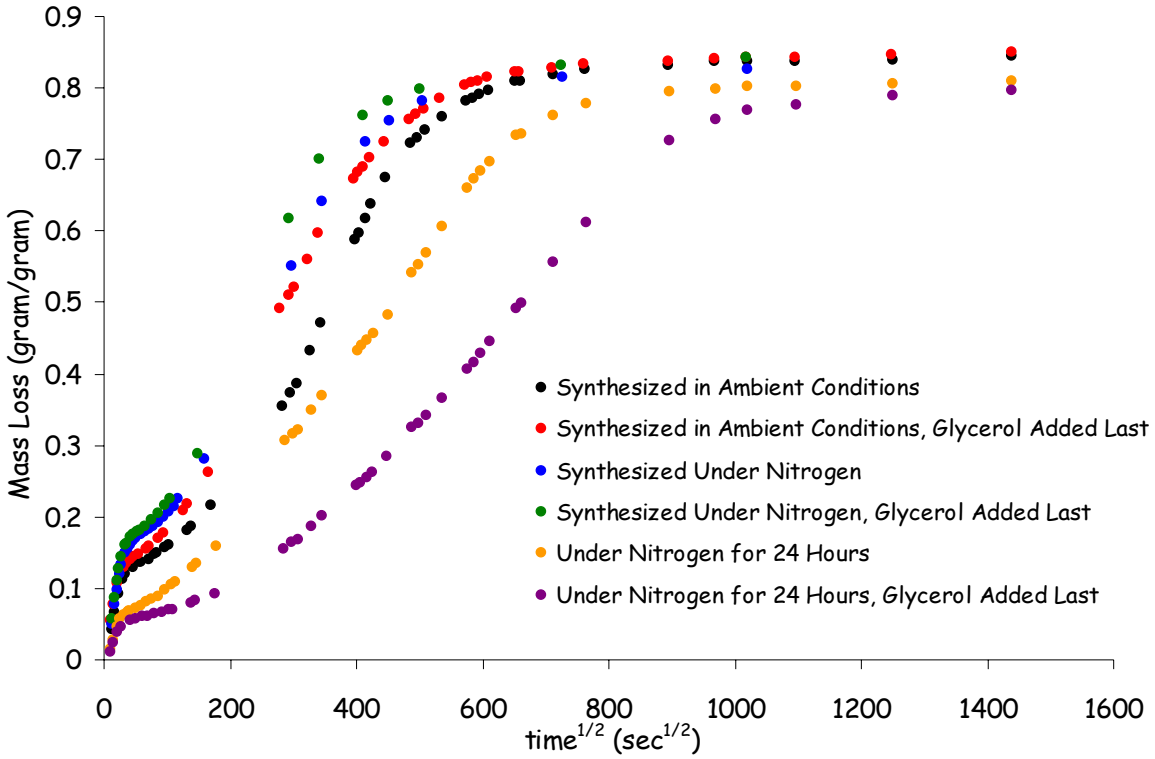

Figure 5-19: Mass loss kinetics at 70°C for melt-point depressant synthesized under different conditions

FT-IR data presented earlier in this chapter indicates that the number of Ti-O-R-O-Ti bonds (R = glycerol, TPG) in the system increases with time under nitrogen. This reaction consumes TPG and glycerol, which reduces the amount

that can be released. The presence of these crosslinks could also slow down the diffusion process.

The samples left under nitrogen for 24 hours were prepared in a different container and did not achieve a thin film geometry. When removed, they were a solid gel, which was cut into particles and placed in a Petri dish for mass-loss measurements (figure 5-20). The diffusion geometry for these 'particulate' samples is different than that of the other samples which remained monolithic thin films throughout most of the sol-gel process. Thus, mass loss data for the particulate samples may not be directly comparable to the other samples.

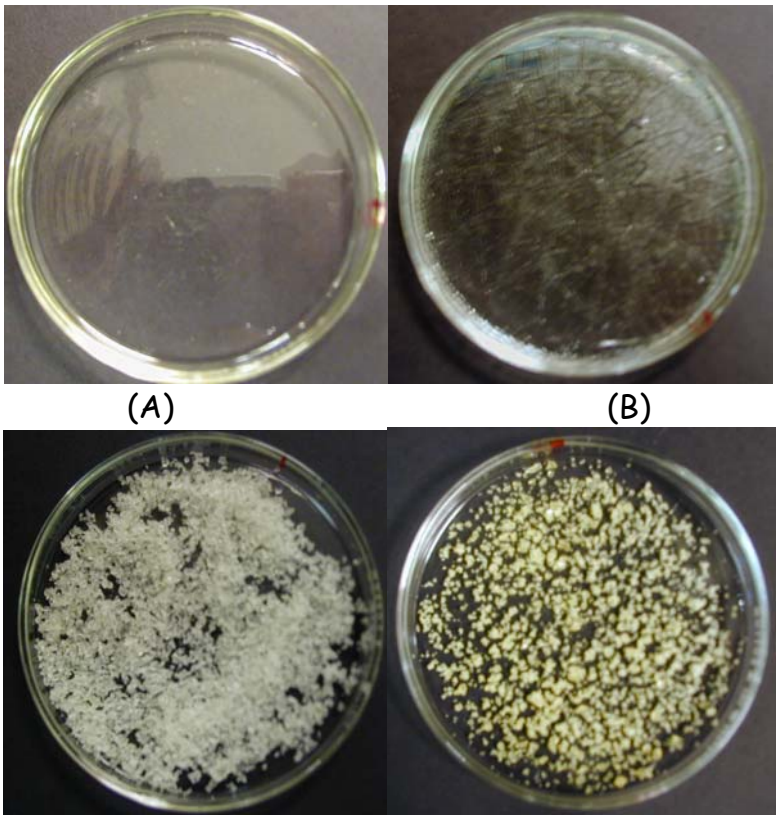

(A) (B)

(C) (D)

Figure 5-20: Physical changes in melt point depressant
(A) melt-point depressant immediately after mixing in ambient conditions
(B) after 3 Days at 70°C
(C) melt-point depressant after stirring under nitrogen for 24 hours
(D) after an additional 3 Days at 70°C

The data presented in figure 5-19 for samples at 70°C indicate that all samples exhibit three regions of mass loss. The particulate samples exhibit slower diffusion than the other samples, which may be due to either the particulate geometry of these samples or differences in their chemical structure. The diffusion distance in the particulate samples was approximated as the particle

radius. The average radius was determined to be 0.3 – 0.4 mm, significantly less than the diffusion distance of 0.5 mm measured for the thin film samples. Based on both the shorter diffusion distance and the greater surface area associated with their geometry, the particulate samples were expected to exhibit greater mass loss rates than thin films of the same composition. The slower mass loss kinetics actually observed for these samples could therefore not be attributed to differences in sample geometry. Instead, it was concluded that the higher Ti-O-R-O-Ti crosslink density in the particulate samples is responsible for slowing the diffusion of TPG. If the particulate samples had the same thin film geometry as the other samples in figure 5-19, the mass loss kinetics would be expected to be even slower than shown in this figure.

Excluding the particulate samples, figure 5-19 indicates minimal differences in mass loss behavior between systems synthesized under different conditions. As in the previous chapter, mass loss was assumed to be diffusion-limited and divided into two regions: diffusion of IPA out of the system and the loss of TPG and glycerol during subsequent sol-gel reactions. Diffusion coefficients for the IPA diffusion regime are reported in table 5-15.

Table 5-15: Diffusion Coefficients for IPA in Sol-Gel System at 70°C

Reaction Conditions	10^6 *D (cm^2/sec)	Mass Loss in First Region (%)
Synthesized in Ambient Conditions	1.52	13.6
Synthesized in Ambient Conditions. Glycerol Added Last	2.34	14.4
Synthesized Under Nitrogen	2.69	16.5
Synthesized Under Nitrogen, Glycerol Added Last	3.58	17.4

Very little difference is seen in the diffusion coefficients between the four systems; they are all within the same order of magnitude. Any trends in diffusion behavior would require multiple measurements made at several different temperatures to determine the activation energies according to: $D=D_0e^{-E/RT}$. Arrhenius plots are shown in the previous chapter for both regions of mass loss associated with the melt-point depressant synthesized under ambient conditions.

Table 5-15 indicates that the systems under nitrogen lost significantly more IPA in this initial region than those synthesized under ambient conditions. The systems in which glycerol was added last also released an increased amount of IPA this initial region, but to a lesser extent. This supports the model's prediction that alcohol exchange reactions involving TPG and glycerol are more efficient for these systems. More highly substituted precursor molecules

release more IPA during the initial part of the reaction. This region of mass loss only indicates the amount of free IPA, which is able to diffuse in the initial stages of the sol-gel process. FT-IR data indicates that the remainder of the IPA is released as the gel ages and dries.

This mass loss information is consistent with FT-IR and ^{1}H NMR data presented in figures 5-10 and 5-17, respectively. These data indicate smaller concentrations of isopropyl groups for both systems synthesized under nitrogen and those where glycerol was added last. While mass loss measurements started immediately after mixing the reactants, spectroscopic techniques could not be performed for at least 30-60 minutes after mixing. Systems with a greater degree of precursor substitution lost a larger concentration of IPA in the time period between mixing and spectroscopic analysis. Consequently, these spectra indicated a smaller IPA concentration.

In addition to diffusion coefficients for IPA, diffusion coefficients were obtained for the second region of mass loss as described in Chapter 4. This region is associated with the loss of TPG, glycerol and the remaining IPA. The mass loss kinetics in this region are complex. However, as described in section

4-3, mass loss kinetics were assumed to be diffusion-limited and fit to a diffusion model.

Table 5-16: Diffusion Coefficients for Final Region of Mass Loss in Sol-Gel System at 70°C

Reaction Conditions	10^8 * D (cm^2/sec)	Final Mass Loss (gram/gram)
Synthesized Under Ambient Conditions	1.25	0.83
Synthesized Under Ambient Conditions, Glycerol Added Last	1.06	0.84
Synthesized Under Nitrogen	1.64	0.84
Synthesized Under Nitrogen, Glycerol Added Last	1.59	0.83

Table 5-16 indicates minimal differences in the diffusion coefficients associated with the final region of mass loss for systems synthesized under different conditions. A few small differences are noted. However, additional experiments are required in order to confirm any trends. These data indicate slightly faster diffusion for the systems synthesized under nitrogen compared to those synthesized in ambient conditions. This supports the previous assumption that diffusion is the rate-limiting process. If mass loss in the sol-gel system were reaction-limited, systems with greater precursor substitution should exhibit slower mass loss. Diffusion, on the other hand, would be faster in these systems due to the lower concentration of Ti-O-R-O-Ti crosslinks.

However, all mass loss measurements were performed on thin films of melt-point depressant with large surface area to volume ratios. With this sample geometry, a large percentage of the gel was exposed to water in the atmosphere. Hydrolysis would be less rapid in bulk sol-gel systems with smaller surface area to volume ratios and consequently less exposure to water. Kinetic factors may become more evident in those systems.

The model also suggests that a change in the reaction conditions would affect the amount of TPG and glycerol released during the sol-gel reaction. As described earlier, the reaction conditions affect the extent of precursor substitution and consequently the degree of Ti-O-R-O-Ti crosslinking. Limiting the concentration of TPG and glycerol bound in crosslinks should maximize the amount released to the coating surface during condensation. Table 5-16 does not indicate any significant changes in the final percent mass loss determined for all four systems.

The ultimate mass loss percentages reported in table 5-16 reflect IPA, TPG and glycerol losses after data collection began; they do not reflect mass loss (primarily IPA), which may have occurred after initial mixing of the reactants

but before data collection began. The mass loss values reported for both regions of mass loss could therefore be misleading. Different amounts of IPA were most likely lost during this initial time period for each of the different systems. Theoretically, systems that yielded greater precursor substitution would release a greater amount of IPA upon mixing and yield deceptively low values for the amount of mass loss in both regions analyzed. However, no definitive conclusions can be drawn regarding the amount of TPG and glycerol released in each of these systems. Thermogravimetric Analysis was performed to gather more information about mass loss behavior.

Thermogravimetric Analysis

Thermogravimetric Analysis (TGA) was performed on the melt-point depressant synthesized under different conditions in order to observe differences in mass loss behavior. Because each component has a different volatility, TGA has the ability to separate mass loss due to each component. In contrast to the isothermal mass loss data presented earlier which reports mass loss as a function of time, TGA data reflects the mass remaining at each temperature ranging from 25 to 400°C. Figure 5-23 shows three main regions of mass loss, the slow loss of IPA at approximately 72°C, the loss of TPG and glycerol

starting at around 200°C, and then the decomposition of additional organics in the system above 300°C. The organics which remain in the system above 300°C were assumed to be bound to the system through Ti-O-R-O-Ti crosslinks.

Figure 5-21 shows that mass loss in the region of 82°C is greater for systems synthesized under ambient conditions (see inset plot). This supports the previous conclusion that IPA is released much faster for systems where greater precursor substitution is achieved. Systems synthesized under nitrogen undergo a greater degree of substitution before hydrolysis and condensation occur. Consequently, a greater amount of IPA is released in the time between synthesis and TGA analysis (approximately 30-60 minutes) and the TGA scan indicates less IPA in the system.

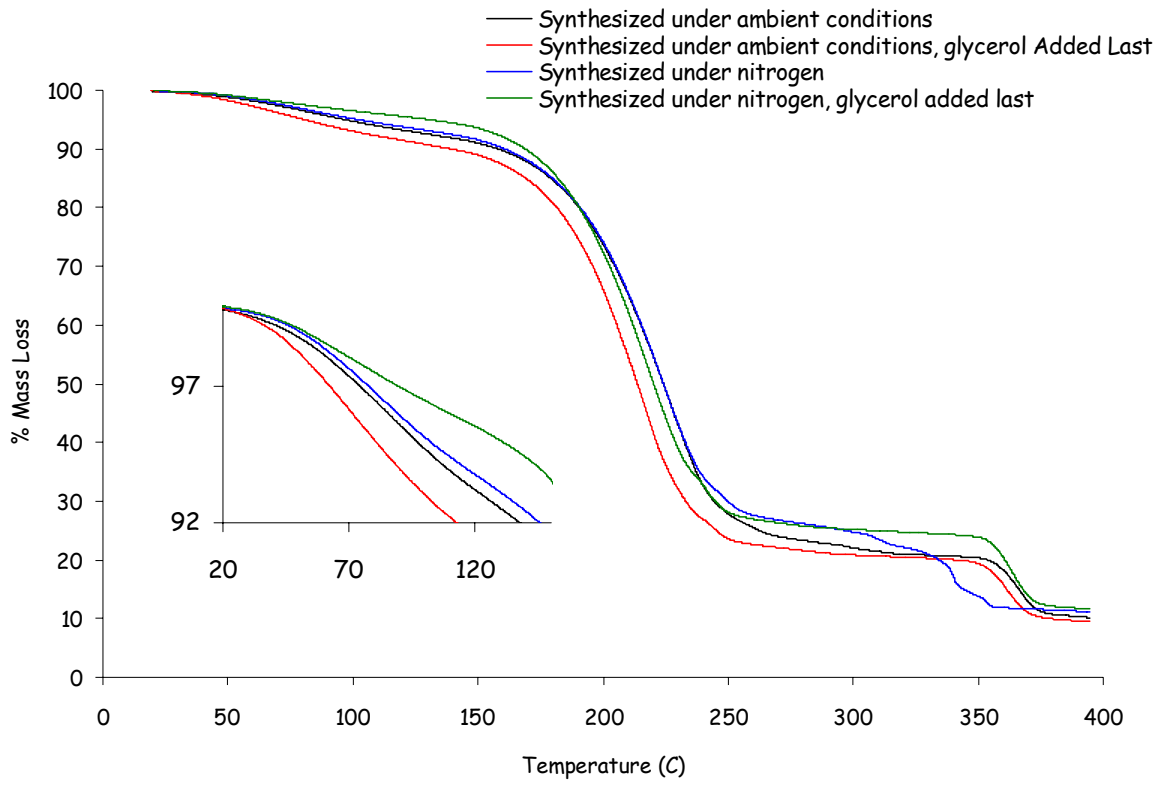

Figure 5-21: Thermogravimetric analysis of melt-point depressant synthesized under different conditions

Because some systems lost significantly more IPA in the period between mixing TGA analysis, the remainder of the mass loss calculations made from this data are slightly misleading. Table 5-17 shows calculated mass percentages for all of the reaction products differ significantly depending on the amount of IPA present when measurements begin. IPA constitutes approximately 25% of the system's mass; therefore, uncertainty in its concentration leads to a significant amount of error in observed mass loss values.

Table 5-17: Calculated Mass Percentages for Sol-Gel System

Reactants			Products		
Compound	**Mass (g/mol)**	**% Mass**	**Compound**	**Mass (g/mol)**	**Observed % Mass**
TIP (1 mole)	284.2	29.8 %	IPA (4 moles)	4 * 60.1	0 - 25.2 %
TPG (3 moles)	3 * 192.3	60.5 %	TPG (3 moles)	3 * 192.3	60.5 – 80.9 %
Glycerol (1 mole)	92.1	9.7 %	Glycerol (1 mole)	92.1	9.7 – 12.9 %
			TiO_2 (1 mole)	79.9	8.4 – 11.2 %
Total	953.2	100%	Total	953.3	100%

Table 5-17 compares these calculated values to those measured in both the TGA scans and the isothermal mass loss kinetics reported in the previous section. Most notable is the difference in IPA percentage between the two measurement techniques, which again reflects IPA lost in the time between synthesis and TGA analysis.

Unlike the isothermal mass loss measurements, TGA analysis distinguishes between TPG and glycerol mass loss and indicates the extent of Ti-O-R-O-Ti crosslinks in the system. It is assumed that the decomposition, which occurs above 300°C is the result of broken Ti-O-R-O-Ti linkages. The model predicts a higher concentration of these linkages in systems with greater precursor substitution. The values determined from TGA data are listed in table 5-18;

however, they are inconclusive due to uncertainty in the IPA concentrations. Greater mass loss percentages associated with Ti-O-R-O-Ti crosslinks were measured for samples prepared under nitrogen, which contradicts the model's prediction. However, these systems had lower IPA concentrations when measurements began so mass loss values obtained from these scans are deceptively high and percentage comparisons are not valid.

Table 5-18: Observed Mass Percentages Loss for Sol-Gel System

	Calculated Values (%)	**Ambient (%)**		**Ambient; Glycerol Added Last (%)**		**Nitrogen (%)**		**Nitrogen; Glycerol Added Last (%)**	
		TGA	Iso-therm	TGA	Iso-therm	TGA	Iso-therm	TGA	Iso-therm
IPA	0-25	8.2	14	10.1	14	7.6	17	5.6	17
TPG	60-81	63.9	69	63.0	70	58.2	67	61.6	66
Glycerol	10-13	3.9		4.3		6.6		6.5	
Ti-ORO-Ti		13.8	17	13.0	16	16.4	16	14.5	17
Final (TiO_2)	8-11	10.2		9.6		11.2		11.8	

The derivative of the mass loss was calculated at each point in figure 5-21 and is shown in figure 5-22, which indicates the rate of mass loss at each temperature. Separate peaks were observed for loss of IPA, TPG and glycerol at approximately 72, 200 and 245°C, respectively. The peaks were identified

by their size and proximity to the boiling points of each species, 82, 273 and 290°C respectively for IPA, TPG and glycerol.

Figure 5-22 shows the loss of IPA is slightly greater for systems synthesized under ambient conditions as discussed above. Slightly greater losses are observed for both TPG and glycerol for systems in which glycerol was added last. This suggests greater concentrations of singly-bound TPG and glycerol in these systems. The system where all reactants were added simultaneously under ambient conditions shows negligible loss of glycerol in this region suggesting, as the model predicts, most of the glycerol is bound in Ti-O-R-O-Ti crosslinks.

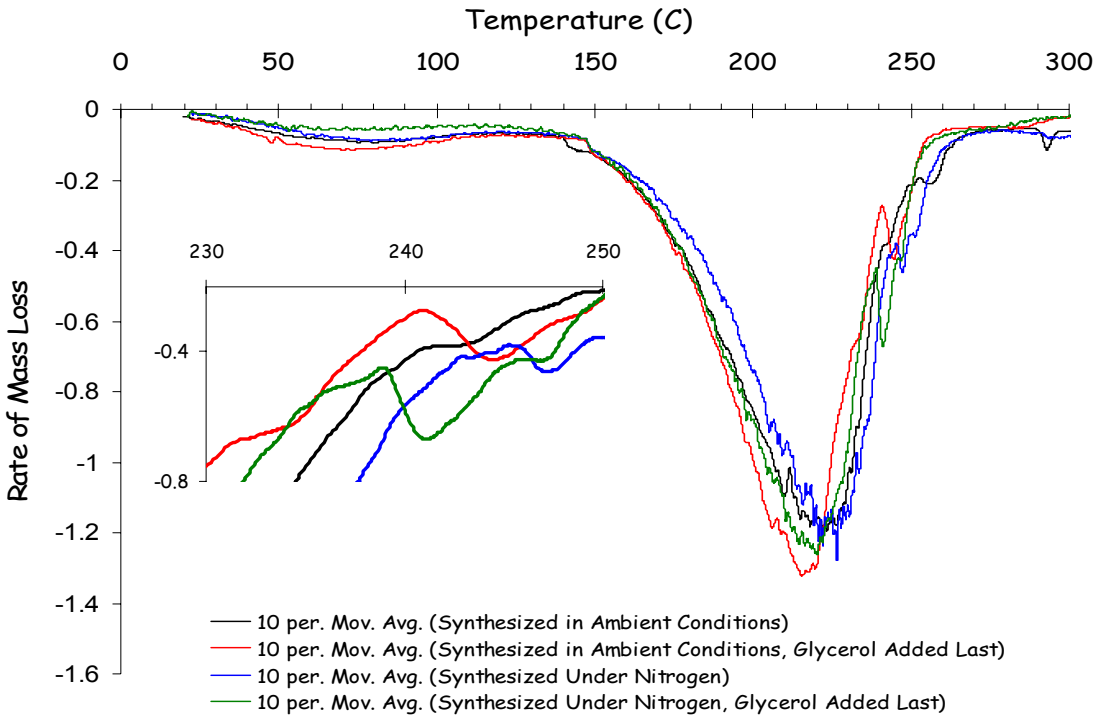

Figure 5-22: Thermogravimetric analysis of melt-point depressant synthesized under different conditions*

* the notation '10 per. Mov. Avg.' indicates data has been smoothed

5.6 Summary and Conclusions

Preliminary FT-IR data indicated that complete condensation did not occur within the melt-point depressant and glycerol remained bound in the gel. Livage and Henry's predictive model for inorganic polymerization was applied to the system in order to explain this phenomenon.[22]

The model indicated that when synthesized under ambient conditions, limited precursor substitution occurs. Both glycerol and water have a stronger affinity for TIP than TPG and as a result a significant amount of TPG remains unreacted within the gel. In this system, alkoxide sites that do not undergo substitution are susceptible to attack by the free end of a glycerol molecule already bound in the gel. This results in Ti-glycerol-Ti crosslinks, which do not undergo condensation and remain bound within the melt-point depressant on drying.

The reaction conditions were altered in order to maximize precursor substitution and limit the concentration of Ti-O-R-O-Ti crosslinks. The model predicted that synthesizing the melt-point depressant under nitrogen and adding glycerol after TPG was allowed to react would maximize precursor substitution yielding a more uniform gel with a high concentration of bound TPG and limited Ti-O-R-O-Ti crosslinks.

FT-IR, NMR and TGA analysis confirm the model's prediction. Limiting hydrolysis by synthesizing the gel under nitrogen appeared to have a greater effect than adding glycerol after TPG was allowed to react for a few minutes.

Despite the different chemistries observed for systems synthesized under different conditions, minimal differences were observed in the mass loss kinetics. The rates were approximated by fitting mass loss data in two different regions to a diffusion model. Data supported the assumption that diffusion is the rate-determining process. Significant differences in reaction kinetics were expected for systems with different chemistries. However, minimal differences were observed between calculated diffusion coefficients. In addition, the small differences observed in the diffusion coefficients indicate faster mass loss for systems synthesized under nitrogen. These systems have smaller concentrations of Ti-O-R-O-Ti crosslinks, which inhibit diffusion.

Although not conclusive, the data presented here suggest that the slow release of TPG and glycerol is controlled by the diffusion of entrapped molecules out of the sol-gel network as illustrated in figure 1-10. The chemistry of the melt-point depressant complex and the degree of precursor substitution affects the structure of the network as shown in figure 1-11-A. This structure, in particular the presence of Ti-O-R-O-Ti crosslinks, can affect the diffusion

behavior. Other than that, the chemistry of the sol-gel should not have a significant effect on the mass loss kinetics.

The 3:1 ratio of TPG:glycerol was chosen empirically, because this ratio yielded the best coating performance (section 1.5). This can be rationalized by the fact the majority of glycerol remains bound to the network, limiting condensation and creating a less dense network. This facilitates diffusion of TPG from the network. In the absence of glycerol, the network would be more highly crosslinked and a higher concentration of TPG should remain entrapped in the network. On the other hand, higher concentrations of glycerol would create a significantly less dense network resulting in faster diffusion. In addition, a smaller concentration of TPG would be released to the surface. Both of these factors would limit the performance lifetime of these coatings.

6. Summary and Conclusions

The coating design, consisting of sub-micron sized phase domains of a hydrophobic matrix and a multi-component melt-point depressant proved effective in preventing the nucleation and adhesion of ice. The multi-component melt-point depressant consisted of a sol-gel system designed to facilitate the slow-release of TPG and glycerol to the coating surface. The hydrophobicity of the matrix was verified using contact angle goniometry and the coating morphology was analyzed using SEM, EDS and AFM techniques.

Mass loss in the two coating formulations was assumed to be diffusion-limited. Arrhenius behavior was observed for the diffusion coefficients of both coating formulations with activiation energies of 21.3 and 22.4 kcal/mol respectively for formulations A and B. While the activation energies for both formulations were comparable, formulation A exhibited diffusion coefficients greater than those obtained for formulation B by approximately a factor of two, indicating that additives can be used to control the mass loss behavior in the coatings.

Mass loss behavior in the melt-point depressant exhibited three regions, the loss of IPA, the loss of TPG and glycerol, and then structural relaxation of the

gel. TGA indicated a fourth region of mass loss at high temperatures associated with the decomposition of organics remaining in the sol-gel network, specifically glycerol bound in Ti-O-R-O-Ti crosslinks. It was assumed that diffusion was the rate-determining process in the loss of IPA and the subsequent loss of TPG and glycerol and mass loss data in both these regions were fit to a diffusion model. Because the majority of mass loss was associated with the loss of TPG and glycerol, it was determined to be most significant to the mass loss properties of the coatings. Mass loss in this region exhibited Arrhenius behavior with an activation energy of 25.1 kcal/mol.

The chemistry of the melt-point depressant complex was predicted using Livage and Henry's model for inorganic polymerization[21] and analyzed using FT-IR, NMR and TGA. Data supported the model's prediction that when TIP is mixed with a 3:1 stoichiometric ratio of TPG:glycerol, the extent of precursor substitution is maximized when the reaction is performed under nitrogen and glycerol is added after TPG has reacted for several minutes. This facilitates the substitution of TPG without competition from glycerol and water, which have higher affinities for TIP. Limiting hydrolysis by synthesizing the gel under nitrogen appeared to have a greater effect than adding glycerol after TPG was allowed to react for a

few minutes. In all sol-gel systems, glycerol remained bound in sol-gel network while TPG was released through condensation reactions.

Despite the different sol-gel structures obtained under different reaction conditions, minimal differences in mass loss kinetics were observed. The small differences that were observed reflected changes in the diffusion environment rather than reaction kinetics, supporting the assumption that mass loss kinetics are diffusion-limited. For the isolated sol-gel, diffusion out of the sol-gel network facilitated the slow release of TPG while diffusion through the coating matrix was rate-determining for the full coating formulations.

While the mechanism for releasing TPG to the coating surface was found different than that on which the coating design was based, it nevertheless proved effective for prevention the nucleation and adhesion of ice on the surface.

7. Future Work

While this study shows that the diffusion of TPG and glycerol out of the matrix can be controlled by including additives that slow down the diffusion process, additional experiments are required to determine the effect of each additive. Systematic variation of coating additives performed in conjunction with performance testing is necessary to correlate diffusion behavior with both the performance and the lifetime of the coating.

Additional experiments could yield more information regarding the structure of the melt-point depressant complex. As discussed in section 5.4, the exact chemistry and structure of the sol-gel could be determined through additional NMR experiments. ^{47}Ti or ^{49}Ti NMR could yield more information about bonds associated with titanium. Heteronuclear Shift Correlation (HETCOR) could also lead o more information about the structure of the sol-gel and verify peak assignments in the ^{1}H NMR spectra. Solution NMR could not be performed at various stages in the sol-gel reaction, because crosslinks limited the solubility of the system. However, a method for performing these measurements in solid-state could reveal how the concentration of bound and unbound IPA, TPG and glycerol change with time.

References

(1) Susan Frankenstein and Andrew M. Tuthill, *"Ice Adhesion to Locks and Dams: Past Work; Future Directions?"* Journal of Cold Regions Engineering **2002**, 16 (2), 83-96.

(2) A.M. Rothrock and R.F. Selden, *"Adhesion of Ice in its Relation to the De-icing of Airplanes"* National Advisory Committee for Aeronautics, Technical Notes #723, **1939**.

(3) US Patent No. 6,693,786

(4) US Patent No. 5,032,641

(5) Ivan A. Ryzhkin and Victor F. Petrenko, *"Physical Mechanisms Responsible for Ice Adhesion"* J. Phys. Chem. B **1997**, 101, 6267-6270.

(6) US Patent No. 5,968,407

(7) US Patent No. 3,940,356

(8) US Patent No. 5,750,047

(9) US Patent No. 6,486,245

(10) Jeffrey C. Brinker, Jeffrey C. and George W. Scherer, *Sol Gel Science: The Physics and Chemistry of Sol-Gel Processing*, Boston Academic Press (1990).

(11) John D. Wright and Nico A.J.M. Sommerdijk, *Sol-Gel Materials, Chemistry and Applications*, Gordon and Breach Science Publishers (2001).

(12) Jerzy Zarzycki, *"Past and Present of Sol-Gel Science and Technology"*, Journal of Sol-Gel Science and Technology **1997**, 8, 17-22.

(13) Chaitanya K. Narula, *Ceramic Precursor Technology and Its Applications*, Marcel Dekker, Inc. (1995).

(14) Helmut Schmidt, *"Preparation, Application and Potential of ORMOCERS"* in *Sol-Gel Science and Technology*, ed. M.A. Aegerter, M. Jafelicci Jr., D.F. de Souza and E.D. Zanotto, World Scientific Publishing (1989).

(15) Karl-Heinz Haas, Sabine Amberg-Schwab and Klaus Rose, *"Functionalized Coating Materials Based on Inorganic-Organic Polymers"*, Thin Solid Films **1999**, 351, 198-203

(16) J. Wen, K. Jordens and G.L. Wilkes, *"Hybrid Organic/Inorganic Coatings for Abrasion Resistance on Plastic and Metal Substrates"*, in *Better Ceramics Through Chemistry VII: Organic/Inorganic Hybrid Materials*, ed. Bradley K. Coltrain, Clement Sahnchez, Dale W. Schaefer and Garth L. Wilkes, Materials Research Society Symposium, 1996.

(17) Zhang, Jun, Shengcheng Luo, Linlin Gui and Youqi Tang, *"Poly(Methyl Methacrylate)-Titania Hybrid Materials by Sol-Gel Processing"*, in *Better Ceramics Through Chemistry VII: Organic/Inorganic Hybrid Materials*, ed. Bradley K. Coltrain, Clement Sanchez, Dale W. Schaefer and Garth L. Wilkes, Materials Research Society Symposium, 1996.

(18) C.S. Deng, P.V. Wright and P.F. James, *"ORMOCER Coatings Based on Titanium and Poly(tetraethylene glycol malonate)"* Journal of Sol-Gel Science and Technology **1998**, 13, 489-493.

(19) C.M. Balik, *"On the Extraction of Diffusion Coefficients from Gravimetric Data for Sorption of Small Molecules by Polymer Thin Films"* Macromolecules **1996**, 29(8), 3025-3029.

(20) Marek W. Urban, *"Vibrational Spectroscopy of Molecules and Macromolecules on Surfaces"* John Wiley & Sons, Inc. (1993)

(21) Livage, J., *"Sol-Gel Chemistry of Transition Metal Oxides"* in *Sol-Gel Science and Technology*, ed. M.A. Aegerter, M. Jafelicci Jr., D.F. de Souza and E.D. Zanotto, World Scientific Publishing (1989).

(22) J. Livage and M. Henry, *"A Predictive Model for Inorganic Polymerization Reactions"* in *Ultrastructure Processing of Advanced Ceramics*, ed. John D. MacKenzie and Donald R. Ulrich (1988).

(23) J. Livage, M. Henry and J. Sanchez, *"Sol-Gel Chemistry of Transition Metal Oxides,"* Prog. Solid St. Chem. **1988**, 18, 259-341

(24) Mackenzie, John D., *"Present and Future Directions in Sol-Gel Science and Technology"*, in *Sol-Gel Science and Technology*, ed. Edward J.A. Pope, Sumio Sakke and Lisa C. Klein, American Ceramic Society, 1995.

(25) Birnie, Dunbar P., III and Norbert J. Bendzko, *"1H and 13C NMR Observation of the Reaction of Acetic Acid with Titanium Isopropoxide"* Materials Chemistry and Physics, **1999**, 59, 26-35.

(26) G.C. Wang, Y.H. Sun and B. Zhong, *"Calculation of Solid Metal Atom's Electronegativity and its Application (II)"* Acta Physico-Chimica Sinica **1998**, 14 (3), 204-209.

(27) Dipankar Datta and S. Nabakishwar Singh, *"Pearson's Chemical Hardness, Heterolytic Dissociative Version of Pauling's Bond-energy Equation and Novel Approach towards Understanding Pearson's Hard-Soft Acid-Base Principle"* Journal of the Chemical Society – Dalton Transactions **1992**, 6, 1541-1549.

(28) Jose L. Gazquez, *"Bond Energies and Hardness Differences"* J. Phys. Chem. A **1997**, 101, 9464-9469.

(29) Stanislaus S. Wong and M.A. Whitehead, *"Calculating Energies and Thermodynamic Relationships of Heteronuclear Diatomic Molecules at Electronegativity Equalization"* Journal of Molecular Structure (Theochem) **1994**, 313, 205-311.

(30) Lynne Reed Murphy, Terry L. Meek, A. Louis Allred and Leland C. Allen, *"Evaluation and Test of Pauling's Electronegativity Scale"* **2000**, 104, 5867-5871

(31) Tapan K. Ghanty and Swapan K. Ghosh, *"Electronegativity, Hardness, and Chemical Binding in Simple Molecular Systems"* **1992**, 31, 1951-1955.

Appendices

Appendices 1-4 contain flowcharts describing reaction paths predicted according to Livage and Henry's Predictive Model for sol-gel systems in four different reaction environments. All possible reaction paths are indicated by a branch in a flowchart as shown in figure 5-9. When a branch ends, no further reactions occur.

Each reaction in the flow chart is accompanied by a factor, Δ^2, which corresponds to the square of the electronegativity difference, $(\chi_{alkoxide} - \chi_{ligand})^2$, and indicates the driving force for the reaction.

Appendix 1: Possible Reaction Paths for Sol-Gel System Synthesized Under Ambient Conditions

Appendix 2: Possible Reaction Paths for Sol-Gel System Synthesized Under Ambient Conditions; Glycerol Added Last

Appendix 3: Possible Reaction Paths for Sol-Gel System Synthesized Under Nitrogen

Appendix 4: Possible Reaction Paths for Sol-Gel System Synthesized Under Nitrogen; Glycerol Added Last

Appendix 1: Possible Reaction Paths for Sol-Gel System Synthesized Under Ambient Conditions

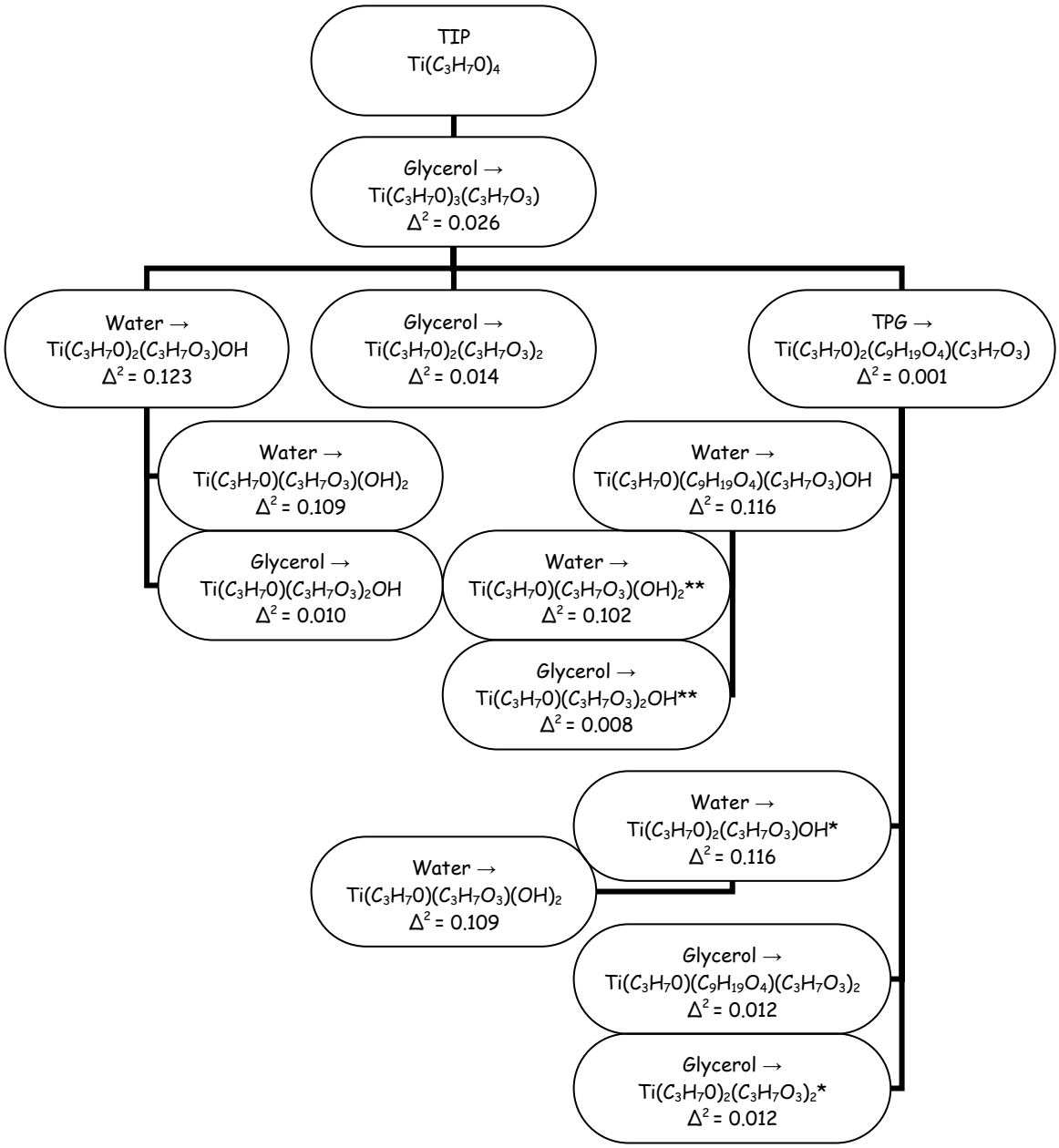

*Substituting group can replace either the isopropyl or the TPG group

Figure A1-1: Possible reaction paths for TIP after initial reaction with glycerol; ambient conditions

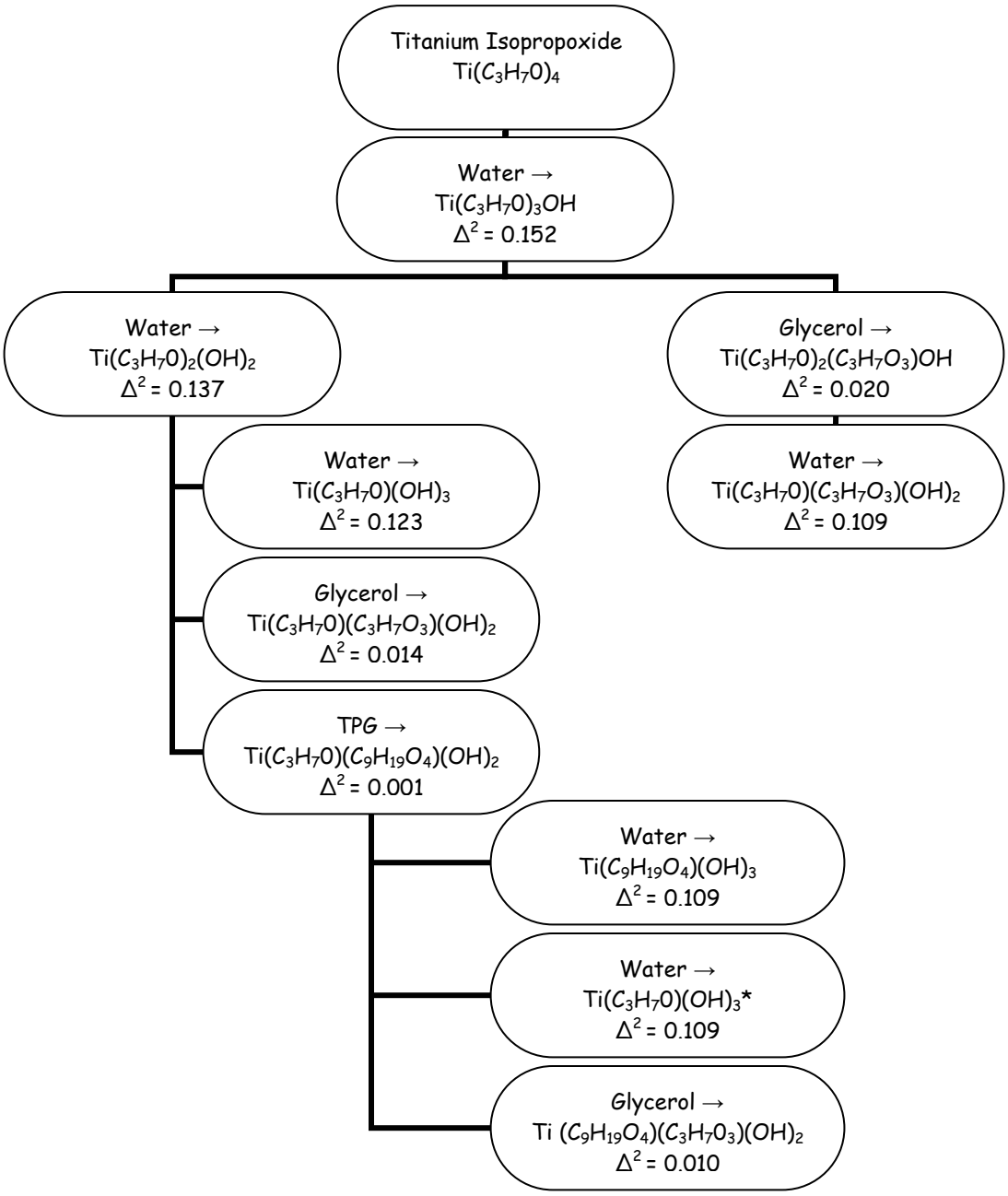

* Water can replace either the isopropyl or the TPG group

Figure A1-2; Possible reaction paths for TIP after initial reaction with water; ambient conditions

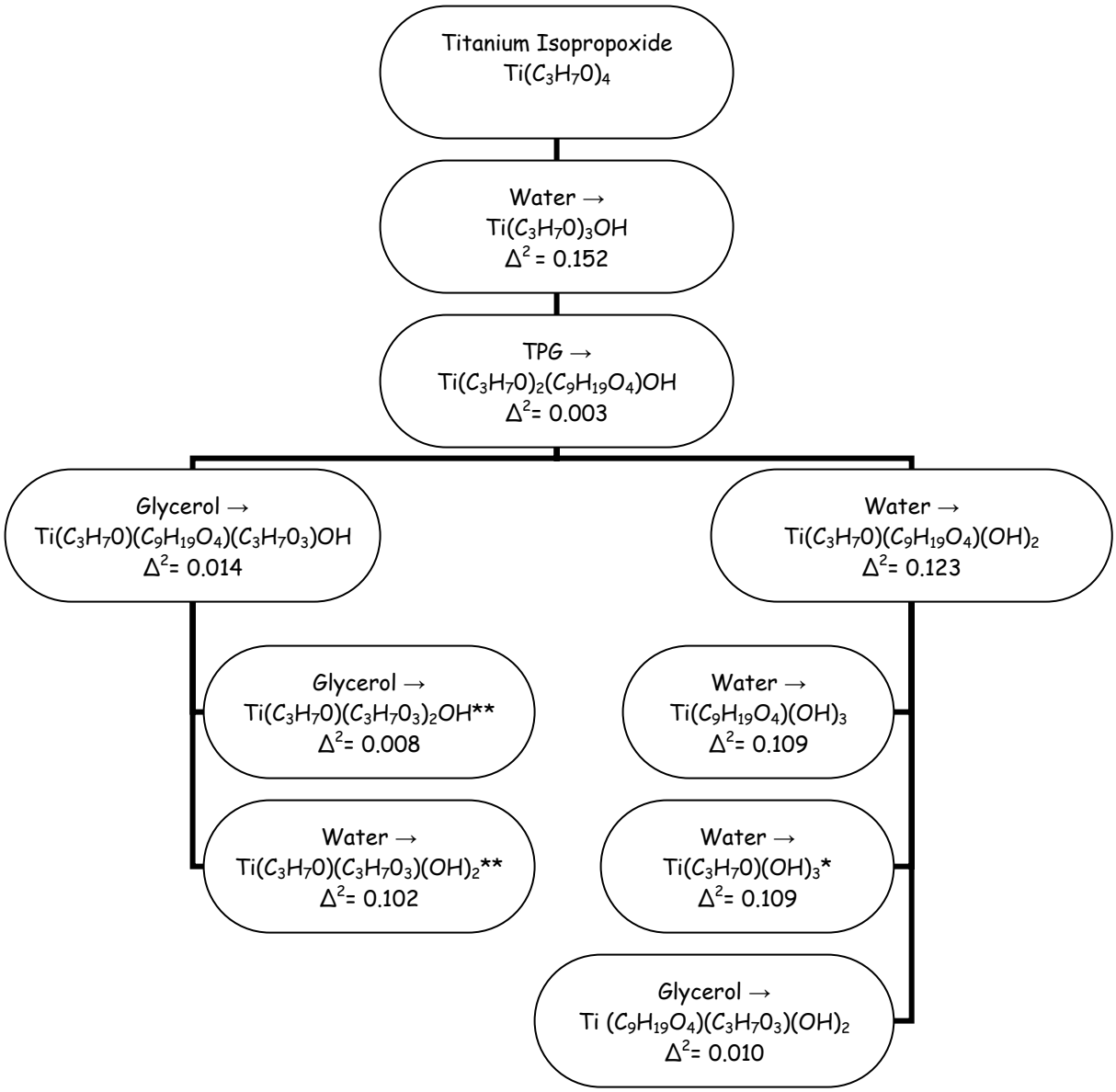

* Water can replace either the isopropyl or the TPG group

** Substituting group replaces the TPG rather than the isopropyl group

Figure A1-3: Possible reaction paths for TIP after initial reaction with water and TPG; ambient conditions

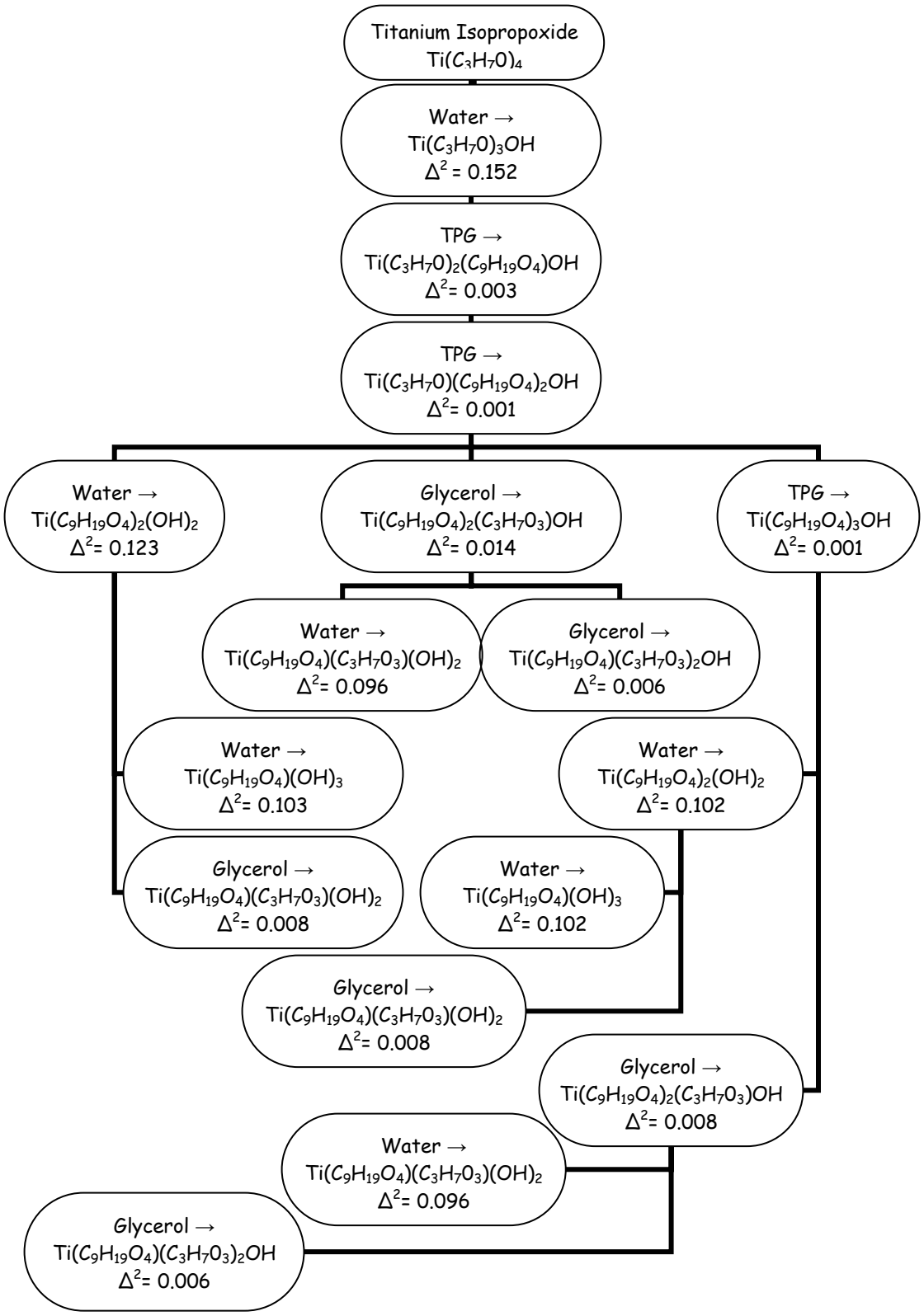

Figure A1-4: Possible reaction paths for TIP after initial reaction with water and two TPG groups; ambient conditions

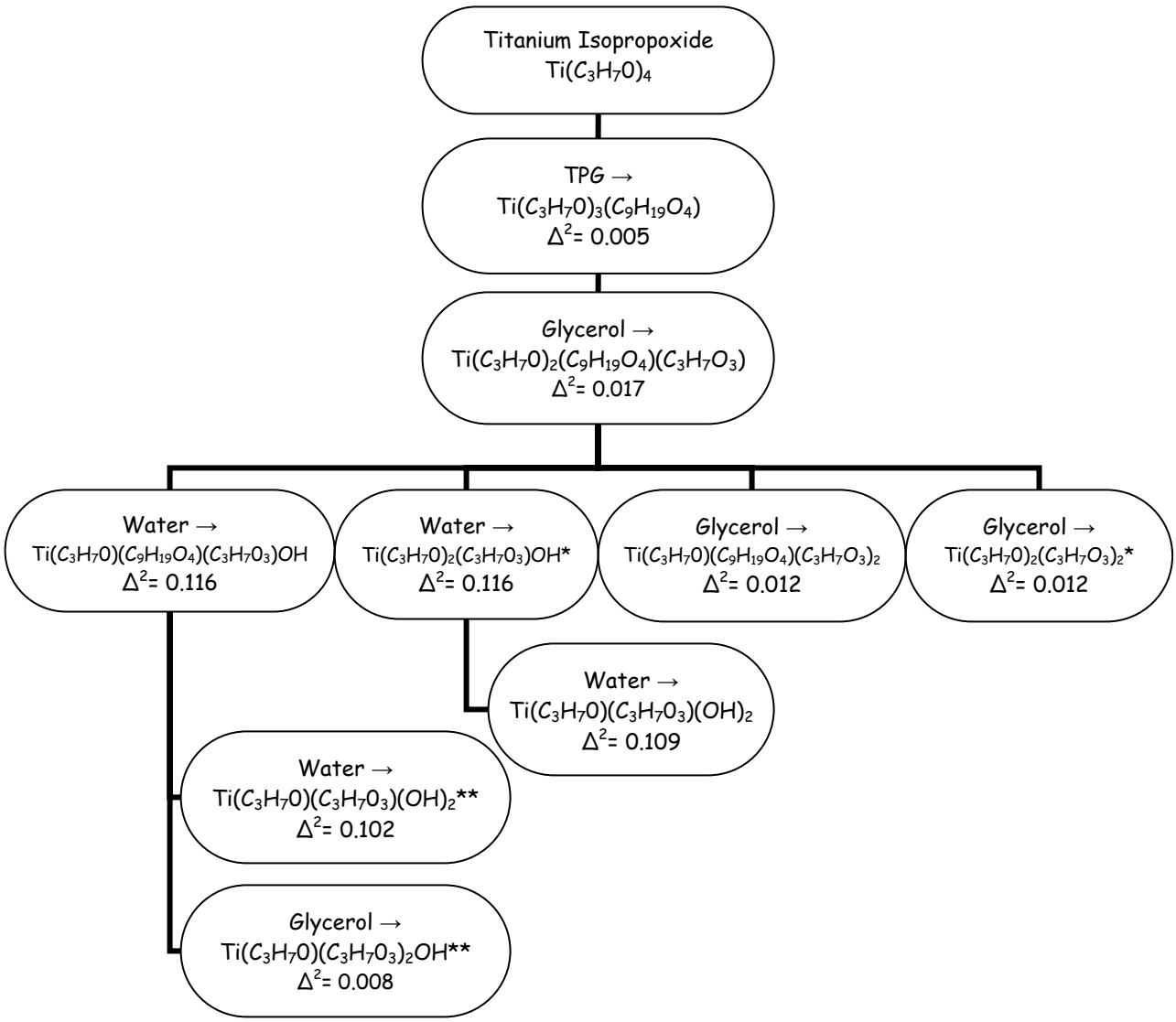

* Water can replace either the isopropyl or the TPG group

** Substituting group replaces the TPG rather than the isopropyl group

Figure A1-5: Possible reaction paths for TIP After initial reaction with TPG and glycerol; ambient conditions

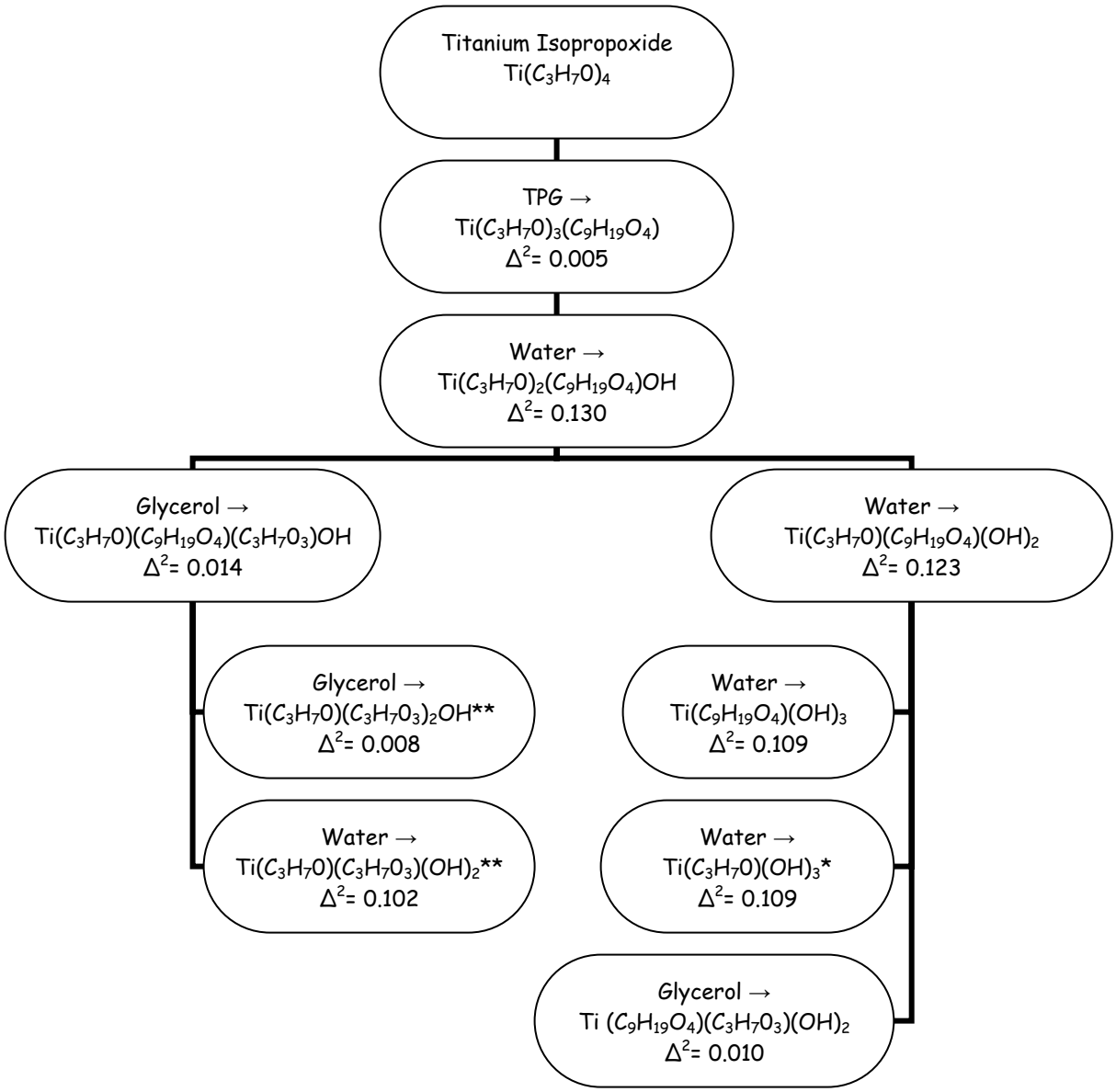

** Substituting group replaces the TPG rather than the isopropyl group

Figure A1-6: Possible reaction paths for TIP after initial reaction with TPG and water; ambient conditions

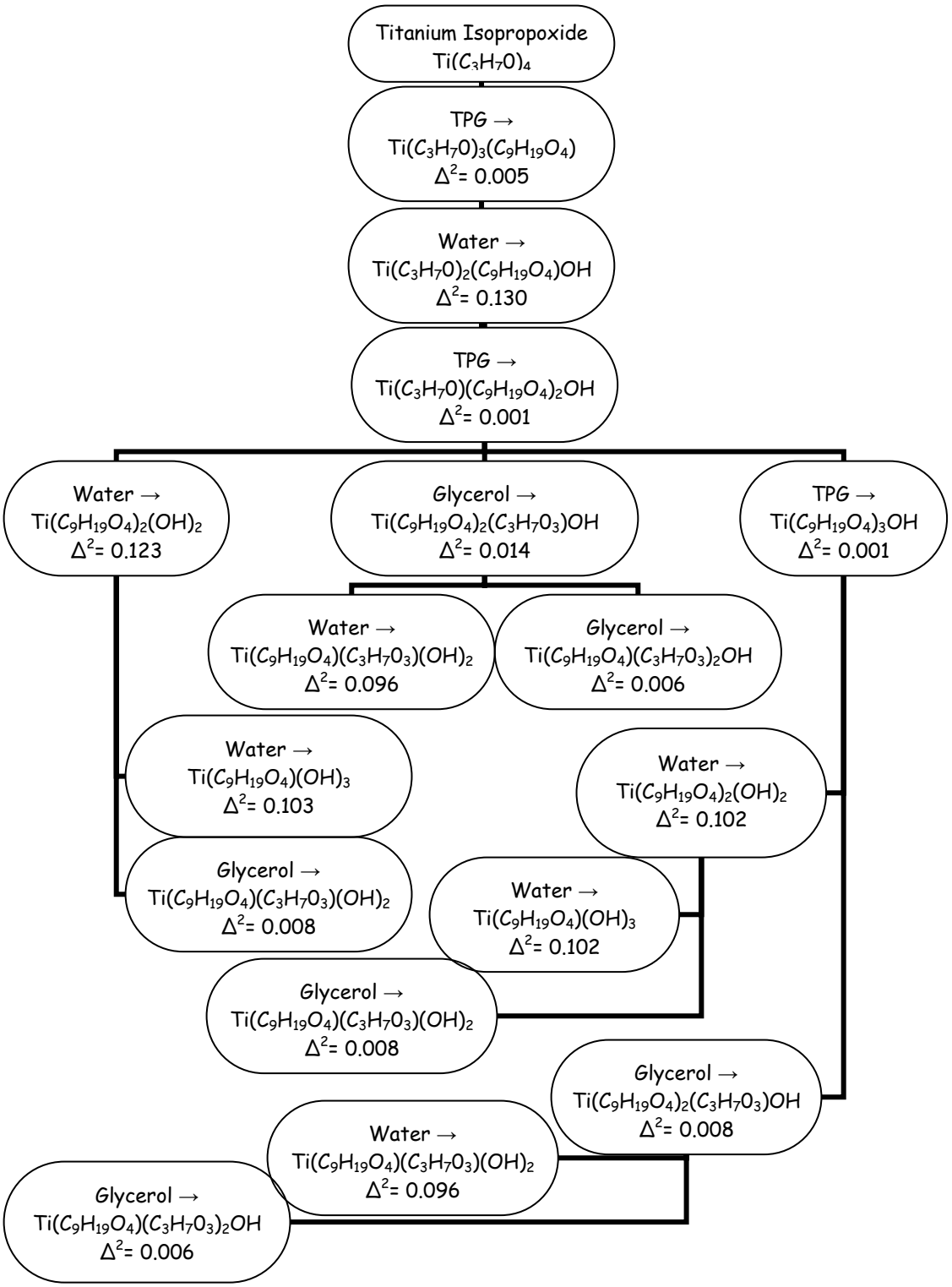

** Substituting group replaces the TPG rather than the isopropyl group

Figure A1-7: Possible reaction paths for sol-gel system TIP after initial reaction with TPG, water and then a second TPG group; ambient conditions

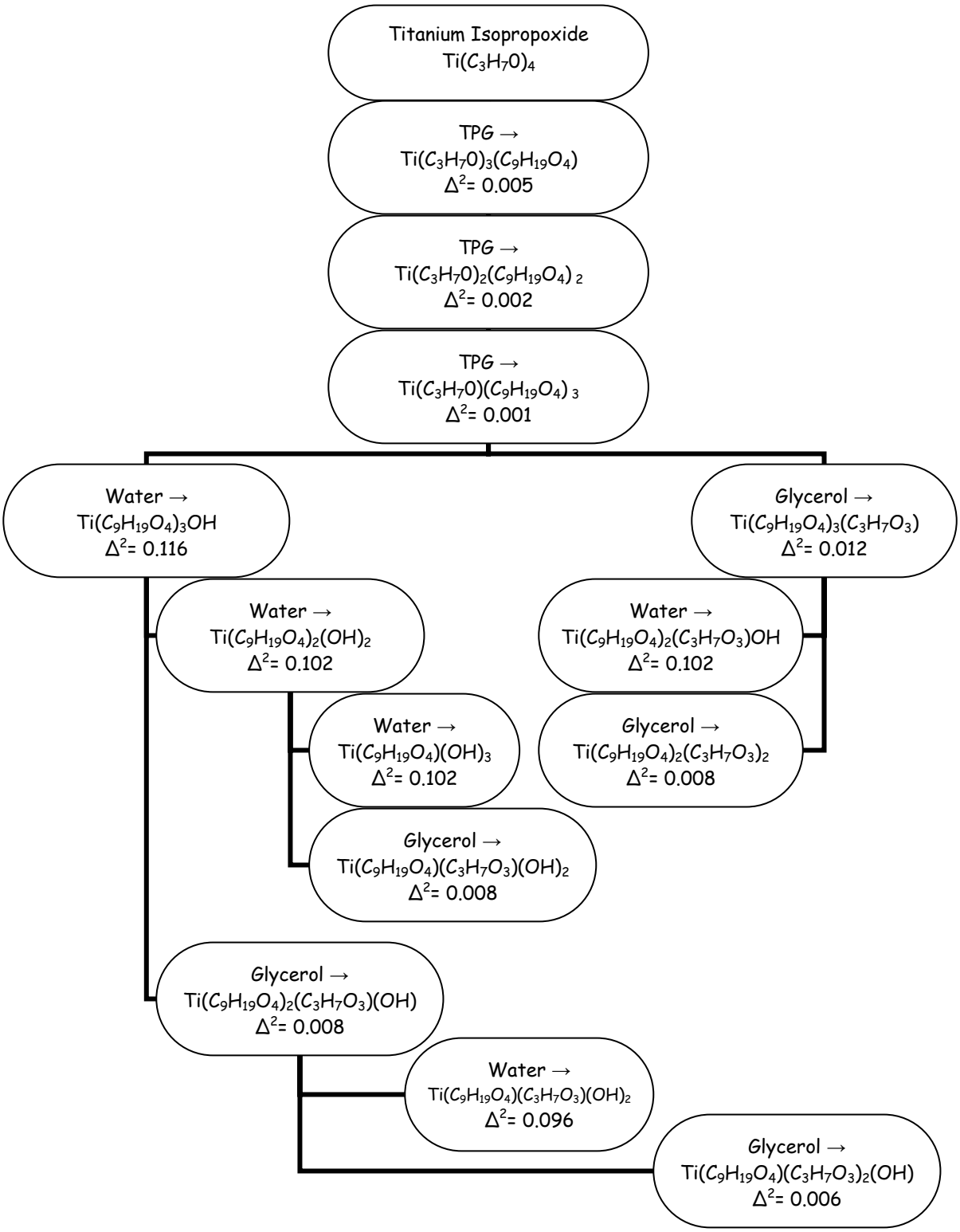

Figure A1-8: Possible reaction paths for TIP after initial reaction with three TPG groups; ambient conditions

Appendix 2: Possible Reaction Paths for Sol-Gel System Synthesized Under Ambient Conditions; Glycerol Added Last

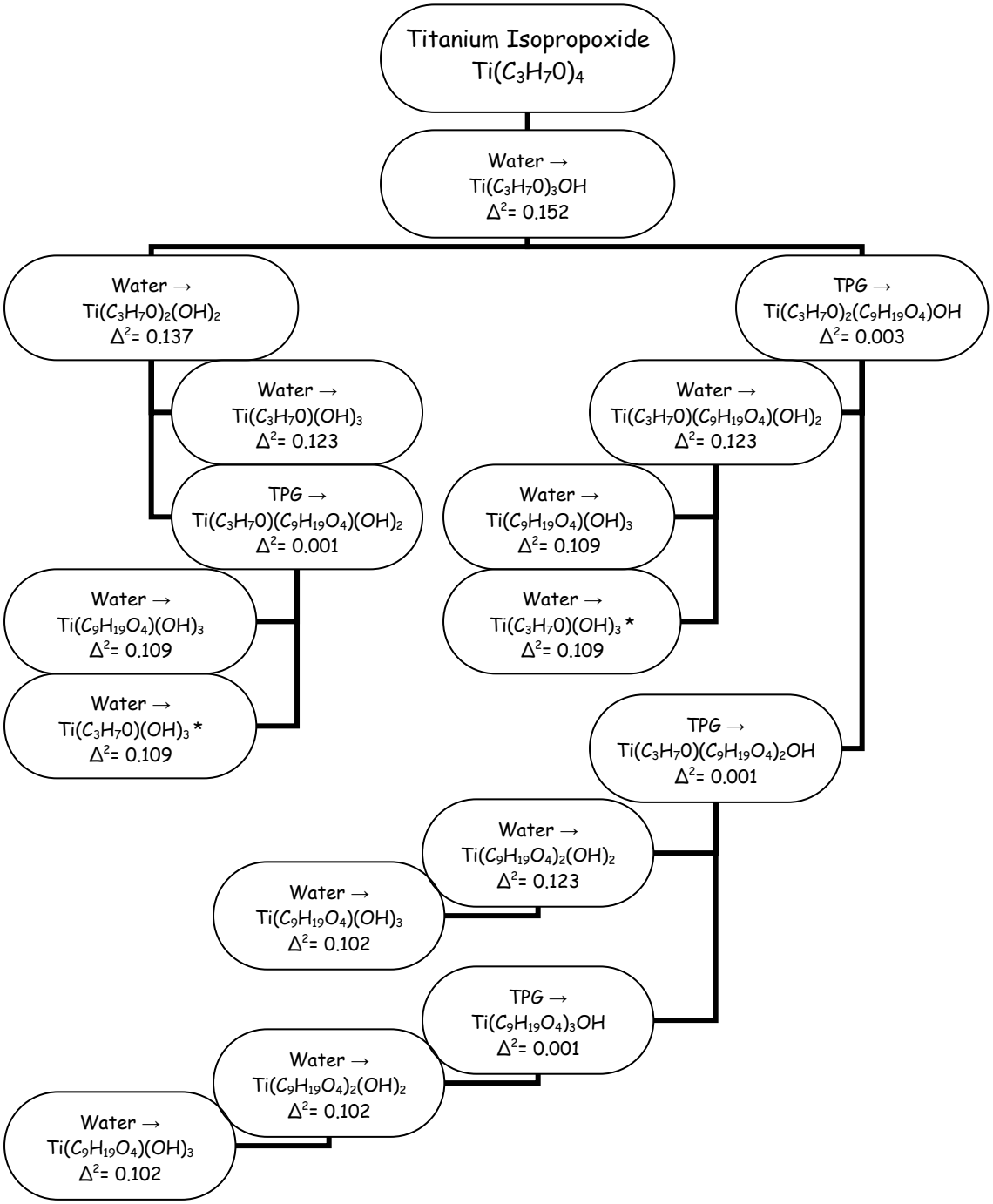

* Water can replace either the isopropyl or the TPG group

Figure A2-1: Possible reaction paths for TIP after initial reaction with water; ambient conditions, glycerol not yet added

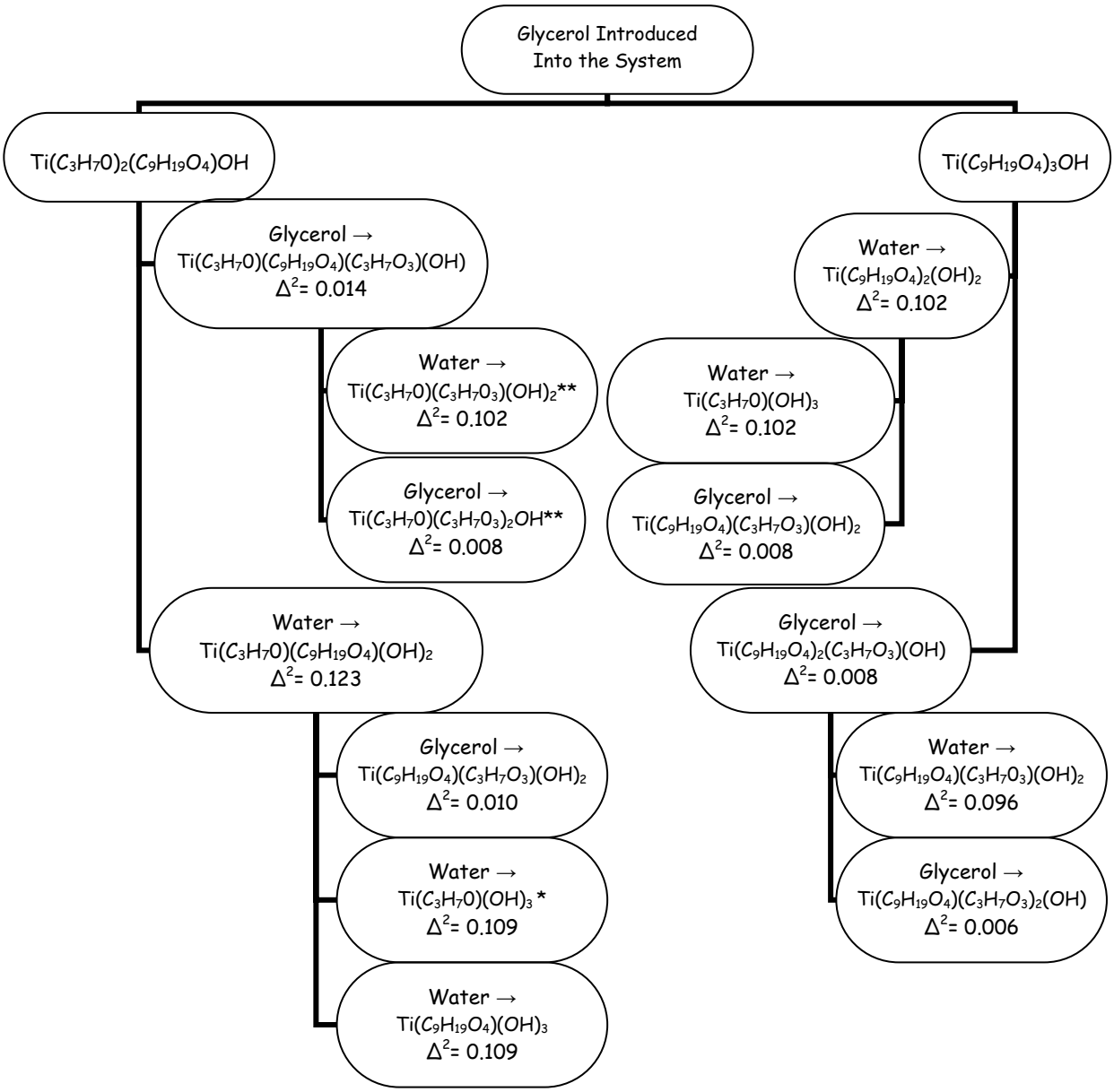

* Water can replace either the isopropyl or the TPG group

Figure A2-2: Possible reaction paths for TIP after initial reaction with water; ambient conditions, glycerol added to system

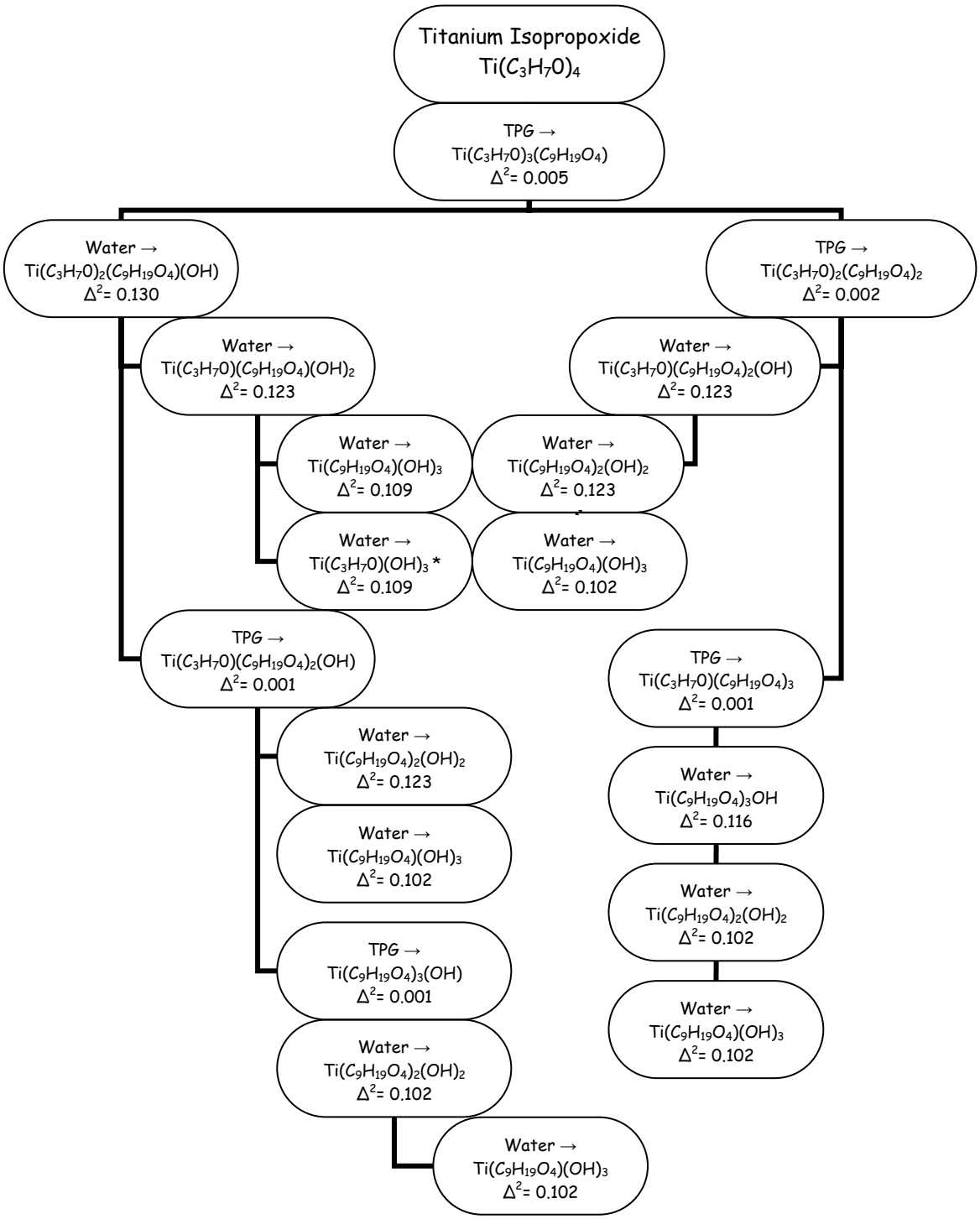

* Water can replace either the isopropyl or the TPG group
** Substituting group replaces the TPG rather than the isopropyl group

Figure A2-3: Possible reaction paths for TIP after initial reaction with TPG; ambient conditions, glycerol not yet added to the system

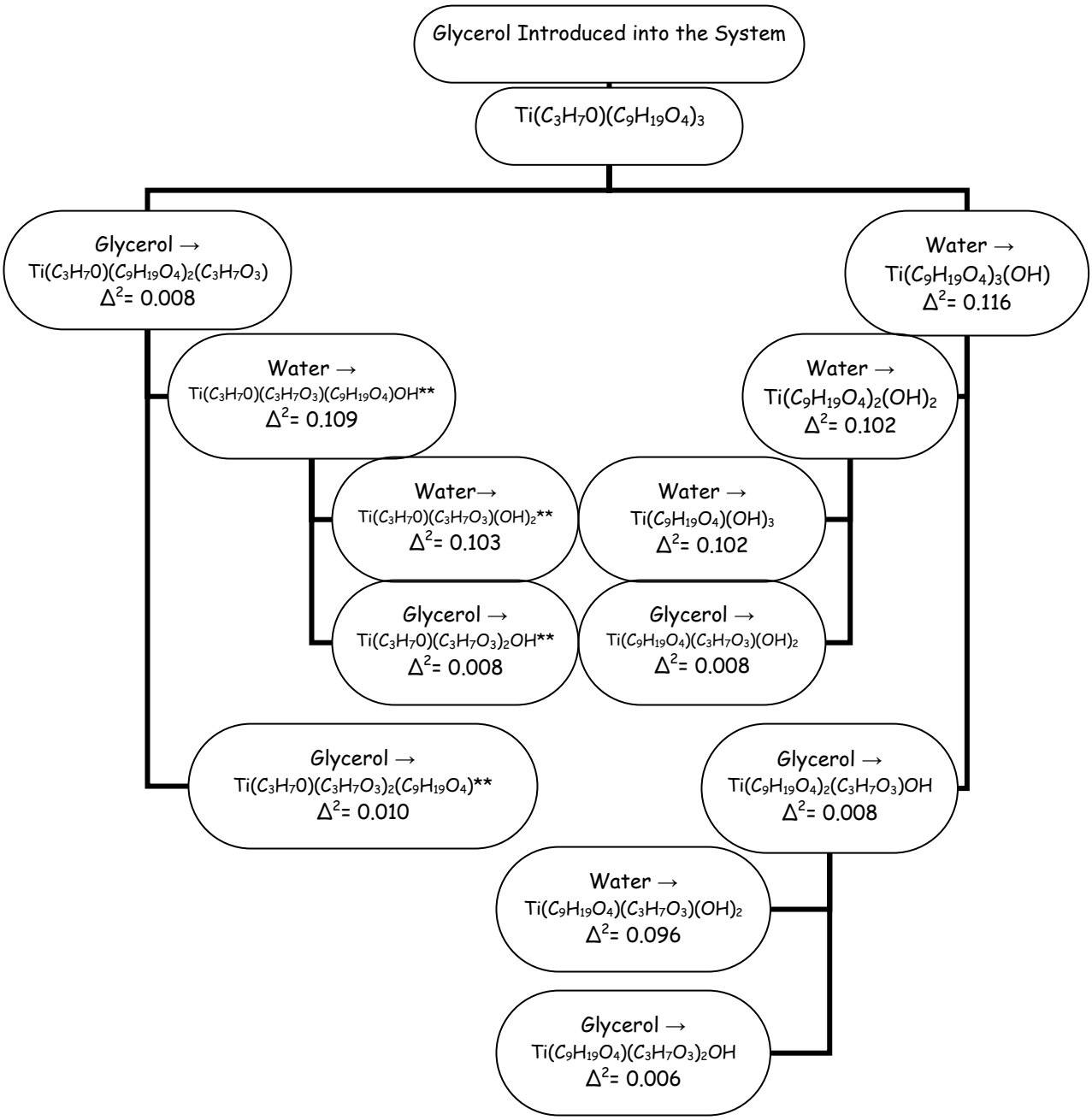

** Substituting group replaces the TPG rather than the isopropyl group

Figure A2-4: Possible reaction paths for $Ti(C_3H_70)(C_9H_{19}O_4)_3$ upon addition of glycerol; ambient conditions

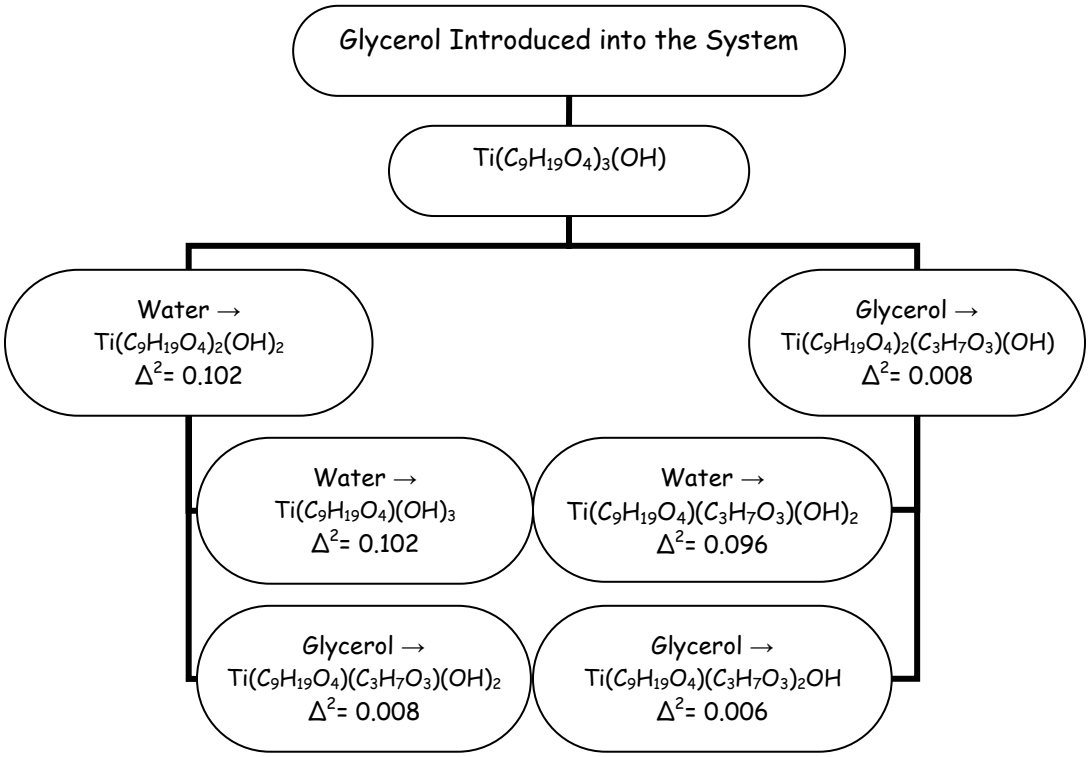

** Substituting group replaces the TPG rather than the isopropyl group

Figure A2-5: Possible reaction paths for $Ti(C_9H_{19}O_4)_3OH$ upon addition of glycerol; ambient conditions

Appendix 3: Possible Reaction Paths for Sol-Gel System Synthesized Under Nitrogen

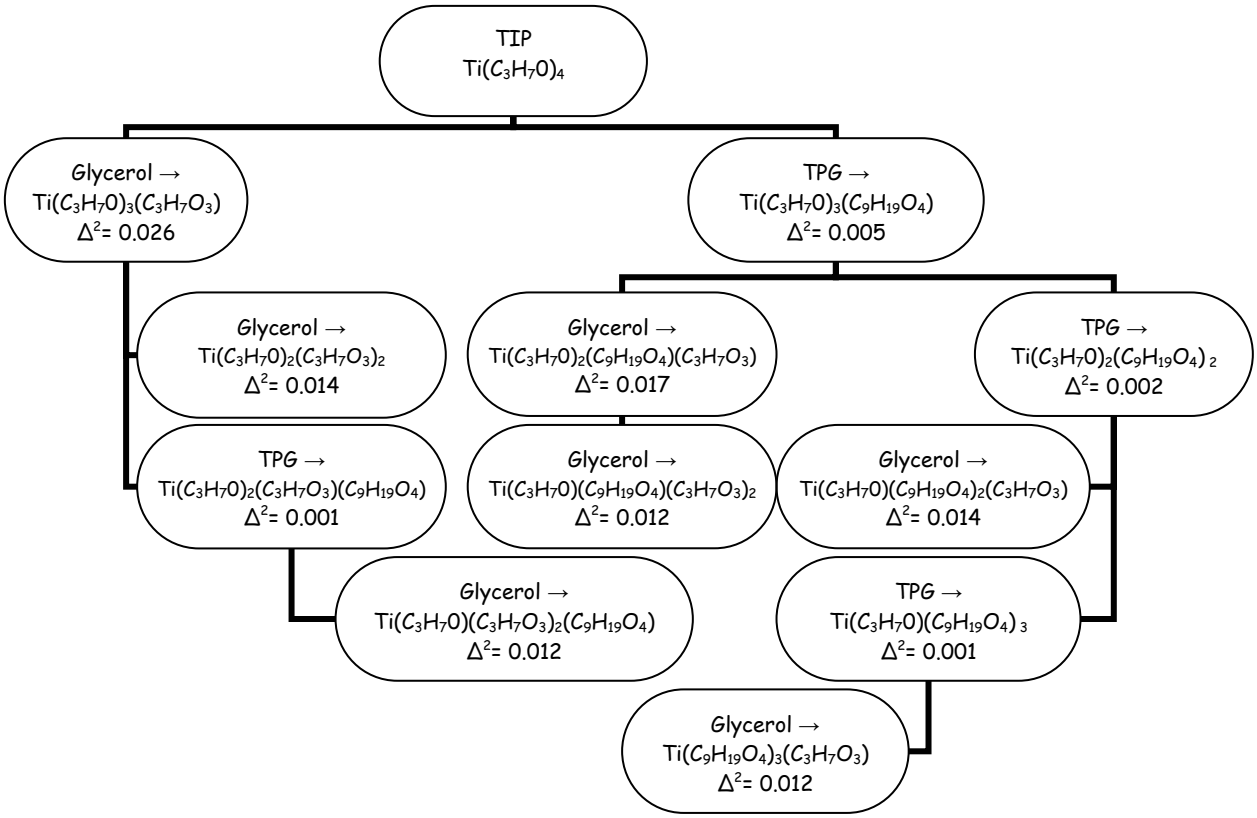

Figure A3-1: Possible reaction paths for TIP under nitrogen

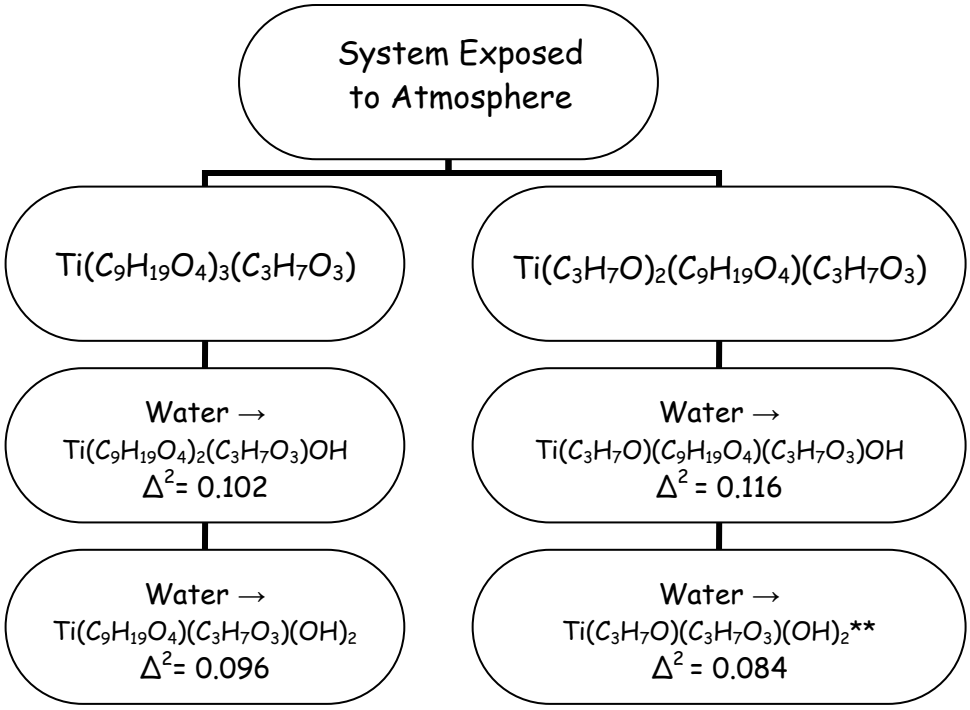

Figure A3-2: Possible reaction paths for $Ti(C_9H_{19}O_4)_3(C_3H_7O_3)$ and $Ti(C_3H_7O)_2(C_9H_{19}O_4)(C_3H_7O_3)$ upon exposure to atmosphere

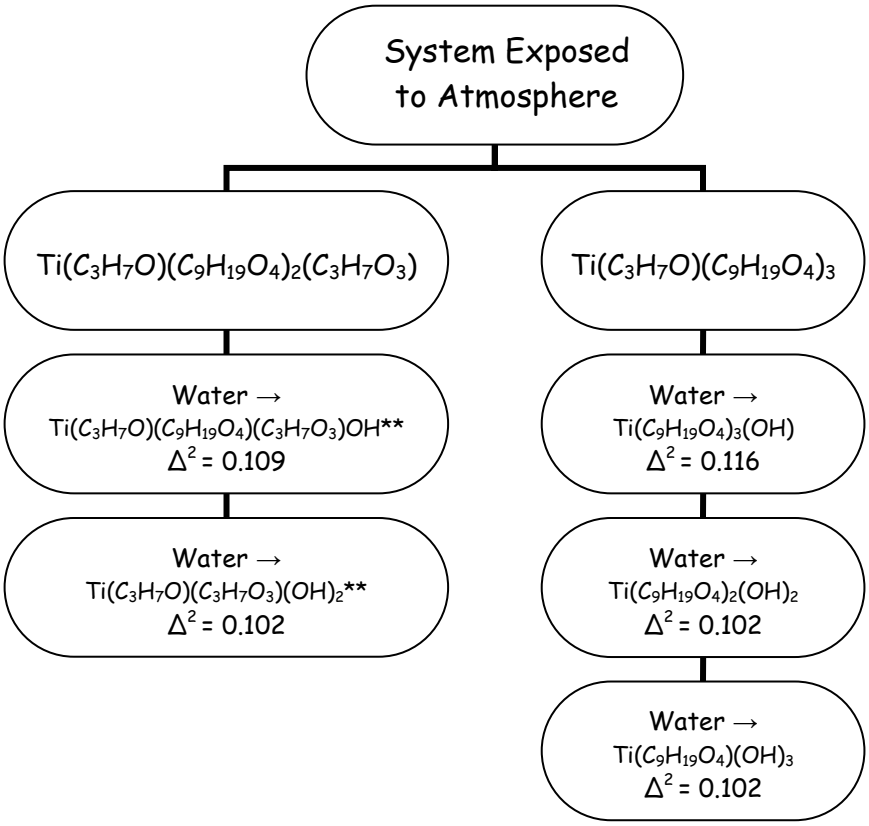

Figure A3-3: Possible reaction paths for $Ti(C_3H_7O)(C_9H_{19}O_4)_2(C_3H_7O_3)$ and $Ti(C_3H_7O)(C_9H_{19}O_4)_3$ upon exposure to atmosphere

Appendix 4: Possible Reaction Paths for Sol-Gel System Synthesized Under Nitrogen; Glycerol Added Last

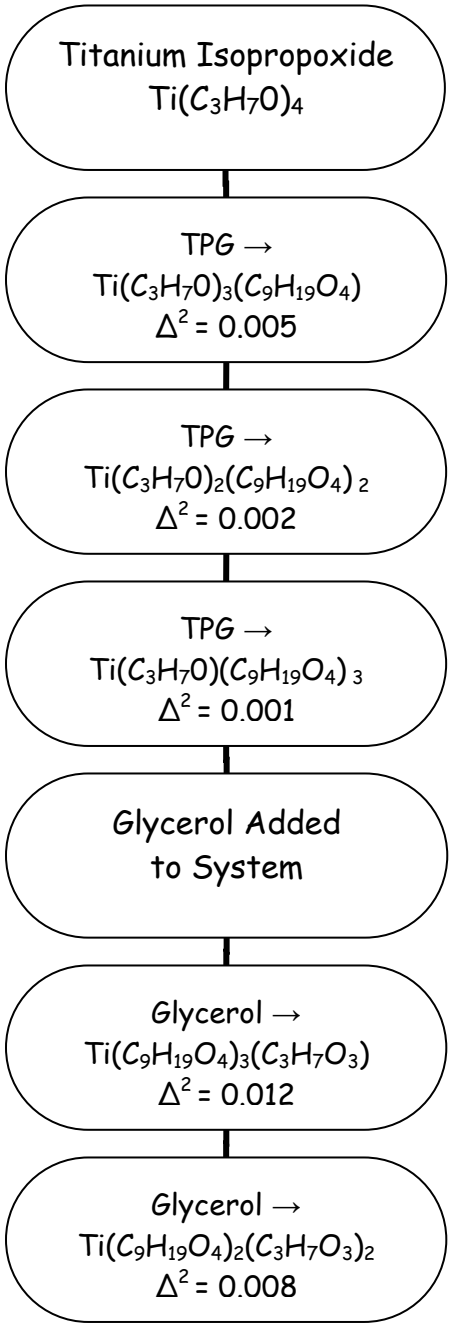

Figure A4-1: Possible reaction paths for TIP under nitrogen, glycerol added last

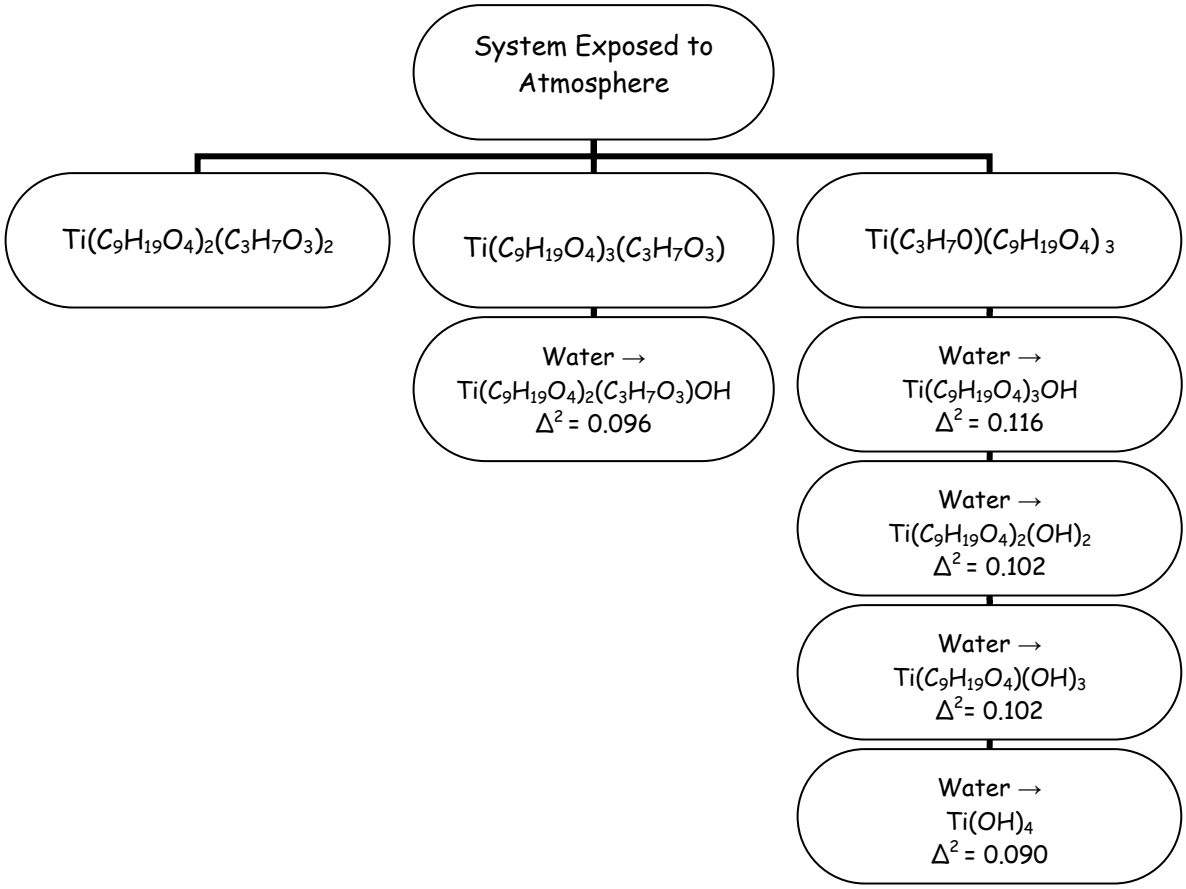

Figure A4-2: Possible reaction paths for system reacted under nitrogen; glycerol added last, exposed to atmosphere